High-Temperature Gas-Cooled Microreactors in Continuous Recycle Nuclear Fuel Cycles for Reducing Nuclear Waste and Environmental Impact

A Thesis Presented for the

Master of Science

Degree

The University of Tennessee, Knoxville

Venkata S. Vallabhaneni

May 2025

ACKNOWLEDGEMENTS

The author would like to thank his advisor, Prof. Nicholas R. Brown, for his mentorship and guidance. The author thanks Dr. Edward Duchnowski and Donald Doyle for providing the initial Serpent models of micro-HTGRs used in this work and guidance on the optimization sweep methodology. The author would also like to thank Dr. Annie Berens and Donald Doyle for their collaboration and input on this work. The author thanks their committee, Profs. Sandra Bogetic and Ivan Maldonado, for their feedback. The author also thanks Prof. Jason R. Trelewicz Prof. Lance L. Snead, and Sai Balla for their collaboration and input.

Finally, the author would like to thank their family and friends for their support and encouragement.

This work was funded by the DOE ARPA-E under contract DE-AR0001620 as part of the "MATRICY: Matrix Engineered TRISO Compacts Enabling Advanced Reactor Fuel Cycles" Program.

Portions of this thesis will be published in the following journal article: Venkata S. Vallabhaneni, Donald L. Doyle, Jason R. Trelewicz, and Nicholas R. Brown. Prismatic and Pebble-Bed Micro-HTGRs in Continuous Recycle Nuclear Fuel Cycles.

ABSTRACT

This work adapts both prismatic and pebble-bed micro high-temperature gas-cooled reactor (HTGR) point designs for Pu/TRU driver fuel under a continuous recycle fuel cycle. The adapted prismatic and pebble-bed micro-HTGR point designs are optimized to maximize fuel discharge burnup to reduce waste disposed, fuel cycle costs, and environmental impact. Optimization was performed for inert matrix fuel (IMF) concepts using different composite moderators in prismatic and pebble-bed designs. The prismatic and pebble-bed designs use (TRU) oxide tristructural-isotropic (TRISO) fuel. Moderator material includes beryllium (Be), beryllium oxide (BeO), yttrium hydride ($YH_{x=1.9}$), or zirconium hydride ($ZrH_{x=1.6}$) entrained in a MgO host matrix. For each prismatic IMF concept, optimization studies were performed to maximize discharge burnup by varying the TRISO packing fraction and assembly lattice pitch. For each pebble-bed IMF concept, optimization studies were performed by varying the TRISO packing fraction, the pebble fueled radius, the ratio of fueled to unfueled pebbles, and the active reactor core radius. Energy-normalized metrics for the mass of spent nuclear fuel and high-level waste (SNF&HLW) disposed, volume of low-level waste (LLW) disposed, metric tons of natural uranium (MTNU) used, area of land used, volume of water used, mass of carbon dioxide (CO_2) produced, and activity of SNF&HLW at 100 and 100,000 years are calculated for the continuous recycle prismatic and pebble-bed IMF concepts. These metric results are compared to those of a graphite reference design, once-through prismatic and pebble-bed IMF concepts, a light water reactor (LWR), and a small modular reactor (SMR). All continuous recycle IMF concepts outperformed the graphite reference case for all evaluated metrics. Additionally, all continuous recycle IMF concepts outperformed their once-through counterparts, the LWR, and SMR for nearly all evaluated metrics. For the mass of SNF&HLW disposed, the continuous recycle designs saw a 92.7% reduction. For the volume of LLW disposed, the continuous recycle designs saw between 29.7% to 31.1% reduction. Overall, the continuous recycle IMF concepts significantly reduced waste disposed, fuel cycle cost, and environmental impact compared to conventional once-through designs.

TABLE OF CONTENTS

LIST OF TABLES

LIST OF FIGURES

Chapter 1 Introduction

Increasing concerns about not only meeting the growing demand for electricity but also climate change and environmental pollution have made nuclear energy an attractive candidate for a low carbon energy source [1]. The next generation of nuclear reactors focuses on increased safety, increased efficiency, and reduced cost. However, nuclear reactors suffer from producing a significant amount of nuclear waste during operation. Properly processing and disposing of nuclear waste is expensive and does raise concerns about proliferation [2]. Large reactors are not always the best choice for meeting certain energy needs, which has sparked interest in small reactors that produce 300 megawatts of electricity (MWe) or less. There are scenarios where these small modular reactors (SMRs) are focused on producing even lower power outputs to address energy needs in remote locations and industrial sites that are not connected to the power grid [3].

1.1 Microreactors

Microreactors, which are SMRs that produce 20 MWe or less, can produce electricity in areas where large reactors are not well suited due to their small size and reduced power. The smaller size of microreactors means they can be fabricated in a factory, shipped by train, truck, or ship, quickly installed on a site, and quickly removed from the same site to be replaced by a new microreactor or transported to a different site [4]. Shown in **Figure 1** is a concept of a microreactor inside a shipping container. This can reduce installation time and cost, which is a major issue for large reactors. Microreactors can operate as part of the power grid, independently of the power grid, or as part of a microgrid. Microreactors, like SMRs, can be built in remote communities and industrial sites that are off-grid, countries with small and medium electricity grids, and rapidly growing cities in developing countries [5]. Additionally, critical facilities that are connected to the grid, such as hospitals and water treatment plants, can continue to operate during a power outage if powered by one or more microreactors [4]. Similar to large reactors, there are concerns about cost, safety, and proliferation when designing microreactors. These concerns can be addressed by designing the microreactor to be a high-temperature gas-cooled reactor (HTGR).

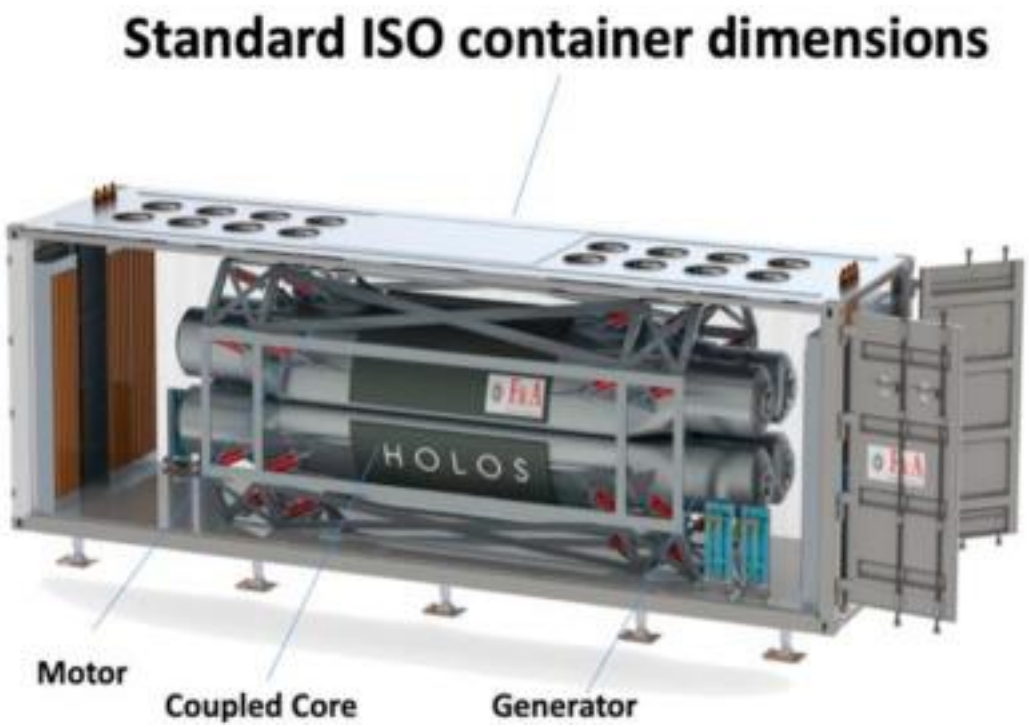

Figure 1. 3D rendering of a microreactor inside a standard shipping container [4].

1.2 High-Temperature Gas-Cooled Reactors

Microreactor designs include designs that use light water, high-temperature gas, molten salt, and liquid metal technologies. HTGRs are a promising nuclear reactor design due to their passive safety characteristics. These include ceramic-coated particle fuel, passive heat removal, and negative temperature feedback reactivity [6]. Ceramic coated-particle fuel enables fission product retention. Passive heat removal prevents accidents from occurring in the event of loss of power. Negative temperature feedback is when reactor reactivity decreases in response to the reactor core temperature increasing. This prevents reactor meltdown as decreasing the reactivity will decrease temperature before fuel can melt. In addition to these passive safety characteristics, HTGRs have been built and operated in the past and are still in operation. Due to their high operating temperatures, HTGRs can also be coupled to chemical plants to provide process heat, making them an even more attractive reactor design candidate for microreactors [7] [8].

The two primary types of HTGRs are prismatic and pebble-bed reactors. The prismatic reactor core is comprised of hexagonal blocks with fuel, which passes through the reactor once, and coolant channels. The pebble-bed reactor core uses fueled pebbles that pass through the core multiple times. Compared to other advanced reactor concepts, HTGRs have prior experience in their construction and operation. Both prismatic and pebble-bed reactors have been constructed and operated in the past or even currently.

The first HTGR that was built was Dragon, which was a prismatic test reactor built in the UK in 1956 and operated until 1968 [9]. The Arbeitgemeinschaft Versuschreaktor (AVR) was a pebble-bed HTGR built in Germany and first went critical in 1966 and operated until 1988. The AVR generated 15 MWe and started commercial operations in 1969 [9]. Peach Bottom I was a prismatic HTGR built in the US and first went critical in 1966 and operated until 1974. Peach Bottom I generated 40 MWe and started commercial operations in 1967 [9]. The Fort Saint Vrain nuclear reactor was a 330 MWe commercial prismatic HTGR located outside Denver, Colorado, and operated commercially from 1979 to 1989 [10]. Its reactor core consisted of hexagonal graphite block fuel elements surrounded by a graphite reflector [11]. Shown in **Figure 2** is the Fort Saint Vrain core arrangement. The High Temperature Gas-cooled Test Reactor (HTR-10) is a 10 megawatt thermal (MWth) test modular pebble-bed HTGR in China [12]. Shown in **Figure 3** is a cross-section of the HTR-10 reactor structure. The HTR-10 reactor core contains roughly 27,000 spherical fuel elements and is surrounded by a graphite reflector [12].

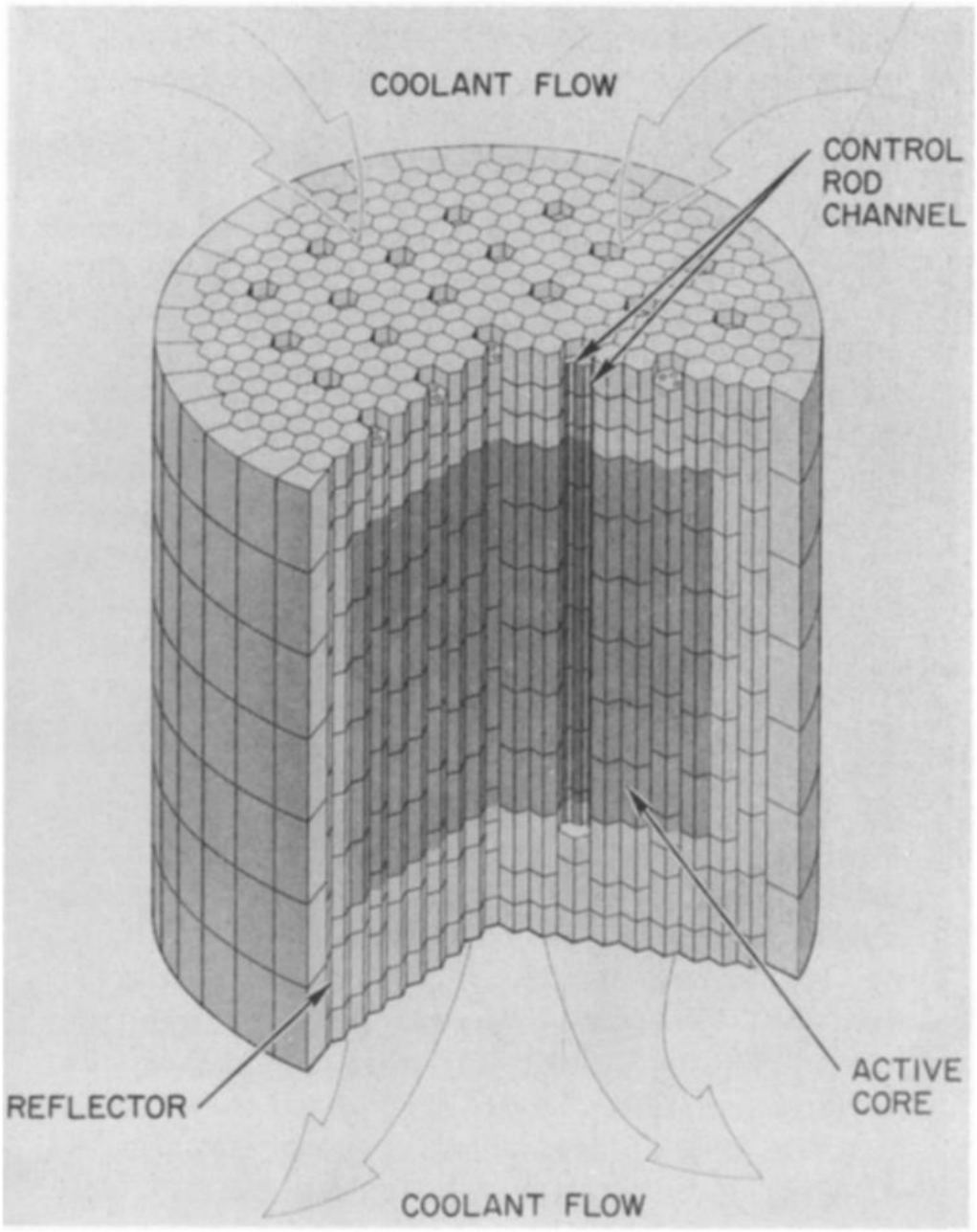

Figure 2. Core arrangement of Fort Saint Vrain [11].

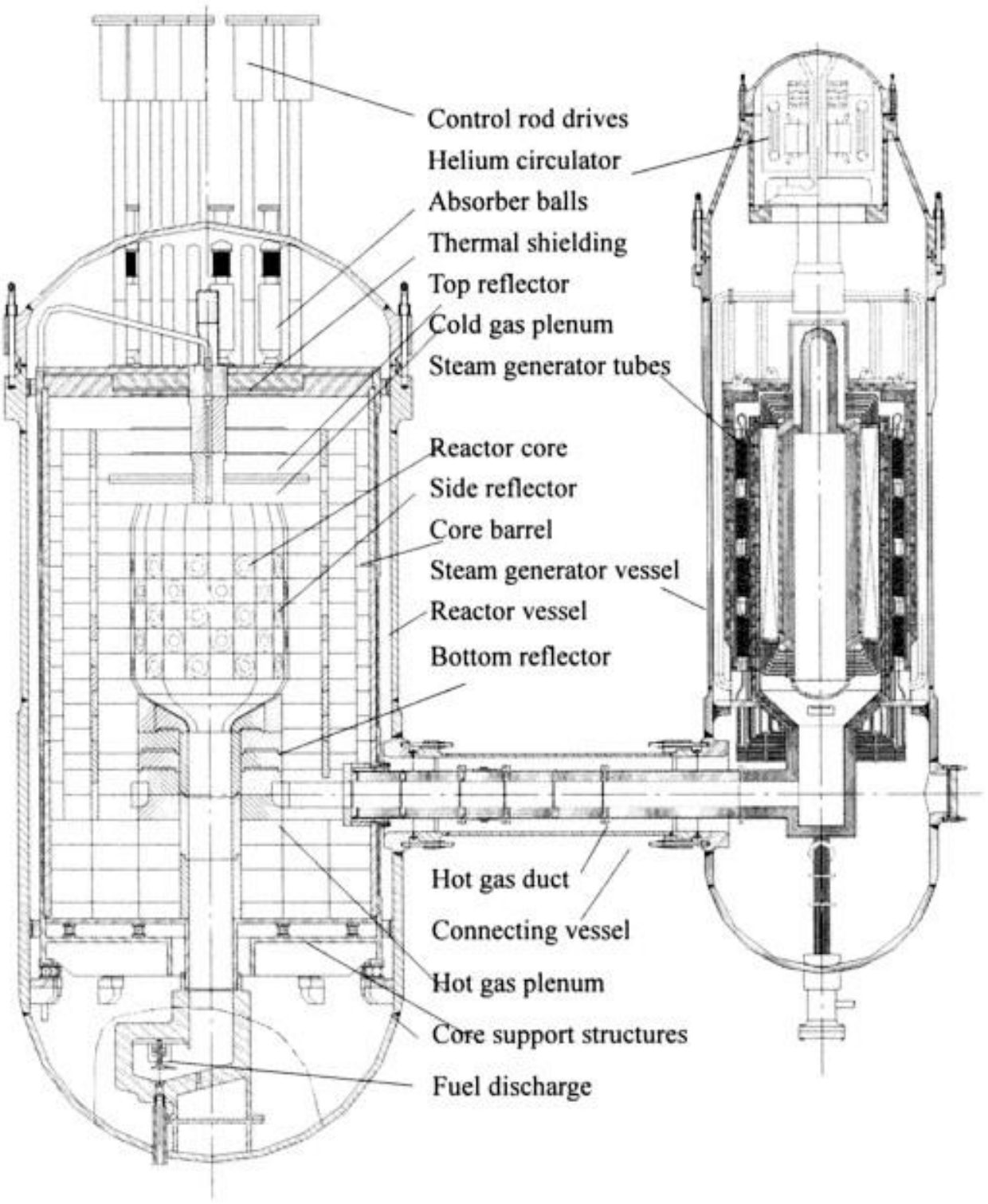

Figure 3. HTR-10 reactor design [12].

1.3 Nuclear Fuel

The use of ceramic coated-particle fuel is one of the safety features of HTGRs as it enables retention of fission products. Current HTGRs use TRISO fuel. Various forms of encapsulated fuel have been used in HTGRs historically, with the earliest form being fuel kernels coated with a single layer of pyrolytic carbon (PyC). Peach Bottom initially used PyC-only coated fuel particles and later used bistructural-isotropic (BISO) particles [13]. BISO particles include a buffer layer between the fuel kernel and the PyC layer. The AVR initially used BISO fuel but later switched to using TRISO fuel [13]. The Fort Saint Vrain reactor used coated-particle fuel with a PyC layer and silicon carbide (SiC) layer. The HTR-10 uses uranium dioxide (UO_2) TRISO fuel. The use of TRISO particles in microreactors has been proposed before [14].

The TRISO fuel particle consists of a fuel kernel surrounded by a graphite buffer layer, an inner PyC layer, a SiC layer, and an outer PyC layer [13]. TRISO particles are encased in a ceramic matrix, which has conventionally been graphite [15]. Shown in Figure 4 are the cross-sections of a UO_2 TRISO particle and a UCO TRISO particle, in which the layers are visible. The buffer layer is made of porous pyrocarbon and provides a void space for fission gases released by the fuel kernel. The inner PyC layer protects the fuel kernel from interacting with the SiC layer and adds to fission gas retention. The SiC layer retains fission products - that could not be retained within the fuel kernel or by the inner PyC layer – and provides structural strength. The outer PyC layer protects the SiC layer during handling and provides further retention of fission gases [13]. These layers work together to enable significant fission retention. TRISO particles can be formed into pebbles or cylindrical compacts, which are used in pebble-bed and prismatic reactors respectively as seen in **Figure 5**.

TRISO fuel has historically used fuel kernels composed of UO_2 or uranium carbide (UC). The use of UCO in HTGRs has been proposed to address corrosion of the SiC layer caused by carbon monoxide (CO) produced by excess O reacting with nearby carbon. The inclusion of additional uranium in carbide form mitigates CO formation [16]. However, UCO does not provide that much more uranium density than UO_2. Compared to UO_2 and UCO, UN has a significantly higher uranium density [17] [18]. The greater uranium mass that can be achieved makes UN TRISO desirable for use in smaller reactors, like micro-HTGRs, to increase fuel loading. While UN enables greater fuel loading, this work looks at transuranic (TRU) fuel in oxide form.

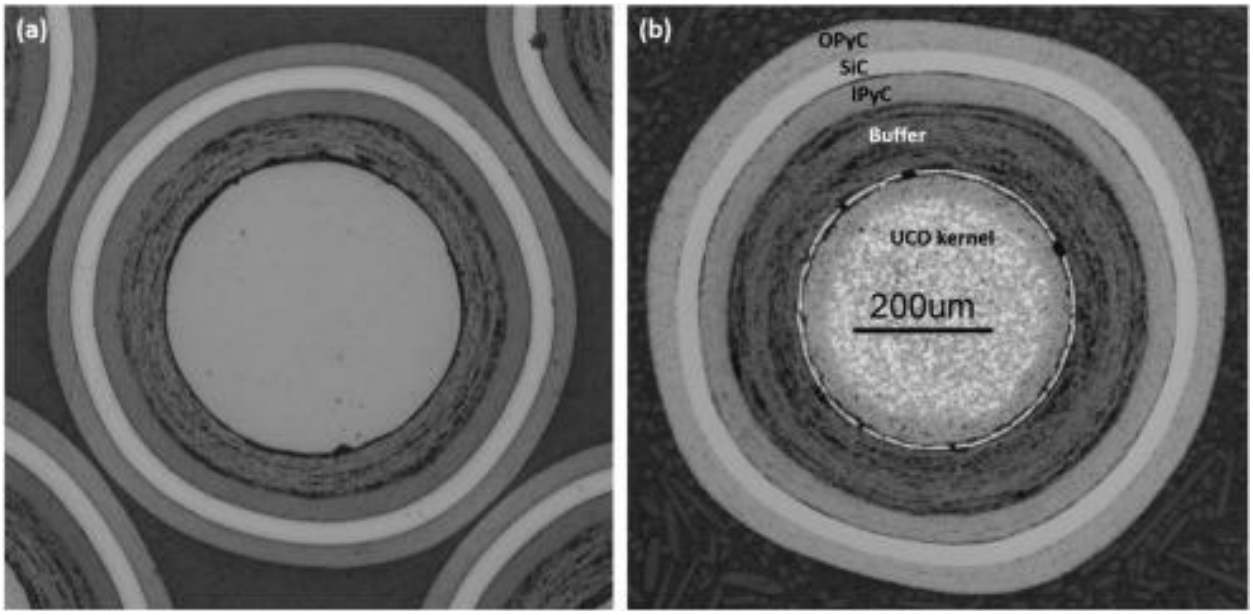

Figure 4. Cross-section of (a) UO_2 TRISO particle and (b) UCO TRISO particle [13].

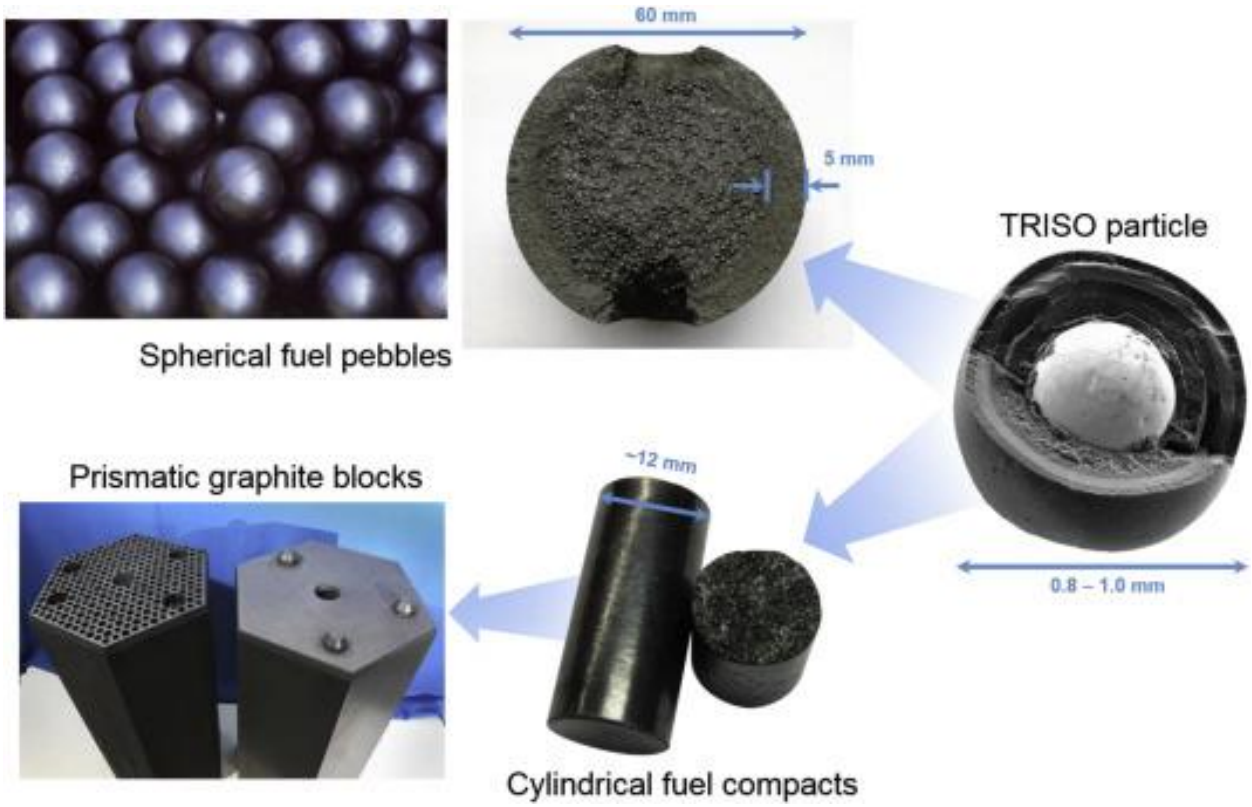

Figure 5. The use of a TRISO particle in spherical (pebble) and cylindrical (compact) fuel forms, where pebbles are used in pebble-bed reactors and compacts are used in prismatic reactors [13].

1.4 Composite Moderators

TRISO particles in HTGRs are traditionally surrounded by a graphite matrix. Some problems can occur when using graphite in the high-temperature environment of an HTGR. Graphite can undergo changes in its volume under high-temperature irradiation, experiencing up to an 8% change in its original volume after initially shrinking and then swelling [19] [20]. Additionally, the thermophysical properties of graphite can change under high-temperature irradiation [21] [22] [23]. These changes in graphite can negatively impact reactor core lifetime. An alternative to graphite is SiC, which is used in fully ceramic microencapsulated (FCM) fuel. SiC has higher stability under irradiation, higher fission product retention, and higher oxidation resistance compared to graphite [27]. However, using SiC in the fuel matrix reduces moderation, which reduces discharge burnup [27]. The reduced discharge burnup can result in increased waste disposed and increased environmental impact. To address the poor irradiation stability of graphite and the weaker moderating strength of SiC, the use of composite moderators in HTGRs has been proposed.

Composite moderators composed of an irradiation stable host matrix and highly moderating entrained phase are an attractive alternative to both graphite and SiC for use in HTGRs. Shown in **Figure 6** are the composite moderator concept and properties of the host matrix and entrained phase. The matrix provides good irradiation stability, good thermal conductivity, and good structural strength; the entrained phase provides strong moderation. The use of composite moderators in HTGRs has been studied and shown to improve reactor performance compared to traditional graphite reactors, where Be, BeO, $YH_{x=1.9}$, and $ZrH_{x=1.6}$ are entrained phase material options [24] [25] [26]. Beryllium and hydride moderators have previously been used in their monolithic form as moderating material in reactors such as the Aircraft Reactor Experiment (ARE) and the Heat Transfer Experiment No. 3 (HTRE3) [28] [29]. These materials are strong moderators but have poor irradiation resistance, which limits the maximum operating temperature. MgO is a commercially available and inexpensive matrix host material. TRISO can also be removed from MgO through thermochemical dissolution of MgO using aqueous chloride [30] and acid solutions [31]. Combining these moderator materials with MgO in composite moderator form can leverage the advantages of both materials. The impact of MgO-based composite moderators and UN TRISO fuel in optimizing micro-HTGR performance has been evaluated in previous work [32] [33].

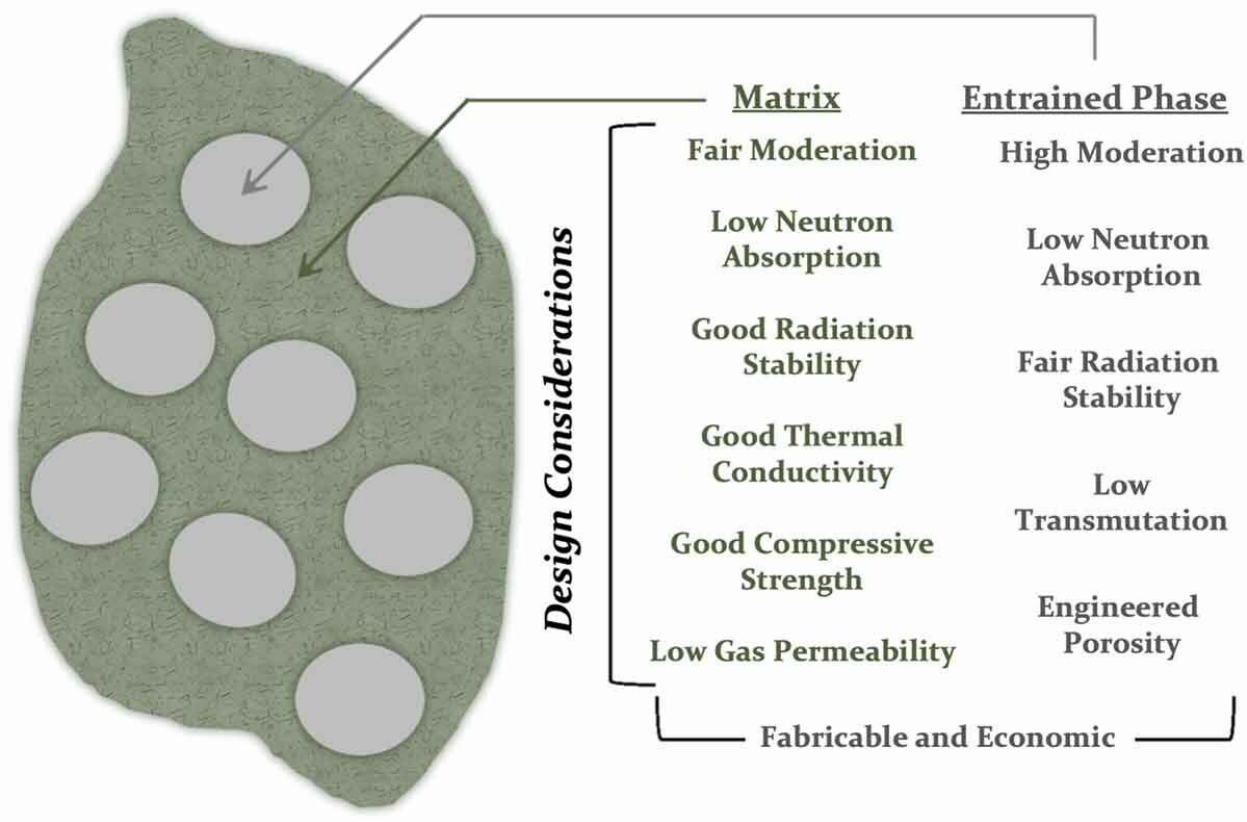

Figure 6. Composite moderator concept and associated attributes [24].

1.5 Transuranic Fuel

Removing TRU and minor actinides (MA) from discharged fuel and recycling them into fresh fuel can provide several benefits. These benefits include reducing environmental impact, more efficient use of permanent disposal space, and reduced proliferation risks. At the rate that the current US nuclear reactor fleet produces waste, new repository capacity equal to that of Yucca Mountain would be needed about every 20 to 30 years [34]. Deep-burn (DB) and IMF concepts that use TRISO fuel to transmute TRU nuclides such as plutonium (Pu), neptunium (Np), and americium (Am) have been proposed to address the need for more practical nuclear waste management [34]. Transuranium extraction (TRUEX) is the process used for actinide recovery in the US. In the TRUEX process, Pu and Np are separated from Am and curium (Cm) [35] [36] [37]. In the DB concept, the recovered TRU is fabricated into TRISO fuel and irradiated in a modular helium reactor (MHR). **Figure 7** shows the cross-section of two TRISO fuel particles containing plutonium oxide or thorium-plutonium oxide after irradiation. Neutronic analysis of these concepts has shown TRU consumption of 58.1% and 55.1% for the DB and IMF concepts respectively [38]. This work uses the TRU fuel vector from the DB-MHR concept in oxide form.

1.6 Continuous Recycle Fuel Cycles

All civilian nuclear energy in the US uses an open-ended once-through fuel cycle. The once-through fuel cycle is not very efficient in its utilization of uranium resources and waste minimization as uranium is mined, enriched, used once in reactors, and disposed of afterward. Continuous recycle fuel cycles have been found to be promising due to their improvements in waste generation and fuel resource utilization compared to the current fuel cycle used in the US. Continuous recycle fuel cycles always reprocess spent fuel for recycling and only HLW is disposed of. Recycling of actinide elements such as Pu, Np, and Am can result in more efficient use of fuel resources and reduce waste generated. The US Department of Energy Office of Nuclear Energy (DOE-NE) chartered an evaluation of the performance of different fuel cycle options [39]. The U/TRU continuous recycle fuel cycle in both fast and thermal critical reactors was identified as one of the most promising options [39]. This work adapts once-through prismatic and pebble-bed IMF concepts to the U/TRU continuous recycle fuel cycle, where the thermal critical reactor is the micro-HTGR.

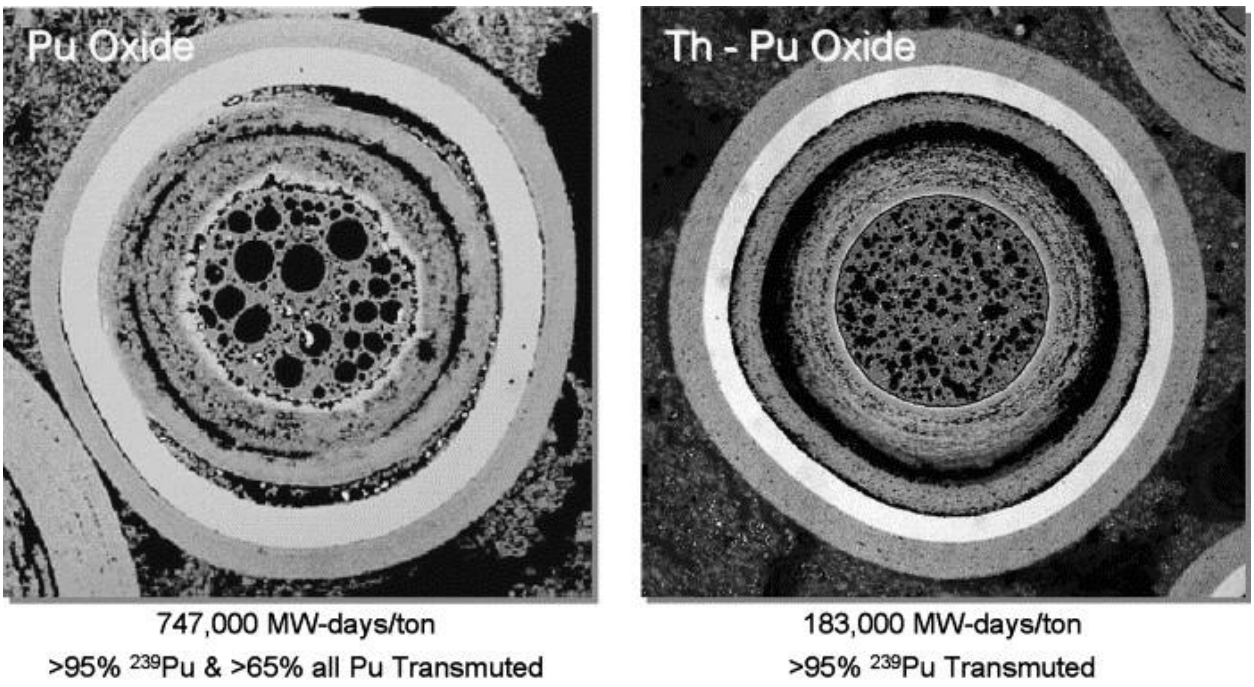

Figure 7. Cross-section of plutonium fueled TRISO particles after irradiation testing.

Chapter 2 Methodology

The performance of the continuous recycle IMF concepts was evaluated by determining the quantity of nuclear waste, fuel cycle cost, and environmental impact. The DOE-NE Evaluation and Screening (E&S) study is a study on the evaluation and screening of nuclear fuel cycle options, which considers the entire fuel cycle from mining to disposal for once-through, limited recycle, and continuous recycle fuel cycles [22]. A total of 40 evaluation groups were studied, including the one that the fuel cycle evaluated in this work is based on. Examples of leveraging the methodology used and lessons learned in the E&S study can be found in previous works [27] [40] [41] [42], including examples of waste reduction technology similar to what is evaluated in this work [32] [24]. The E&S study was done with the goal of identifying a few promising fuel cycles that showed significant improvement compared to the currently used nuclear fuel cycle in the US. The evaluation methods used in the E&S study were used in this work to calculate energy-normalized metrics which provide a one-to-one comparison between the different reactor concepts and sizes. These energy-normalized metrics include mass of SNF&HLW disposed, volume of LLW disposed, MTNU used, area of land used, volume of water used, mass of CO_2 produced, and activity of SNF&HLW at 100 and 100,000 years. Metric results from the continuous recycle microreactor IMF concepts are compared to those of a graphite reference, once-through microreactor IMF concepts, an LWR, and an SMR [43].

2.1 Continuous Recycle Fuel Cycle

The evaluated fuel cycle option is a continuous recycle fuel cycle management scheme. **Figure 8** shows a graphical representation of the fuel cycle that is being evaluated. The fuel cycle that is evaluated is a two-stage fuel cycle where the first stage is a 1000 MWth sodium-cooled fast reactor (SFR) and the second stage is a 10 MWth prismatic or pebble-bed micro-HTGR. This is based on the EG30 recycled fuel cycle from the E&S study [39]. EG30 is a fuel cycle concept in which Stage 1 is a 1000 MWth SFR and Stage 2 is a 3000 MWth PWR that uses recycled MOX fuel. This fuel cycle option was identified as one of the most promising designs due to the improvements it offered in comparison to the fuel cycle currently used in the US [39]. All uranium, plutonium, and minor actinides are recycled in this continuous recycle fuel cycle. Unlike the PWR, the micro-HTGR does not require any uranium. In the fuel cycle evaluated in this work, only the SFR requires uranium for its driver and blanket fuel.

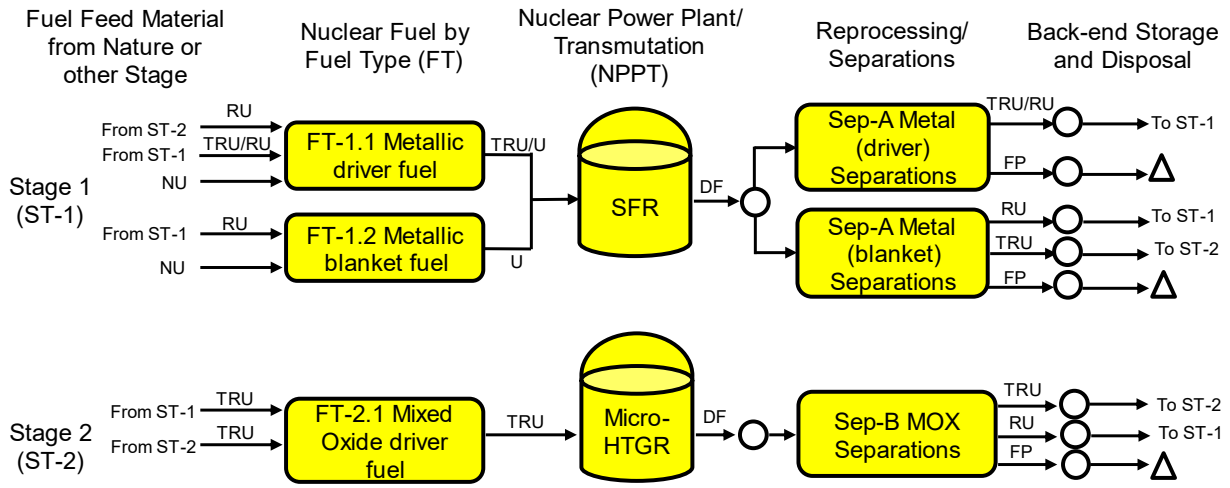

Figure 8. Schematic overview of the two-stage fuel cycle from SFR(TRU/U) to PWR (TRU/Pu). Reproduced from the E&S study [39].

The Stage 1 SFR produces TRU for the Stage 2 micro-HTGR. TRU/U recovered from Stage 1 and MA recovered from Stage 2 are mixed with NU to create the Stage 1 driver fuel and RU from Stage 1 is mixed with natural uranium (NU) to create the Stage 1 blanket fuel. Discharged SNF from the Stage 1 driver fuel is reprocessed to recover TRU/RU, which is recycled back into Stage 1 by using it to make new driver fuel. Excess TRU from reprocessing Stage 1 discharged blanket fuel and Pu recovered from Stage 2 are used to make TRU mixed oxide (MOX) driver fuel for Stage 2. Discharged fuel from Stage 2 is reprocessed, where recovered Pu and MA are recycled back into Stage 2, and recovered RU and excess MA are recycled back into Stage 1. LLW, FP, and material losses during reprocessing of Stages 1 and 2 are sent to disposal [39].

2.2 Reactor Concepts

Prismatic and pebble-bed micro-HTGRs using TRU TRISO fuel in IMF form and different composite moderators are evaluated in this work. The size constraints of both the prismatic and pebble-bed designs were set to a total radius of 90 cm and a total height of 395.5 cm. The power was set to 10 MWth in both the prismatic and pebble-bed designs to match the power of the HTR-10 [12].

The graphite reference design comes from previous work evaluating the impact of composite moderators in once-through prismatic IMF designs [24]. The graphite reference is a prismatic micro-HTGR that uses 19.9% enriched uranium carbide (UCO) TRISO fuel and adheres to the same size constraints as the continuous recycle micro-HTGRs. The once-through prismatic and pebble-bed designs also adhere to the same size constraints. These once-through designs use 19.9% enriched uranium nitride (UN) TRISO fuel instead of UCO. The size of TRISO particles used is the same in the graphite reference, once-through IMF concepts, and continuous recycle IMF concepts. The only difference is the density of the fuel kernel due to using UCO, UN, or TRU oxide respectively. The radius and densities of the TRU oxide TRISO can be seen in **Table 1**. The heavy metal vector of the fuel consists of only plutonium, neptunium, and americium isotopes of TRU recovered from spent fuel. The vector is based on the one used in the Deep-Burn Modular Helium Cooled Reactor Design [38]. **Table 2** contains the mass percentage of isotopes present in the TRU fuel heavy metal vector. Cm is excluded from the fuel vector because of its high spontaneous fission rate and decay heat, which can make fuel fabrication difficult [38].

Table 1. TRU oxide TRISO layer radii and density for continuous recycle micro-HTGRs.

Layer	**Radius [cm]**	**Density [g/cm^3]**
TRU oxide kernel	0.0425	11.09
Buffer	0.0475	1.0
Inner PyC layer	0.0510	1.90
SiC layer	0.0545	3.20
Outer PyC layer	0.0580	1.90

Table 2. Heavy metal vector of TRU fuel [38].

Isotope	**Percent Mass (%)**
Np-237	4.5941
Pu-238	1.3340
Pu-239	50.9975
Pu-240	20.7970
Pu-241	7.5689
Pu-242	4.9457
Am-241	8.2207
Am-242m	0.0304
Am-243	1.5118

Am and Cm are typically co-extracted by most extractants used in actinide partitioning. Am and Cm are most stable in their trivalent oxidation state, which is Am(III) and Cm(III) respectively. Separating Am and Cm in this state is very difficult because of their chemical similarity. Efficient separation of Am(III) and Cm(III) can be achieved by using nitric acid solutions [45]. The use of such solutions in separation of Am and Cm would be desirable for use in the continuous recycle fuel cycle evaluated in this work, as Cm is excluded from the microreactor fuel vector.

In the prismatic IMF concept, TRISO particles are embedded in pure MgO, which is surrounded by the composite moderator. In the pebble-bed IMF concept, TRISO particles are embedded in the composite moderator. The composite moderator used consists of a MgO host matrix with an entrained phase that is either Be, BeO, $YH_{x=1.9}$, or $ZrH_{x=1.6}$. The volume percent of the host matrix and entrained moderator for each composite moderator is found in

Table 3. Shown in **Figure 9** is an example of TRISO particle distribution in the prismatic IMF compact (left) and in the pebble-bed IMF pebble (right).

The prismatic micro-HTGR design used in this work is based on designs from previous works looking at advanced moderator concepts and evaluating their performance in a once-through fuel cycle [44]. **Figure 10** shows the radial and axial cross-sections of the prismatic micro-HTGR and **Figure 11** shows the radial and axial cross-section of the pebble-bed microreactor. The reactors were simulated using Serpent [46], a continuous-energy Monte Carlo transport code, and the ENDF/B-VII.1 cross-section data library. The prismatic microreactors were depleted until they reached subcriticality. Discharge burnup in the prismatic reactors was calculated when effective criticality reached one, or reactivity reached zero. Discharge burnup was calculated differently in the pebble-bed reactors. The linear and quadratic reactivity models were used to calculate discharge burnup in the pebble-bed reactors, assuming an eight-batch fuel management scheme [47]. The prismatic microreactor simulations were run with lattice pitches of 2.0, 2.2, 2.4, and 2.5 cm and TRISO packing fractions between 5% and 50% in increments of 5% for each lattice pitch value. The pebble-bed microreactor simulations were run with pebble fueled radii of 0.5, 1.0, 1.5, 2.0, 2.5, and 3.0 cm, TRISO packing fractions between 5% and 55% in increments of 10%, ratio of fueled to unfueled pebbles between 10% and 100% in increments of 10%, and active core radii of 30, 40, 50, 60, 70, 80, and 85 cm. Adjusting these parameters means adjusting the ratio of fuel to moderator as well.

Optimization sweeps were performed for each of the four IMF concepts for both the prismatic and pebble-bed designs. These optimization sweeps plotted discharge burnup as a function of two reactor core parameters. The optimal configuration was the configuration that produced the highest fuel discharge burnup. High discharge burnup was targeted due to the evaluated metrics being dependent on discharge burnup.

Table 3. Two-phase composite moderator materials and volume percent.

Composite Moderator	Host Material	Moderator Material
MgO Be	60% MgO	40% Be
MgO BeO	60% MgO	40% BeO
MgO $YH_{x=1.9}$	85% MgO	15% YH
MgO $ZrH_{x=1.6}$	85% MgO	15% ZrH

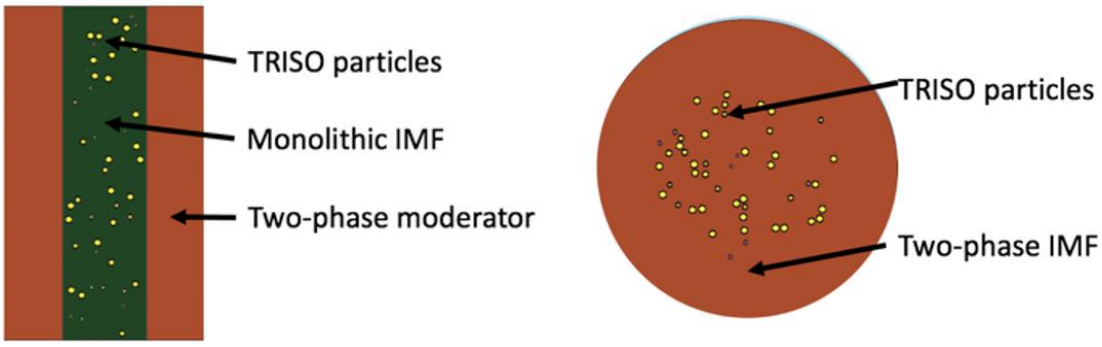

Figure 9. IMF within a prismatic (left) and pebble-bed (right) reactor platform.

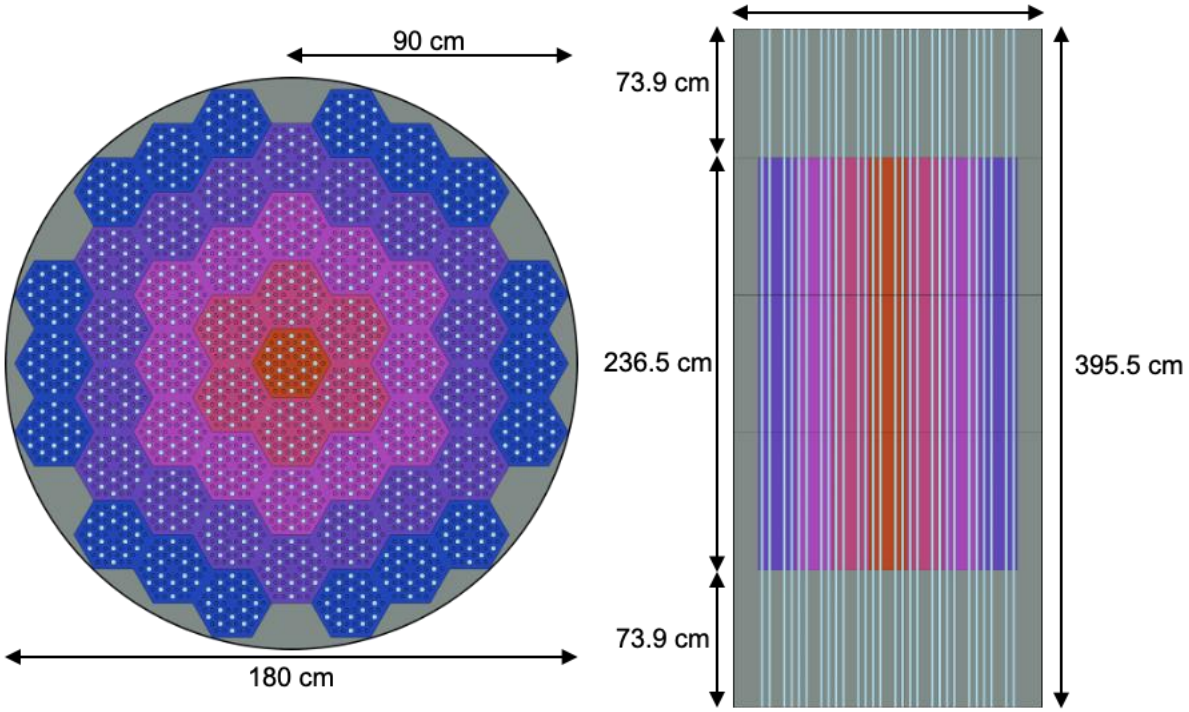

Figure 10. Radial (left) and axial (right) cross-section of the prismatic microreactor.

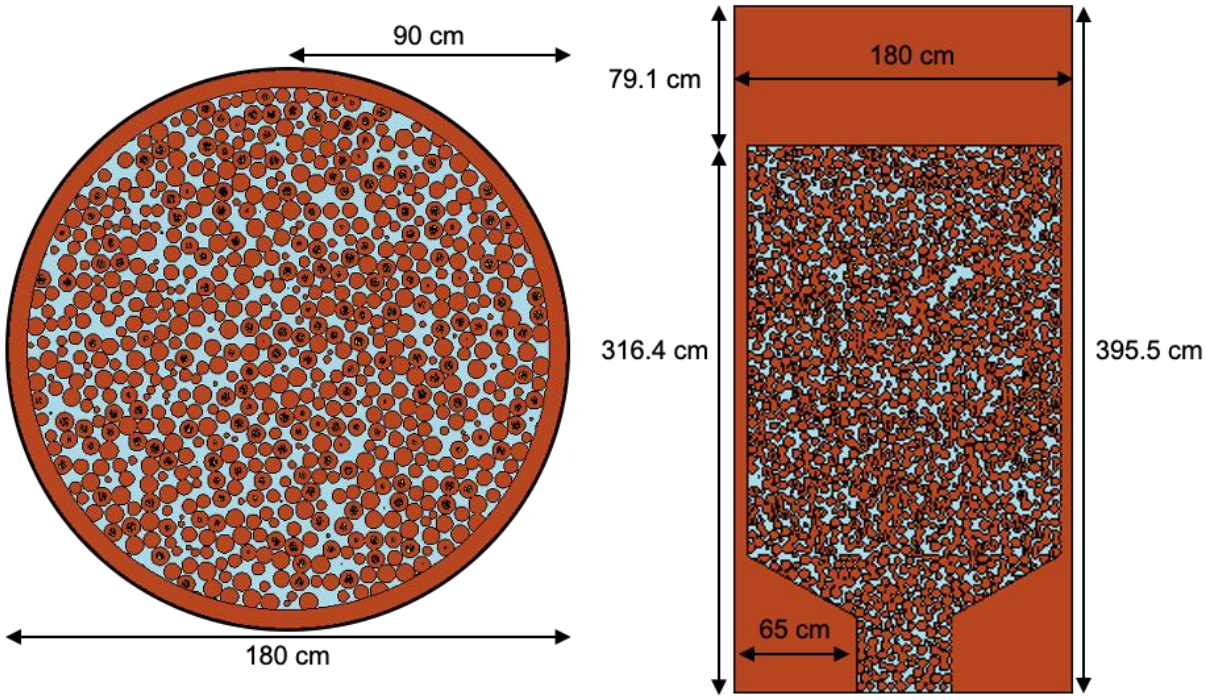

Figure 11. Radial (left) and axial (right) cross-section of the pebble-bed microreactor point design.

2.3 Normalized Mass Flow Calculation

After finding an optimal configuration for each prismatic and pebble-bed IMF concept, normalized mass flow data is calculated for the fuel cycle. The mass flow data is normalized based on the electrical energy generated in a year, which is assumed to be 100 gigawatt electric (GWe) per year according to the E&S study [39]. Compositions for charge and discharge fuel of Stages 1 and 2 are also calculated. Charge fuel in the Stage 2 micro-HTGR comes from TRU recovered from Stage 1 discharged blanket fuel and Pu recovered from Stage 2 discharge fuel. Both stages are balanced to where the Stage 1 SFR produces just enough TRU needed to feed the Stage 2 micro-HTGR. **Figure 12** shows an annotated mass flow table with explanations of important terms and the flow of material. It is divided into two stages, which are divided into three technologies: fuel, nuclear power plant transmutation (NPPT), and reprocessing and separation (rep/sep). Neptunium is included in the plutonium row in the mass flow table because it is included in the plutonium stream during TRUEX [35] [36] [37]. The mass flow table shown is for the continuous recycle prismatic MgO ZrH design.

The electricity share of the two stages is calculated according to how much TRU is available from Stage 1 and much how TRU is needed in Stage 2. *N*, which is the number of Stage 2 reactors that can be sustained by one Stage 1 reactor, is calculated using Equation 1, where $M_{TRU,2}$ is the mass flow rate of TRU required to feed one Stage 2 reactor and $M_{TRU,1}$ is the mass flow rate of excess TRU generated by Stage 1.

$$(1)\ N = \frac{M_{TRU,2}}{M_{TRU,1}}$$

The initial heavy metal mass of Stage 2 M_2 can be calculated using Equation 2, where P_2 is the Stage 2 reactor thermal power in MWth, $T_{C,2}$ is the Stage 2 reactor cycle length in effective full power days (EFPD), and BU_2 is the Stage 2 reactor fuel discharge burnup in megawatt-days per kilogram of heavy metal (MWd/kgHM).

$$(2)\ M_2 = \frac{P_2 T_{C,2}}{BU_2}$$

The electrical energy generation share of Stage 1 f_1 is calculated using Equation 3, where E_i is the electrical energy generated per year per Stage *i* reactor.

$$(3)\ f_1 = \frac{E_1 N}{E_1 N + E_2}$$

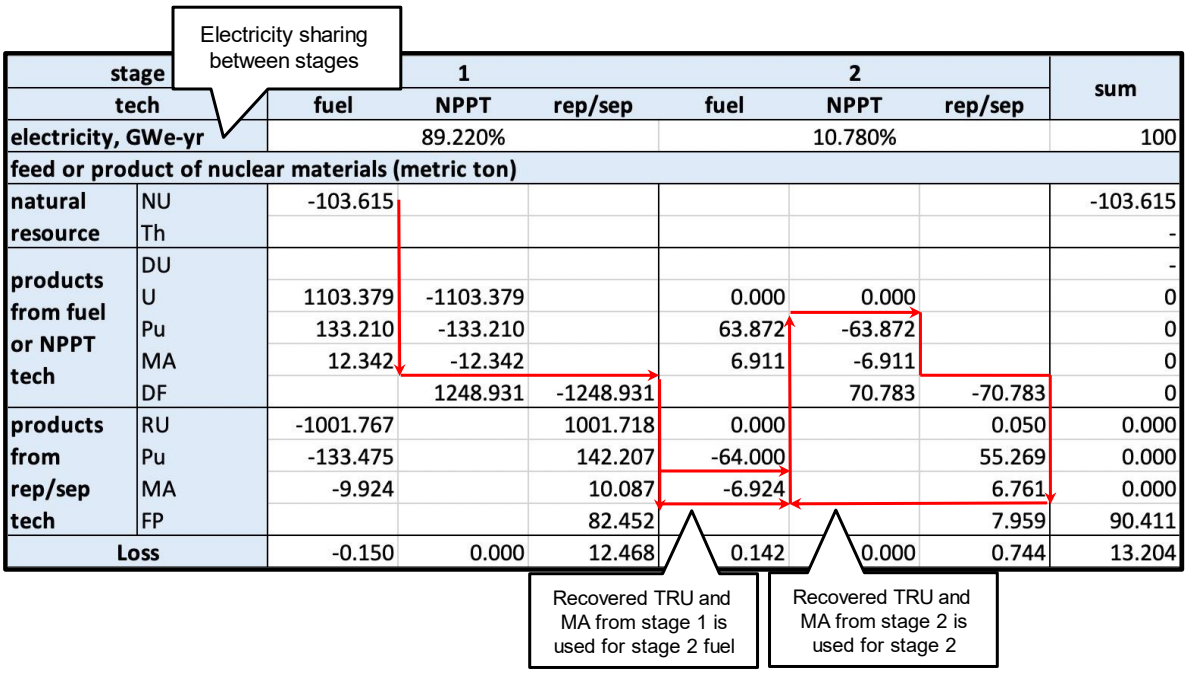

stage		1			2			sum
tech		fuel	NPPT	rep/sep	fuel	NPPT	rep/sep	
electricity, GWe-yr			89.220%			10.780%		100
feed or product of nuclear materials (metric ton)								
natural resource	NU	-103.615						-103.615
	Th							-
products from fuel or NPPT tech	DU							-
	U	1103.379	-1103.379		0.000	0.000		0
	Pu	133.210	-133.210		63.872	-63.872		0
	MA	12.342	-12.342		6.911	-6.911		0
	DF		1248.931	-1248.931		70.783	-70.783	0
products from rep/sep tech	RU	-1001.767		1001.718	0.000		0.050	0.000
	Pu	-133.475		142.207	-64.000		55.269	0.000
	MA	-9.924		10.087	-6.924		6.761	0.000
	FP			82.452			7.959	90.411
Loss		-0.150	0.000	12.468	0.142	0.000	0.744	13.204

Figure 12. Annotated table of normalized mass flow for the prismatic MgO ZrH concept.

E_i can be calculated using Equation 4, where P_i is Stage i reactor thermal power, η_i is Stage i reactor thermal efficiency, and CP_i is Stage i capacity factor. The capacity factor is assumed to be 0.9 for both stages. The thermal efficiency of the Stage 1 SFR is 40% and the thermal efficiency of the Stage 2 micro-HTGR is 50%.

$$(4)\ E_i = P_i \eta_i CP_i$$

Equation 5 can be used to convert mass flow $M_{x,o}$ in units of kilogram per reactor-year to M_x in units of metric tons per year instead.

$$(5)\ M_x = M_{x,o}\left(\frac{100 f_i}{E_i}\right)$$

Using Equations 1 through 5, normalized mass flow data is calculated for each of the continuous recycle prismatic and pebble-bed IMF concepts and put into a table. The optimized core configurations are used. Values from these tables are used to calculate levelized metrics for the continuous recycle IMF concepts.

2.4 Fuel Cycle Evaluation Metrics

Metrics from the E&S study are used to evaluate the performance of the continuous recycle IMF concepts. These metrics are mass of SNF&HLW disposed, volume of LLW disposed, area of land used, volume of water used, mass of CO_2 produced, and activity of SNF&HLW at 100 and 100,000 years [21]. All metrics are energy normalized per GWe-yr for better comparison between the different reactors and concepts. In addition to being compared to the graphite reference prismatic microreactor, the continuous recycle IMF concepts are compared to the once-through prismatic and pebble-bed IMF concepts, a large-scale LWR, and an SMR.

The mass of SNF&HLW disposed includes heavy metal and fission products produced during irradiation of the initial fuel mass. This metric does not include any structural materials, for example, the prismatic blocks used in the prismatic HTGR designs. The mass of SNF&HLW disposed for the continuous recycle IMF concepts was determined by calculating the mass of FP produced from reprocessing and separation in both stages. The mass of FP is calculated when calculating normalized mass flow for each continuous recycle IMF concept. RU, Pu, and MA are recycled back into the SFR and micro-HTGR and are not sent to disposal. This recycling of a significant majority of the reprocessing and separation products results in a comparatively lower mass of SNF&HLW disposed for the continuous recycle IMF concepts.

The volume of LLW disposed was calculated using values in the normalized mass flow data tables and multiplier constants found in the E&S study [39]. This metric includes Class A through Class C LLW and greater than Class C (GTCC) wastes. Waste produced by operations and Decontamination and Decommissioning (D&D) of facilities at the end of their lifetime are included. Given the fuel cycle that is being evaluated in this work, multiplier constants for reactor operation, reprocessing, and recycled fuel fabrication were identified. The reactor operation constants were for SFR and HTGR operation. The reprocessing constant was for ADS metal blankets. The recycle fuel fabrication constants were for shielded glove boxes that handle uranium and remote processing of Pu/TRU in oxide and metal form. See **Table 4** for the multiplier constants used to calculate the volume of LLW disposed [39].

The environmental impact can be evaluated by calculating the MTNU used, area of land used, volume of water used, and mass of CO_2 produced. The MTNU used in the continuous recycle IMF concepts was determined by calculating how much NU goes into making fuel for both stages. This mass of NU is calculated when calculating normalized mass flow for each continuous recycle IMF concept. Reprocessed uranium (RU) is recycled back into Stage 1, which significantly reduces how much MTNU is required for the continuous recycle IMF concepts. Additionally, the Stage 2 micro-HTGR does not use any uranium in its fuel.

The metrics for area of land used, volume of water used, and mass of CO_2 produced are calculated using multiplier constants and re-normalizing parameters. These multiplier constants, which are found in the E&S study, and the re-normalizing parameters are shown in **Table 5** [39]. Multiplier constants are grouped into four categories for the fuel cycle: front end of the fuel cycle, fuel fabrication, reactor, and disposal and transport. The front end of the fuel cycle category includes mining and milling, conversion, enrichment, and deconversion. The fuel fabrication category includes the fabrication of uranium oxide (UOX) and MOX fuel. The reactor category includes reactor construction, reactor operation, and reprocessing and waste conditioning. The disposal and transport category includes shallow land burial, geological repository, interim storage, and waste packages and drip shields. The re-normalizing parameters are necessary for normalizing values to energy generated per year. These re-normalizing parameters include values found when performing normalized mass flow calculations, including MTNU required and the mass of SNF&HLW disposed. The reactor construction and reactor operation multiplier constants do not have an associated re-normalizing parameter.

Table 4. LLW multipliers along with re-normalization parameters most applicable to the evaluated continuous recycle fuel cycle. Reproduced from the E&S study [39].

Category	Volume of LLW (m^3/-)	Parameter Associated with LLW
Reactor Operation		
SFR (-/GWe-year)	278.6	f_1 (GWe-year)
HTGR (-/GWe-year)	278.6	f_2 (GWe-year)
Reprocessing		
ADS Metal Blanket (-/MTHM)	16.025	M_{flow} (MTHM/GWe-year)
Recycle Fuel Fabrication		
Shielded Glovebox – U - metal (-/MTHM)	1.75	M_{RU} (MTRU/GWe-year)
Remote – Pu/TRU – oxide (-/MTHM)	3.3	$M_{TRU,2}$ (MTHM/GWe-year)
Remote – Pu/TRU – metal (-/MTHM)	2.475	$M_{TRU,1}$ (MTHM/GWe-year)

Table 5. Land, Water, and CO_2 multipliers along with re-normalization parameters. Reproduced from the E&S study [39].

Portion of Nuclear Fuel Cycle	Land Use Multiplier (km^2/-)	Water Use Multiplier (ML/-)	CO_2 Multiplier (kg/-)	Radiologic Exposure Multiplier (Person-mSv/-)	Re-normalizing parameter
Front End of Fuel Cycle					
Mining/Milling-Uranium (-/MTNU)	2.8E0-4	8.5E-1	8.3E4	14.2E-1	$M_{natural}$ (MTNU/GWe-yr)
Conversion-Uranium (-/MTNU)	3.3E-9	6.5E-2	2.2E4	8.8E-1	$M_{natural}$ (MTNU/GWe-yr)
Enrichment-Uranium (-/SWU)	9E-9	2.9E-5	2.8E1	3.1E-2	SWU (SWU/GWe-year)
Deconversion-Uranium (-/MTDU)	9.3E-5	5.3E-4	-3.2E3	2.9E-5	M_{DU} (MTDU/GWe-year)
Fuel Fabrication					
UOX (-/MTIHM)	1.02E-4	1.41E-1	2.85E5	1.43	M_{flow} (MTIHM/GWe-yr)
MOX (-/MTINH)	1.02E-4	5.21E-1	4.45E5	1.17	M_{flow} (MTIHM/GWe-yr)

Table 5. Continued.

Portion of Nuclear Fuel Cycle	Land Use Multiplier (km^2/-)	Water Use Multiplier (ML/-)	CO_2 Multiplier (kg/-)	Radiologic Exposure Multiplier (Person-mSv/-)	Re-normalizing parameter
Reactor					
Reactor Construction (-/GWe-yr)	--	--	1.16E7	--	
Reactor Operation (-/GWe-yr)	7.27E-2	2.37E4	--	7.3E2	
Reprocessing and waste conditioning (-/MTIHM)	4.41E-5	4.83E-1	5.15E5	3.8E-1	$M_{SNF\&HLW}$ (MTIHM/GWe-yr)
Disposal and Transport					
Shallow Land Burial (-/MT waste)	9.74E-6	2.3E-4	1.82	1.32E-1	$M_{DU+RU+RTh}$ (DU+RU+RTh/GWe-yr)
Geologic Repository (-/MTIHM)	1.5E-3	1.43E-1	8.81E4	1.32	$M_{SNF\&HLW}$ (MTIHM/GWe-yr)
Interim Storage (-/MTIHM)	3.0E-5	--	3.11E4	1.16	$M_{SNF\&HLW}$ (MTIHM/GWe-yr)
Waste Packages and Drip Shields (-/MTIHM)	--	--	5.75E4	--	$M_{SNF\&HLW}$ (MTIHM/GWe-yr)

The metrics for the activity of SNF&HLW at 100 and 100,000 years after reactor operation were calculated using Equation 6. The activity *A(t)* and initial fissile mass $M_{fissile}$ were determined using Serpent. Mass flow M_{flow} was calculated using Equation 2. 100 years was chosen to evaluate hazards during handling and storage of SNF&HLW and 100,000 years was chosen to evaluate long-term hazards from disposal of SNF&HLW.

$$(6)\ A_{SNF+HLW}(t) = \frac{A(t)}{M_{fissile}} * M_{flow}$$

Chapter 3 Results

3.1 Prismatic Design Optimization

Using the previously discussed optimization methods, optimal core configurations were identified for each prismatic and pebble-bed IMF concept. The prismatic optimization sweep results across the fueled radius and TRISO packing fraction are shown in **Figure 13** through **Figure 16**.

Figure 13 and **Figure 14** are contour plots of the optimization sweeps performed for the prismatic MgO Be and MgO BeO concepts respectively. In both concepts, discharge burnup increases as the TRISO packing fraction is increased, however, it decreases as lattice pitch increases. The optimal configuration for the prismatic MgO Be and MgO BeO concepts is a lattice pitch of 2.0 cm and a TRISO packing fraction of 50%. This indicates that the Be-based moderator concepts perform better using a higher fuel-to-moderator ratio. The MgO BeO concept achieved a slightly higher peak discharge burnup of 88.484 GWd/MTHM compared to the MgO Be concept which achieved a peak discharge burnup of 86.481 GWd/MTHM.

Figure 15 and **Figure 16** are contour plots of the optimization sweeps performed for the prismatic MgO $YH_{x=1.9}$ and MgO $ZrH_{x=1.6}$ concepts respectively. In the MgO $YH_{x=1.9}$ concept, the discharge burnup is at its highest when the lattice pitch is 2.0 cm or 2.5 cm. At a lattice pitch of 2.0 cm, discharge burnup is highest at a TRISO packing fraction of 50%. At a lattice pitch of 2.5 cm, discharge burnup is highest at a TRISO packing fraction of 10%. Between these two configurations, the optimal configuration for the MgO $YH_{x=1.9}$ concept was found to be a lattice pitch of 2.5 and a TRISO packing fraction of 10%. A somewhat similar trend is observed in the MgO $ZrH_{x=1.6}$ concept, but the discharge burnup is significantly higher when using low TRISO packing fractions. The optimal configuration for the MgO $ZrH_{x=1.6}$ concept is a lattice pitch of 2.2 cm and a TRISO packing fraction of 5%. This indicates that the hydride-based moderator concepts perform better using a lower fuel-to-moderator ratio. The MgO $ZrH_{x=1.6}$ concept achieved a significantly higher peak discharge burnup of 111.253 GWd/MTHM, compared to the MgO $YH_{x=1.9}$ concept which achieved a peak discharge burnup of 52.105 GWd/MTHM.

The optimal core configurations and resulting discharge burnup for each prismatic IMF concept are shown in **Table 6**. The MgO $ZrH_{x=1.6}$ achieves the highest discharge burnup out of the four evaluated concepts.

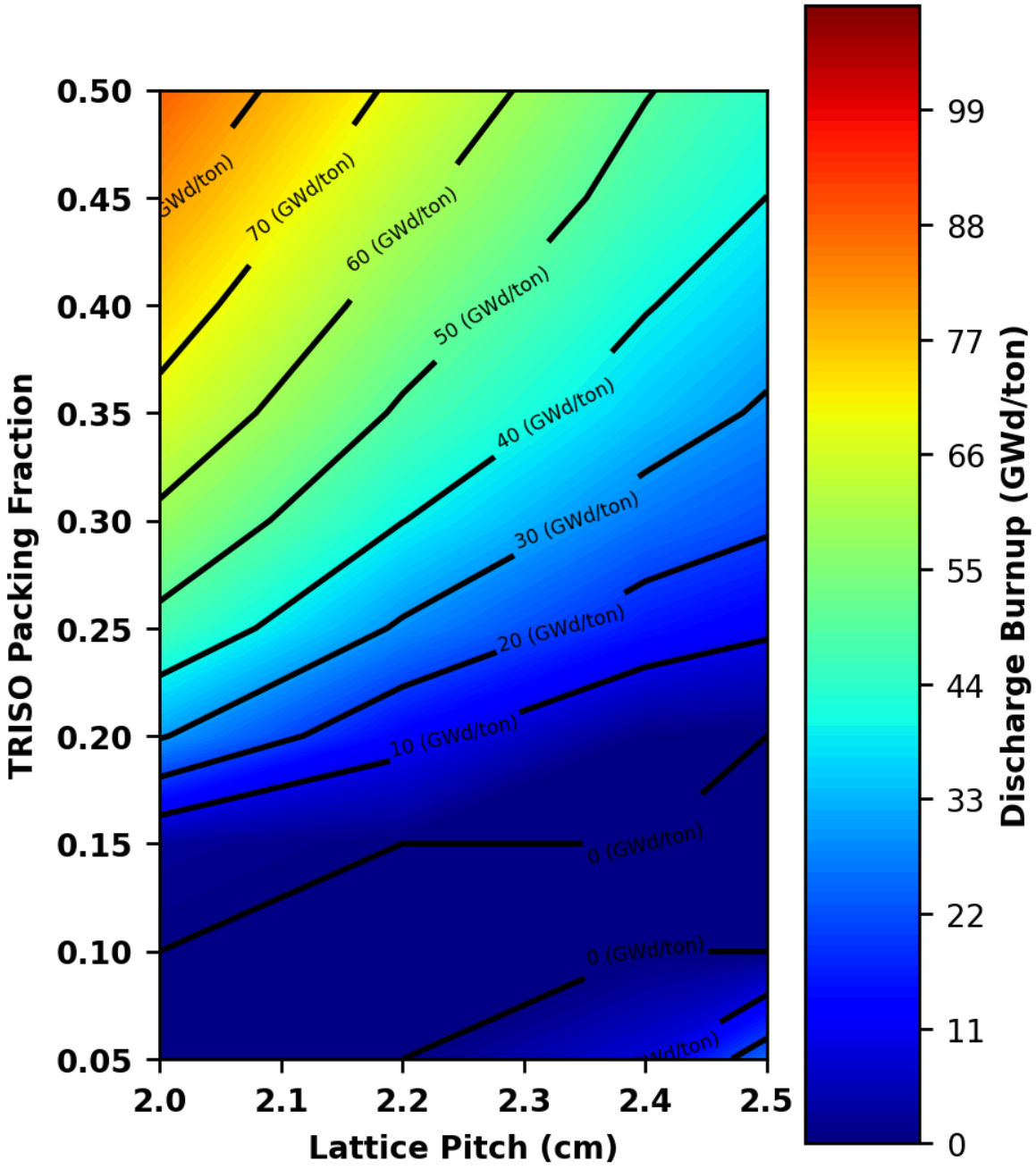

Figure 13. Contour plot of discharge burnup as a function of lattice pitch and TRISO packing fraction for the prismatic MgO Be concept.

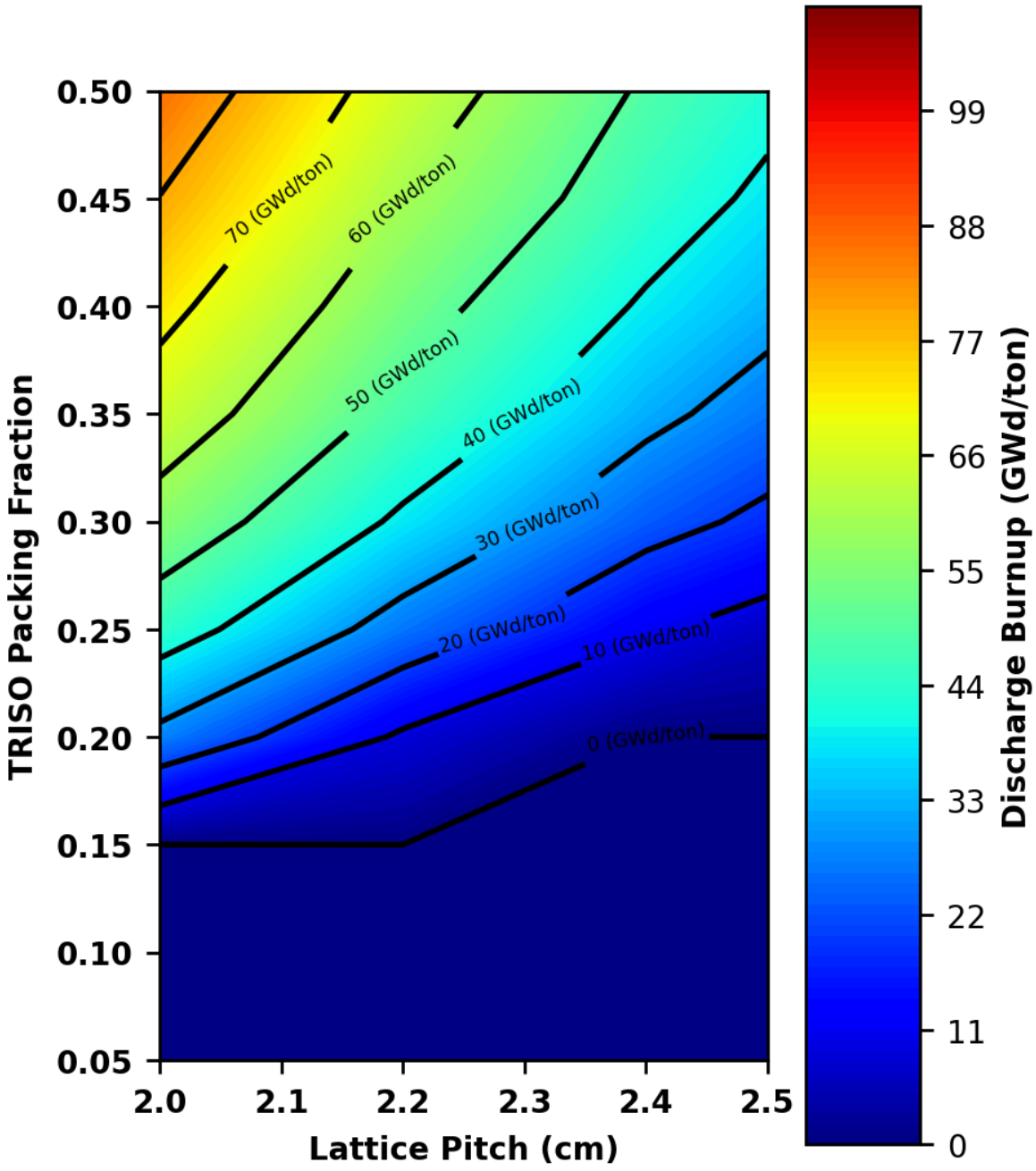

Figure 14. Contour plot of discharge burnup as a function of lattice pitch and TRISO packing fraction for the prismatic MgO BeO concept.

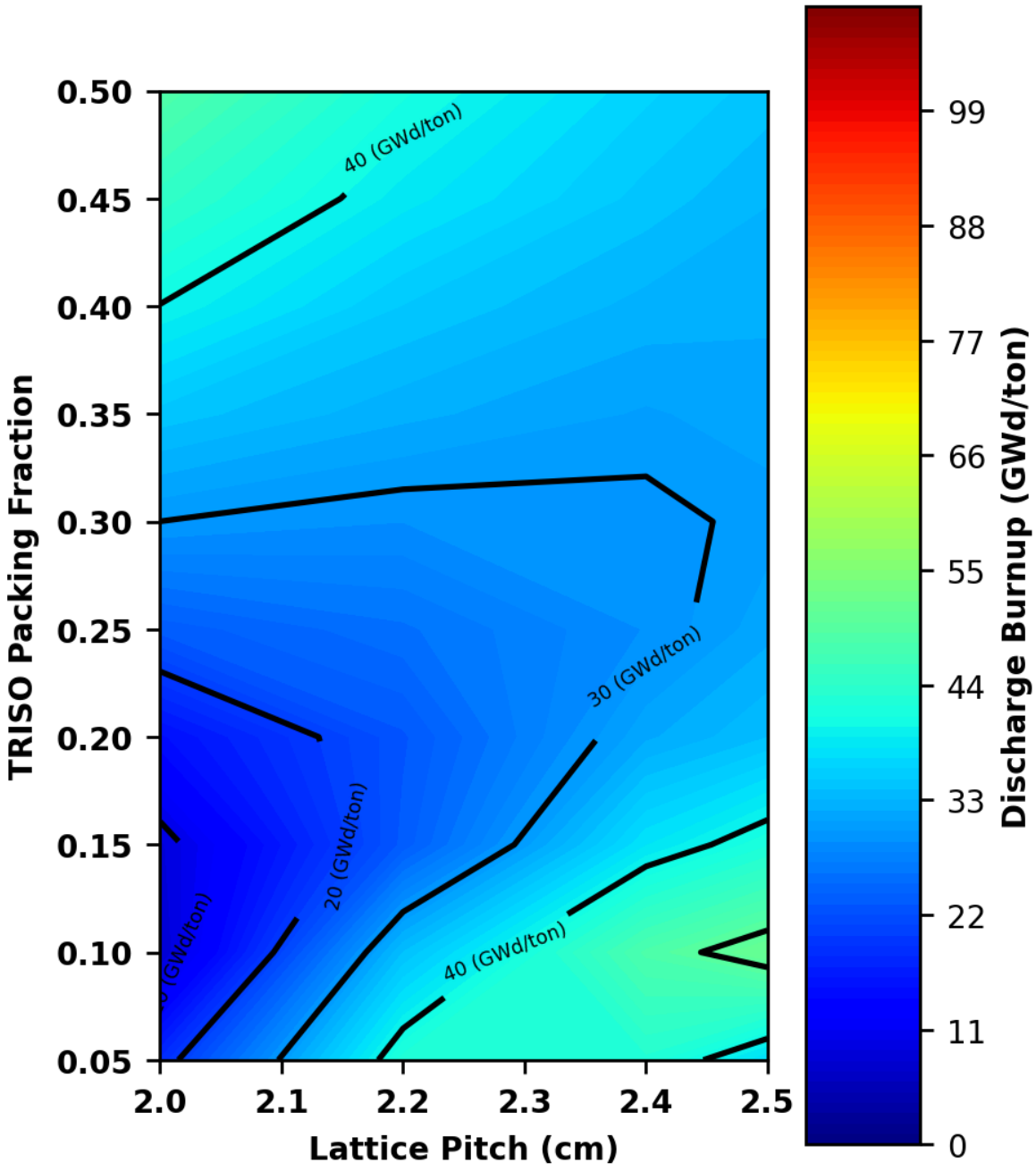

Figure 15. Contour plot of discharge burnup as a function of lattice pitch and TRISO packing fraction for the prismatic MgO $YH_{x=1.9}$ concept.

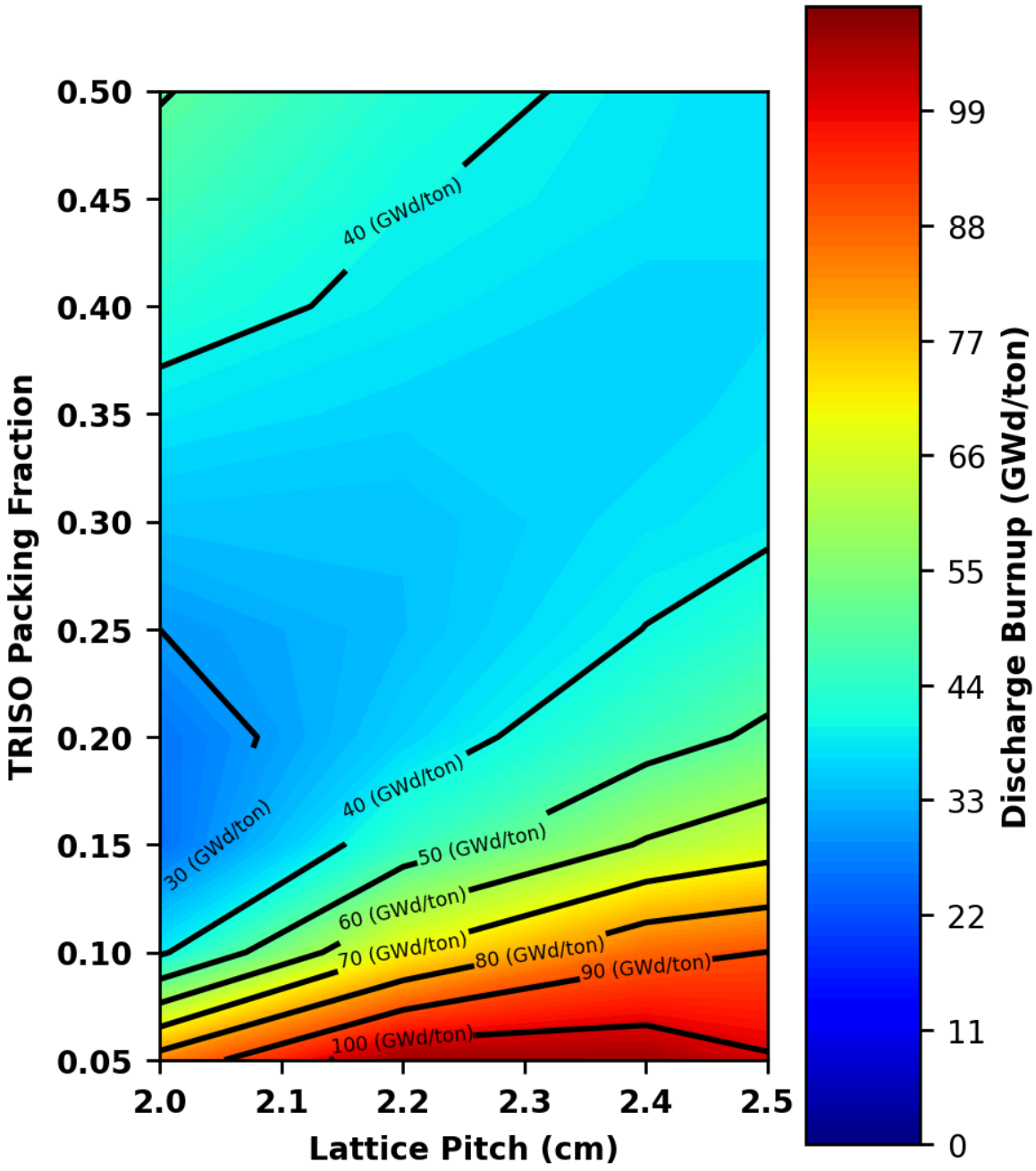

Figure 16. Contour plot of discharge burnup as a function of lattice pitch and TRISO packing fraction for the prismatic MgO $ZrH_{x=1.6}$ concept.

Table 6. Optimal prismatic core configurations for fuel discharge burnup.

Fuel Concept	TRISO packing fraction	Fuel pin lattice pitch (cm)	Discharge Burnup (GWd/MTHM)
MgO BeO	0.5	2.0	88.484
MgO Be	0.5	2.0	86.481
MgO $YH_{x=1.9}$	0.1	2.5	52.105
MgO $ZrH_{x=1.6}$	0.05	2.2	111.253

3.2 Pebble-bed Design Optimization

Unlike the prismatic designs where only two parameters are varied in the optimization sweeps, four parameters are varied in the pebble-bed optimization sweeps. Two optimization sweeps were performed for each pebble-bed design with one optimization sweep varying optimization sweep varying TRISO packing fraction and pebble fueled radius and the other optimization sweep varying the ratio of fueled to unfueled pebbles and active reactor core radius. In the optimization sweeps varying ratio of fueled to unfueled pebbles and active reactor core radius, the TRISO packing fraction was set to 55% and the pebble fueled radius was set to 3 cm. In the optimization sweeps varying TRISO packing fraction and pebble fueled radius, the ratio of fueled to unfueled pebbles was set to 1.0 and the active reactor core radius was set to 30 cm. Something observed in the optimization sweeps regardless of what parameters are being varied is that the fuel in-core residence increases as the quantity of fuel in the reactor core increases. Increasing any one of the pebble-bed parameters increases how much fuel there is.

Figure 17 through **Figure 20** are contour plots of the optimization sweeps varying TRISO packing fraction and pebble fueled radius performed for the pebble-bed MgO Be, MgO BeO, MgO $YH_{x=1.9}$, and MgO $ZrH_{x=1.6}$ concepts respectively. Regions in black are where the configuration failed to reach criticality. As seen in all four of these contour plots, discharge burnup increases as both the TRISO packing fraction and pebble fueled radius increase. This indicates that all four pebble-bed IMF concepts achieve a higher discharge burnup with more fuel per pebble. A 55% TRISO packing fraction and 3 cm fueled pebble radius result in the highest discharge burnup for all four pebble-bed designs, with the MgO BeO design achieving the highest discharge burnup out of the four designs.

Figure 21 through **Figure 24** are contour plots of the optimization sweeps varying the ratio of fueled to unfueled pebbles and active reactor core radius performed for the pebble-bed MgO Be, MgO BeO, MgO $YH_{x=1.9}$, and MgO $ZrH_{x=1.6}$ concepts respectively. Once again, regions in black are where the configuration failed to reach criticality. As seen in all four of these contour plots, discharge burnup increases as the ratio of fueled to unfueled pebbles increases. This is not the case for the core radius, where discharge burnup is highest when the core radius is either 60 or 70 cm. A fueled to unfueled ratio of 1.0 for all four concepts and active core radius of 60 cm for MgO BeO and MgO $ZrH_{x=1.6}$ and active core radius of 70 cm for MgO Be and MgO $YH_{x=1.9}$ achieved the highest discharge burnups, with MgO BeO achieving the highest burnup.

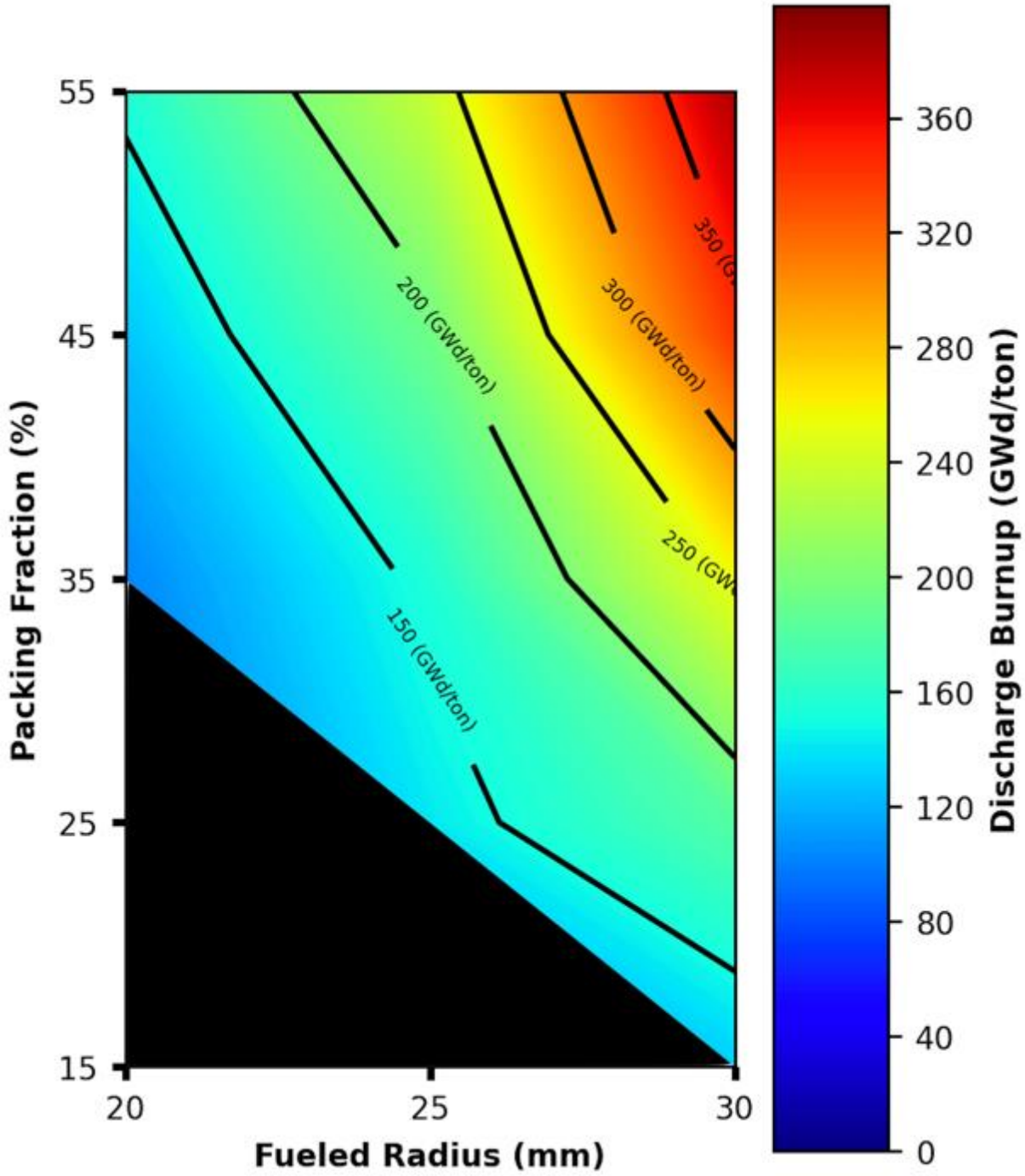

Figure 17. Contour plot of discharge burnup as a function of fueled radius and TRISO packing fraction for the pebble-bed MgO Be concept.

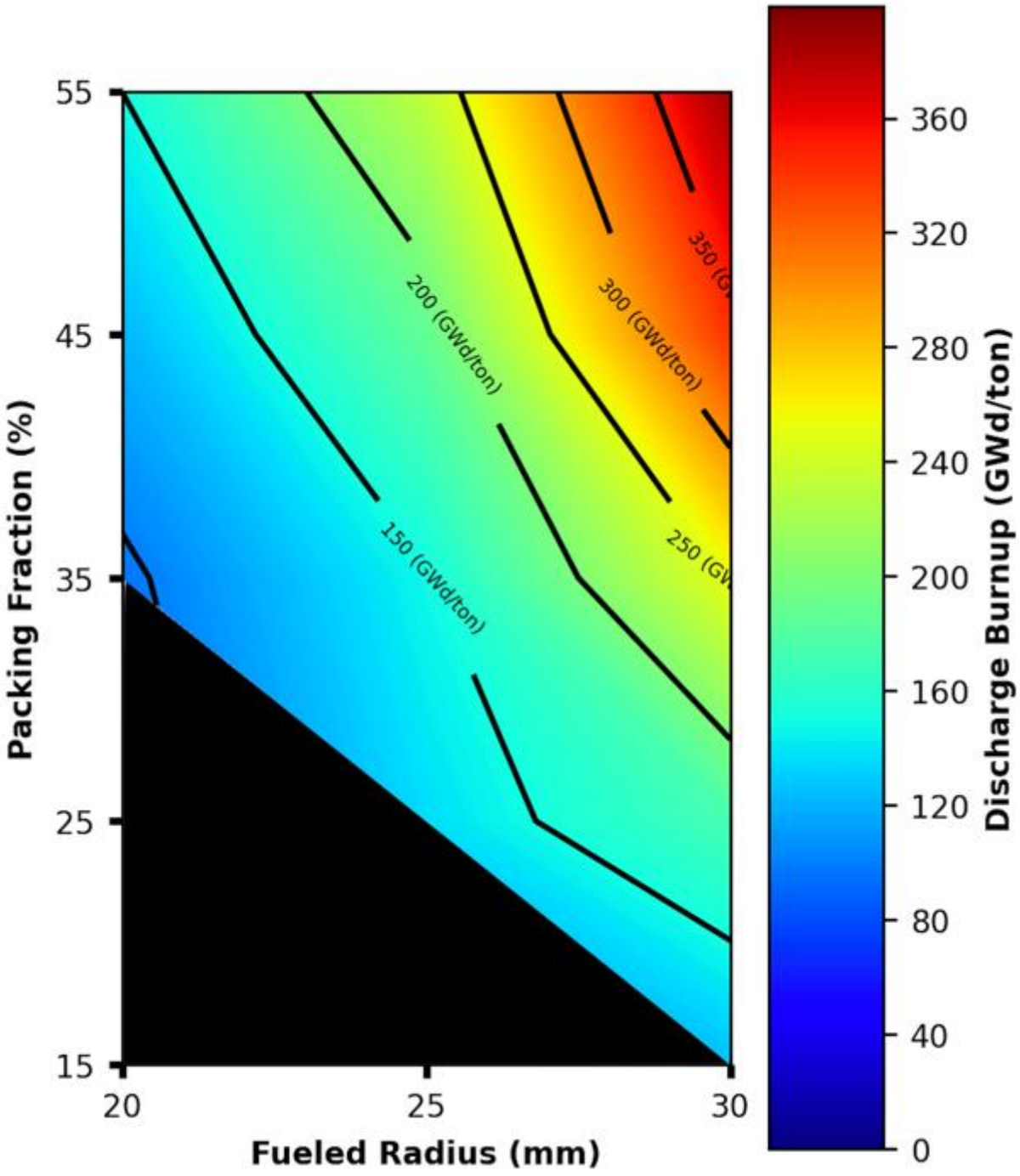

Figure 18. Contour plot of discharge burnup as a function of fueled radius and TRISO packing fraction for the pebble-bed MgO BeO concept.

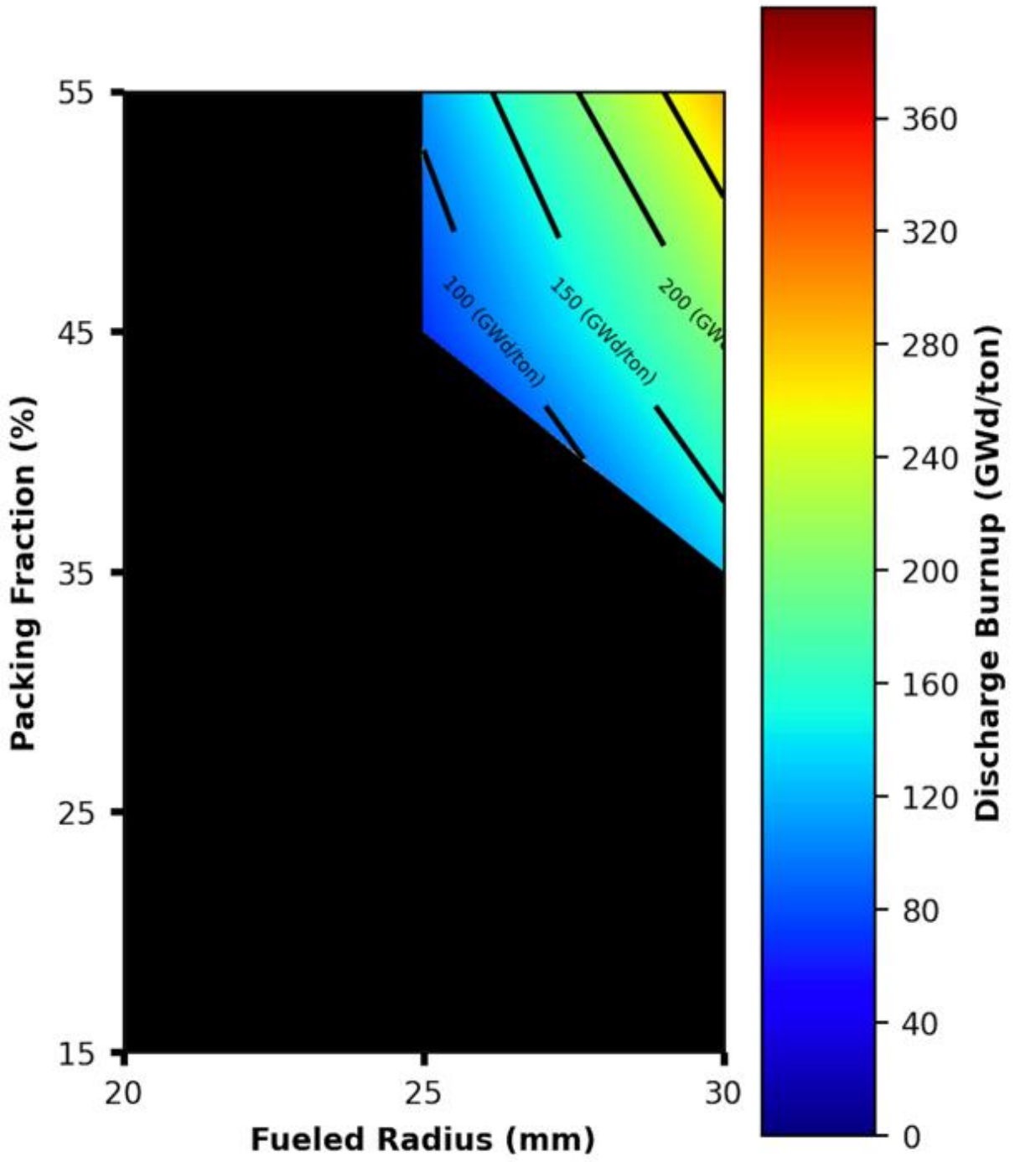

Figure 19. Contour plot of discharge burnup as a function of fueled radius and TRISO packing fraction for the pebble-bed MgO $YH_{x=1.9}$ concept.

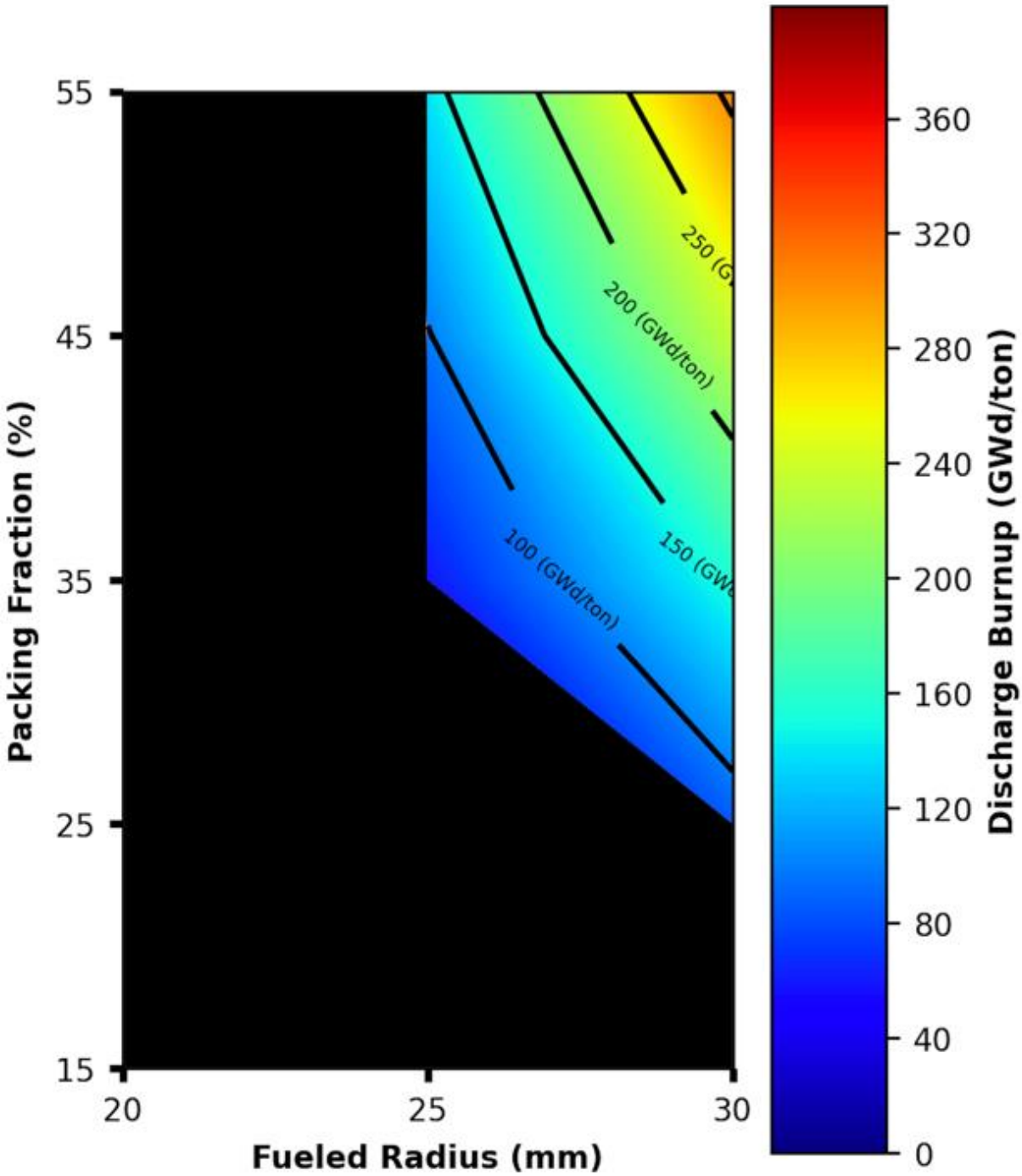

Figure 20. Contour plot of discharge burnup as a function of fueled radius and TRISO packing fraction for the pebble-bed MgO $ZrH_{x=1.6}$ concept.

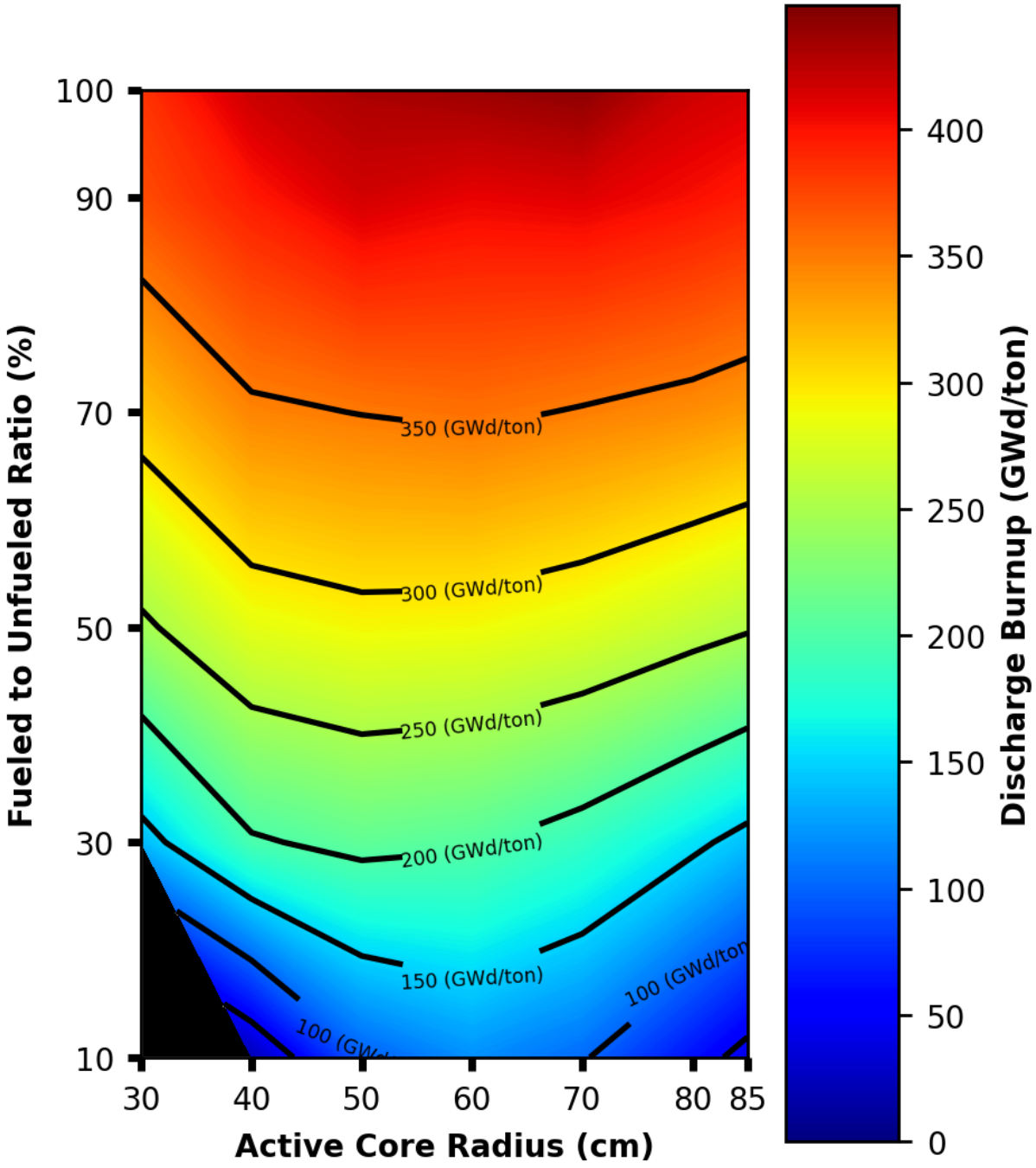

Figure 21. Contour plot of discharge burnup as a function of fueled to unfueled pebble ratio and active core radius for the pebble-bed MgO Be concept.

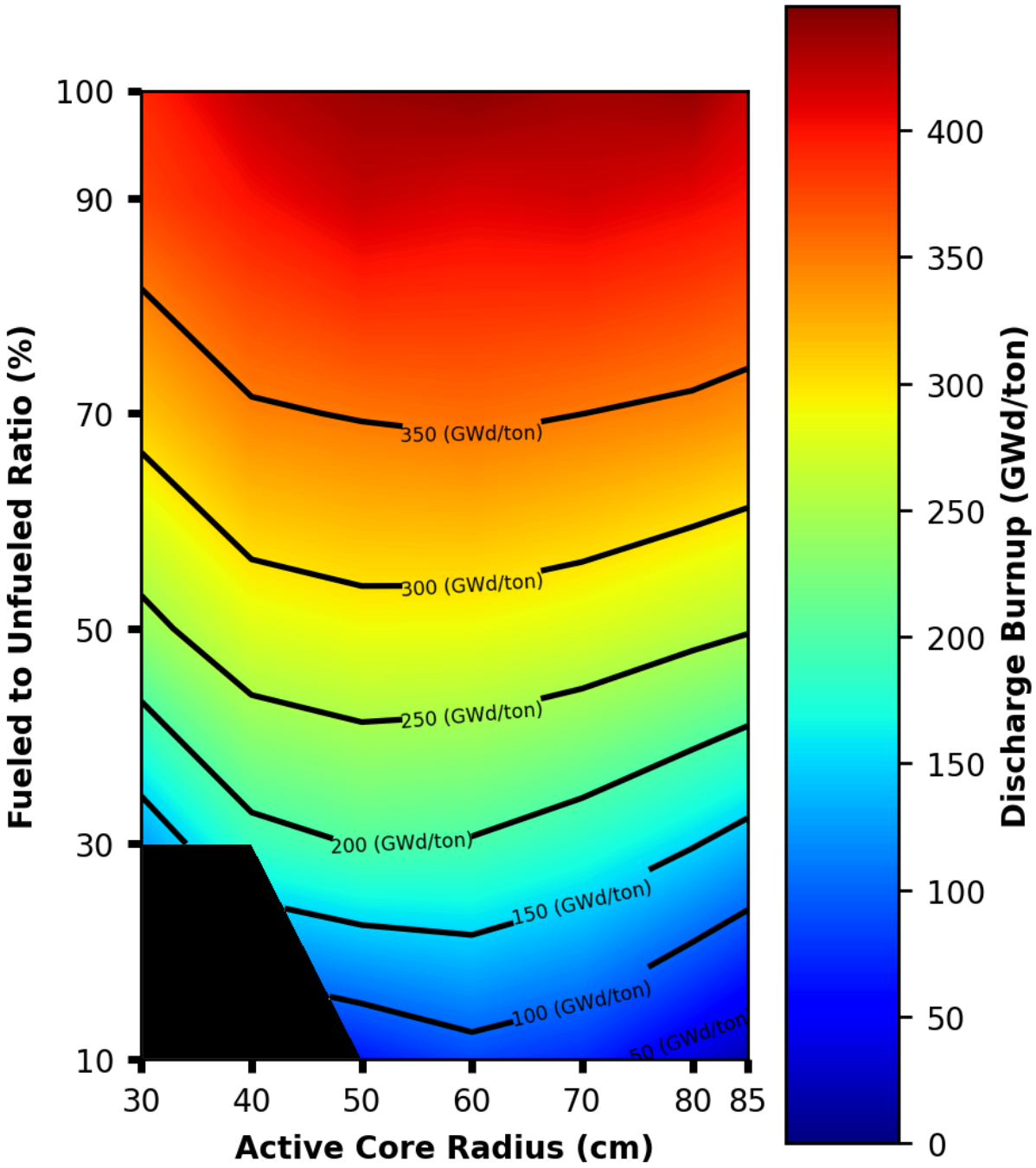

Figure 22. Contour plot of discharge burnup as a function of fueled to unfueled pebble ratio and active core radius for the pebble-bed MgO BeO concept.

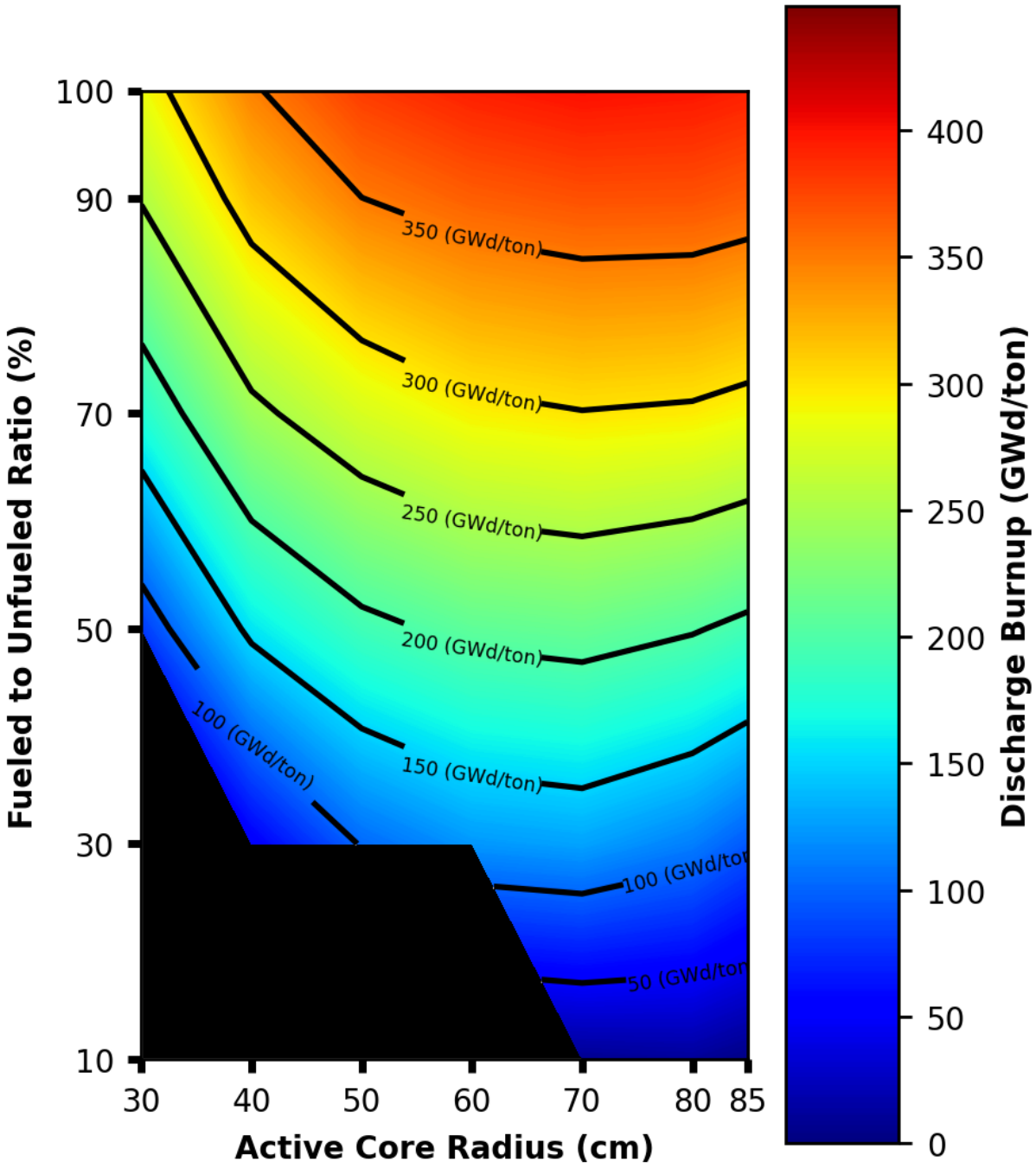

Figure 23. Contour plot of discharge burnup as a function of fueled to unfueled pebble ratio and active core radius for the pebble-bed MgO YH concept.

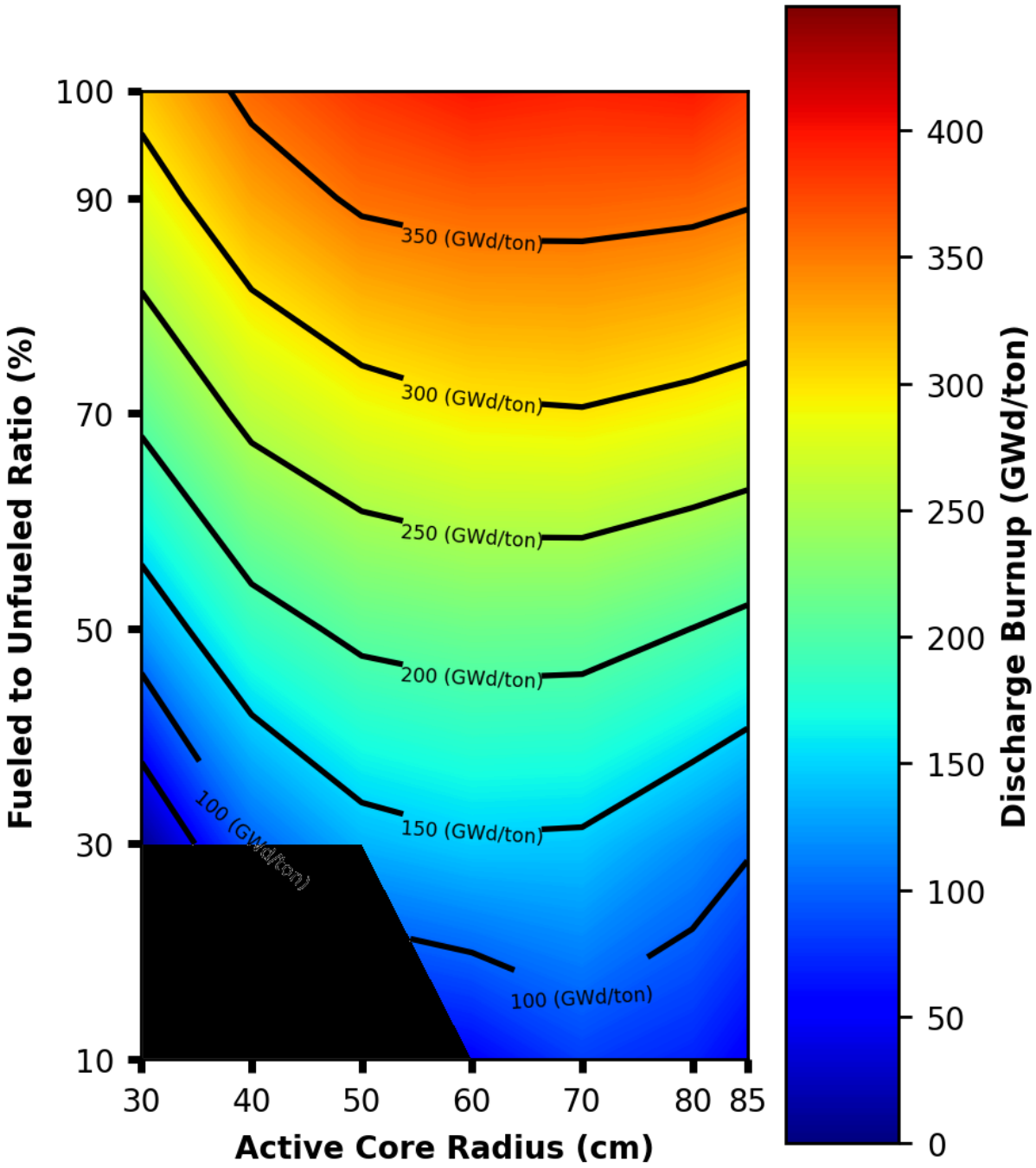

Figure 24. Contour plot of discharge burnup as a function of fueled to unfueled pebble ratio and active core radius for the pebble-bed MgO ZrH concept.

The optimal configuration used for all four pebble-bed IMF concepts uses a ratio of fueled to unfueled pebbles of 1.0, a fueled radius of 3 cm, a TRISO packing fraction of 55%, and an active core radius of 30 cm. Although a larger active core radius results in a higher discharge burnup, it also results in a significantly longer fuel in-core residence time. The fuel in-core residence time of the optimal pebble-bed designs is already long. The shortest in-core residence time in the pebble-bed designs is nearly 70 years for the MgO $YH_{x=1.9}$ concept. Compared to the longest in-core residence time in the prismatic designs, which is roughly 32 years for the MgO BeO concept, there is a significant difference in in-core residence time between the prismatic and pebble-bed designs.

The optimal core configuration used and resulting discharge burnup for each pebble-bed IMF concept are shown in

Table *7*. All four pebble-bed IMF concepts used the same optimal configuration, where a higher ratio of fuel to moderator produces a higher discharge burnup. Unlike the prismatic IMF concepts where the MgO $ZrH_{x=1.9}$ concept achieved the highest discharge burnup, the MgO BeO concept achieved the highest discharge burnup amongst the pebble-bed IMF concepts, which was 415.32 GWd/MTHM. The MgO Be, MgO $YH_{x=1.9}$ and MgO $ZrH_{x=1.6}$ concepts achieved peak discharge burnups of 411.55, 287.47, and 314.08 GWd/MTHM respectively. Shown in **Table 8** are the core configurations that produce the highest possible discharge burnup for each pebble-bed IMF concept. Like the optimal core configurations used, these configurations use a ratio of fueled to unfueled pebbles of 1.0, a fueled radius of 3.0 cm, and TRISO packing fraction of 55%. The only difference is the core radius used, where it is 60 cm for the MgO BeO and MgO $ZrH_{x=1.6}$ concepts and 70 cm for the MgO Be and MgO $YH_{x=1.9}$ concepts compared to 30 cm used in the optimal core configurations. These core configurations achieve higher discharge burnups, with the MgO BeO design using a core radius of 60 cm achieving a 473.61 GWd/MTHM burnup at 166034 days compared to the design using a core radius of 30 cm achieving a 415.32 GWd/MTHM burnup at 36479 days. Seeing as the burnup increases by about 14% at an in-core residence that is about 4.55 times larger, a core configuration with a smaller active core radius was used. The fuel in-core residence time of the optimal pebble-bed designs used is already significantly longer than the in-core residence times of the optimal prismatic designs. While the burnups in the pebble-bed designs may seem incredibly high, previous

experiments have looked at HTGR TRISO fuel achieving high discharge burnups in a similar range [48] [49] [50] [51].

Table 7. Optimal pebble-bed core configurations for fuel discharge burnup that are used.

Fuel Concept	Ratio of fueled to unfueled pebbles	Fueled radius (cm)	TRISO packing fraction	Core radius (cm)	Discharge Burnup (GWd/MTHM)
MgO BeO	1.0	3.0	0.55	30	415.32
MgO Be	1.0	3.0	0.55	30	411.55
MgO $YH_{x=1.9}$	1.0	3.0	0.55	30	287.47
MgO $ZrH_{x=1.6}$	1.0	3.0	0.55	30	314.08

Table 8. Pebble-bed core configurations that achieve the highest discharge burnups.

Fuel Concept	Ratio of fueled to unfueled pebbles	Fueled radius (cm)	TRISO packing fraction	Core radius (cm)	Discharge Burnup (GWd/MTHM)
MgO BeO	1.0	3.0	0.55	60	473.61
MgO Be	1.0	3.0	0.55	70	462.77
MgO $YH_{x=1.9}$	1.0	3.0	0.55	70	422.52
MgO $ZrH_{x=1.6}$	1.0	3.0	0.55	60	415.72

High fuel discharge burnups have been achieved in fuel test elements (FTEs) used in the Fort Saint Vrain reactor in 1976 [49]. Eight FTEs were tested in the reactor core to analyze the effect of test elements on plant operation and safety. All FTEs used TRISO fuel and three of the eight FTEs used BISO in addition to TRISO fuel. Six of the FTEs used UCO TRISO fuel and the remaining two FTEs used (Th, U)C_2 TRISO fuel [49]. Shown in **Table 9** are peak irradiation test temperatures and what burnups the FTEs reached. The test element fuel materials previously underwent full irradiation exposure in test capsules. Testing was performed by General Atomic (GA). The P13 and HRB capsules were tested between 1974 and 1975 and reached high discharge burnups [49]. The HRB capsules used weak-acid resin (WAR) in the fuel fabrication process [49]. Successful performance in the P13 capsules was determined according to whether or not there was less than 1% failure in the outer PyC layer. In the HRB capsules, there needed to be less than 1% failure in all coatings. One source of failure was kernel migration, which could occur depending on fuel temperature. Shown in **Table 10** and **Table 11** are the peak irradiation test temperatures and what burnups the P13 and HRB capsules achieved respectively.

The locations of the TRISO particles used in the Serpent models for both the prismatic and pebble-bed microreactor designs were created using a particle disperser routine in Serpent. This particle disperser routine generates a particle distribution file where particles are randomly distributed in a specified volume. The particle radius, number of particles, and dimensions of the specified volume are used in creating the file. The optimization sweeps for the prismatic and pebble-bed designs varied TRISO packing fraction from 5% to 50% in compacts and from 5% to 55% in pebbles. The packing fraction in two of the optimal prismatic designs, MgO Be and MgO BeO, is 50%. The packing fraction in all four optimal pebble-bed designs is 55%. Given how high these packing fractions are, it is important to discuss the maximum limit on TRISO packing fraction that can be achieved that is feasible and does not compromise the integrity of the TRISO layers.

Table 9. Fuel test element performance in the Fort Saint Vrain reactor [49].

Test Element #	Fuel Temperature (°C)	Burnup (% FIMA)
FTE-3	848	44
FTE-4	893	46
FTE-5	967	55
FTE-6	1036	71

Table 10. GA irradiation tests of UC_2 TRISO fuel [49].

Capsule	# of TRISO Samples	Fuel Temperature (°C)	Burnup (% FIMA)	# of Successful Samples
P13L	15	1400	75	4
P13M	10	1350	70	9
P13N	15	1350	68	10
P13P	20	1350	70	17
P13R	9	1075	75	3
P13S	9	1075	75	5

Table 11. GA irradiation tests of WAR TRISO fuel [49].

Capsule	# of TRISO Samples	Fuel Temperature (°C)	Burnup (% FIMA)	# of Successful Samples
HRB-7	4	1500	80	3
HRB-8	4	1250	80	3
HRB-9	17	1250	80	8
HRB-10	17	1500	80	5

The theoretical maximum packing fraction of uniform spheres packed in an orthorhombic arrangement is 62.5% [52]. According to a fuel fraction packing model, one dimensional compression can limit packing fraction to 48% and die wall constraining effects can further reduce this to 40% [53]. The model is somewhat conservative as it assumes particles cannot pass by one another by 1.5 times the diameter of an overcoated particle during compacting and that there is no horizontal movement [53]. High TRISO packing fractions decrease distance between TRISO particle, which increases the probability of particle-particle interactions. This is known as rupture and can damage TRISO particle layers [55]. Sintering can result in reduced distance between particles and re-arrangement of the particles, which can also lead to increased rupture probability. This is something that needs to be taken into consideration during the fuel fabrication process. Zero-rupture TRISO fuel can be fabricated by stacking layers of TRISO particles and consolidating them by sintering. Discs containing indents for TRISO particles known as green bodies are used [56]. The green body disks are stacked in a graphite die to form a cylindrical green-body pellet which will be plasma sintered. Experimental work showed that packing fractions up to 34% could be achieved after sintering without observing particle-particle contact in optical microscopy or X-ray Computed Tomography (XCT) [55]. The packing fraction could be increased by decreasing distance between planes, enabling the addition of more disks. Packing fractions of up to 43.3% were achieved by using smaller coating for the TRISO particles and hot pressing [57]. These packing fractions achieved through plasma sintering and hot pressing are in a SiC matrix and not a MgO-composite matrix that is evaluated in this work.

3.3 Neutronic Analysis

Evaluating the neutron spectra for each of the continuous prismatic and pebble-bed designs can explain why some designs can achieve higher discharge burnups compared to others. Shown in **Figure 25** through **Figure 30** is the normalized neutron flux per unit lethargy as a function of neutron energy at the beginning of cycle (BOC) or end of the cycle (EOC). The normalized flux per unit lethargy is the fraction of neutrons at a given energy. Shown in **Figure 25** and **Figure 26** are the neutron spectra of the continuous recycle prismatic cases compared to the graphite reference case at BOC and EOC respectively. Shown in **Figure 27** and **Figure 28** are the neutron spectra of the continuous recycle pebble-bed cases compared to the graphite reference case at BOC and EOC respectively. Shown in **Figure 29** and **Figure 30** are the neutron spectra of the continuous recycle prismatic MgO $ZrH_{x=1.6}$ case and pebble-bed MgO BeO case compared to the graphite reference. The MgO $ZrH_{x=1.6}$ and MgO BeO cases were chosen for comparison because they produce the highest discharge burnup out of all the prismatic and pebble-bed cases respectively.

When comparing the neutron flux in the continuous recycle prismatic cases to the graphite reference, the graphite reference has a larger thermal peak at BOC and EOC. The continuous recycle prismatic cases have larger fast peaks compared to the graphite reference at BOC and EOC. Valleys can be seen past 10 keV due to high energy neutron interactions with the moderating material. When comparing the continuous recycle prismatic cases to each other, the Be-based moderator cases have similar neutron flux spectra and hydride-based moderator cases have similar neutron flux spectra. The MgO $ZrH_{x=1.6}$ case has the largest thermal peak out of the four continuous recycle prismatic cases. The thermal peak in the MgO $ZrH_{x=1.6}$ case is larger at EOC relative to BOC and is accompanied by a reduction in the fast peak. This change from BOC to EOC in the thermal and fast peaks is also seen in the MgO Be, MgO BeO, and MgO $YH_{x=1.9}$ cases. At energies between 1 eV and 10 keV, the hydride-based moderator cases have similar neutron fluxes compared to the graphite reference. The Be-based moderator cases see a more pronounced slope in this energy range, with a greater fraction of neutrons being higher energy. The higher discharge burnup achieved by the MgO $ZrH_{x=1.6}$ case can be attributed to a larger fraction of thermal neutrons relative to the other three continuous recycle prismatic cases, which results in a higher probability for thermal fission events to occur within the fuel.

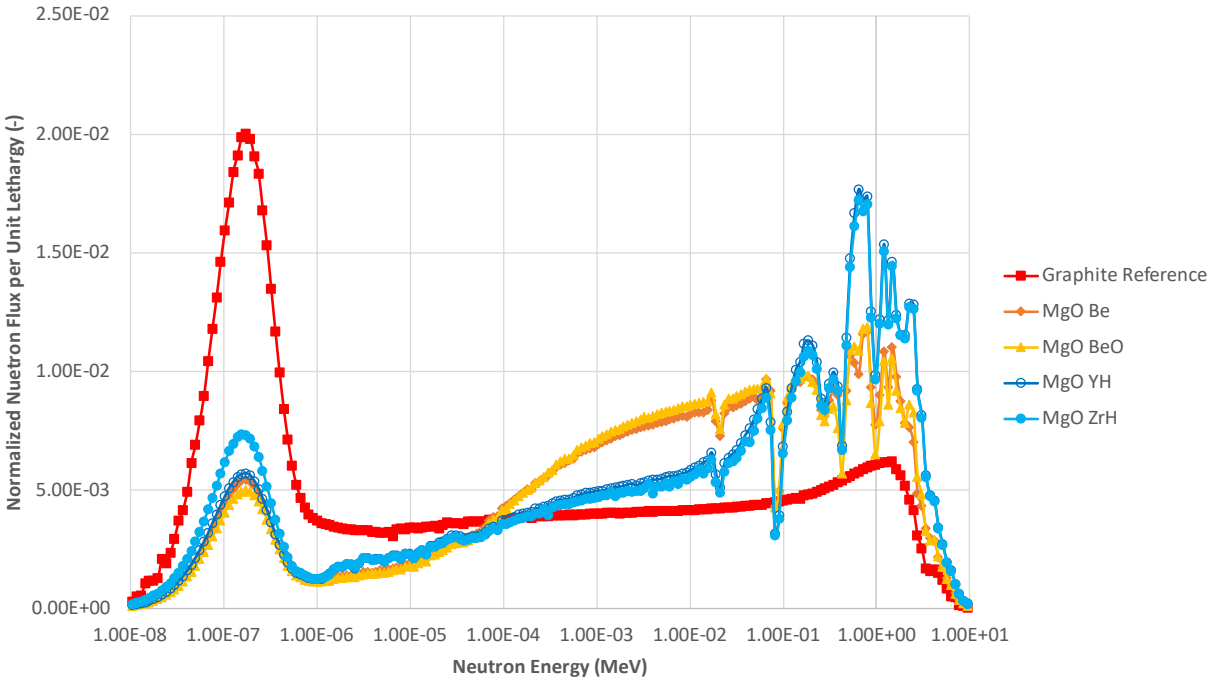

Figure 25. Normalized neutron flux per unit lethargy spectra at BOC for graphite reference case and continuous recycle prismatic cases.

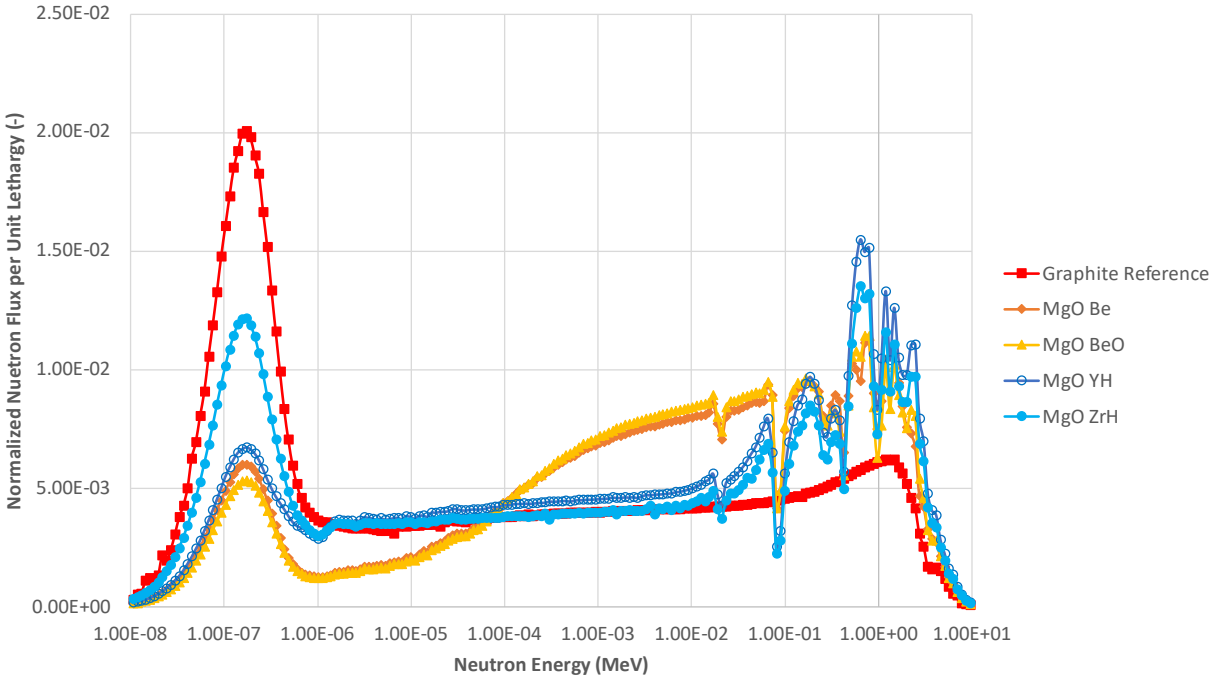

Figure 26. Normalized neutron flux per unit lethargy at EOC for graphite reference case and continuous recycle prismatic cases.

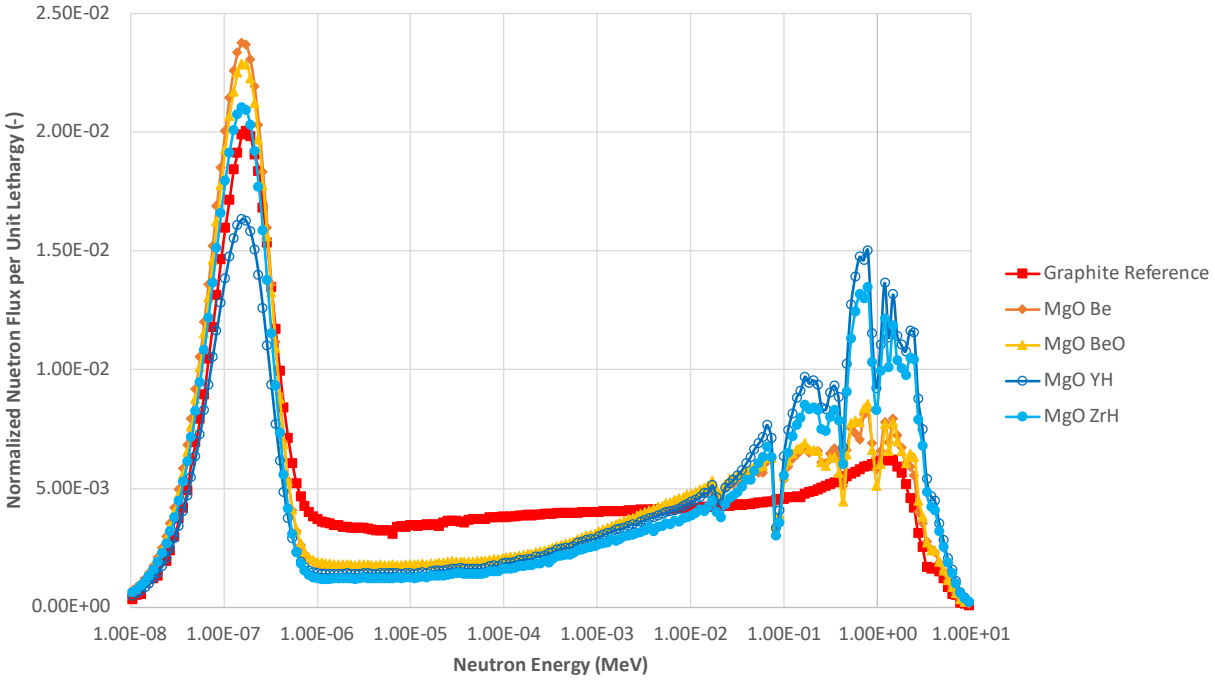

Figure 27. Normalized neutron flux per unit lethargy at BOC for graphite reference case and continuous recycle pebble-bed cases.

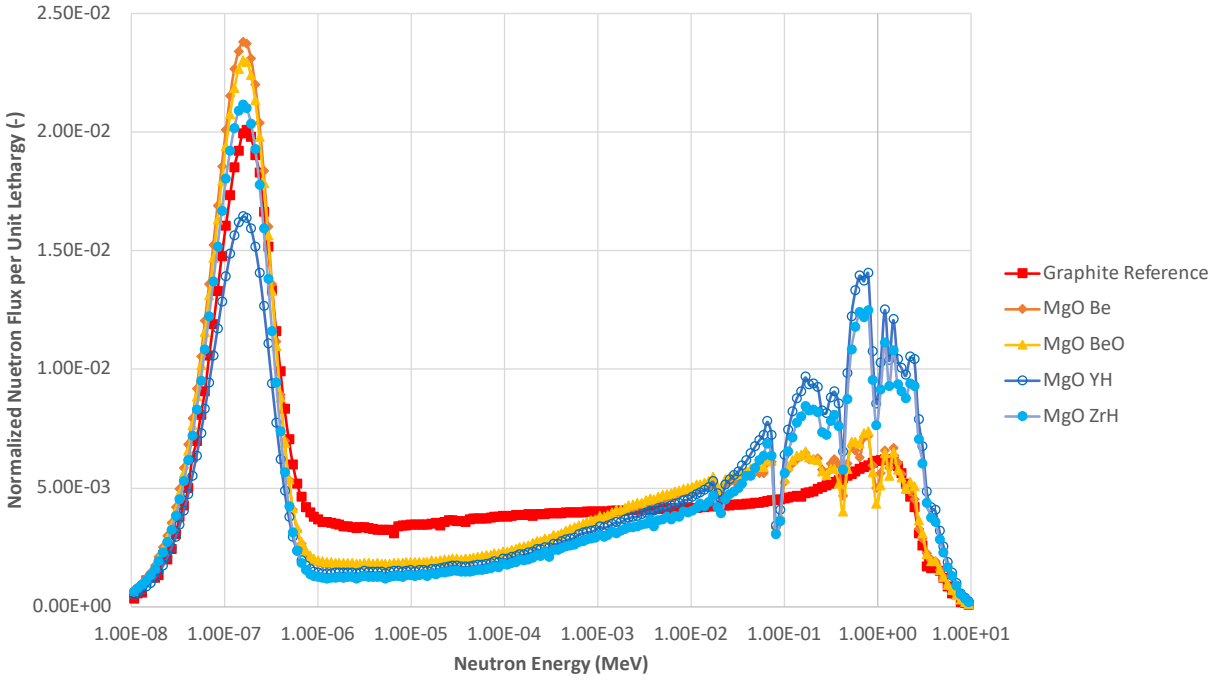

Figure 28. Normalized neutron flux per unit lethargy at EOC for graphite reference case and continuous recycle pebble-bed cases.

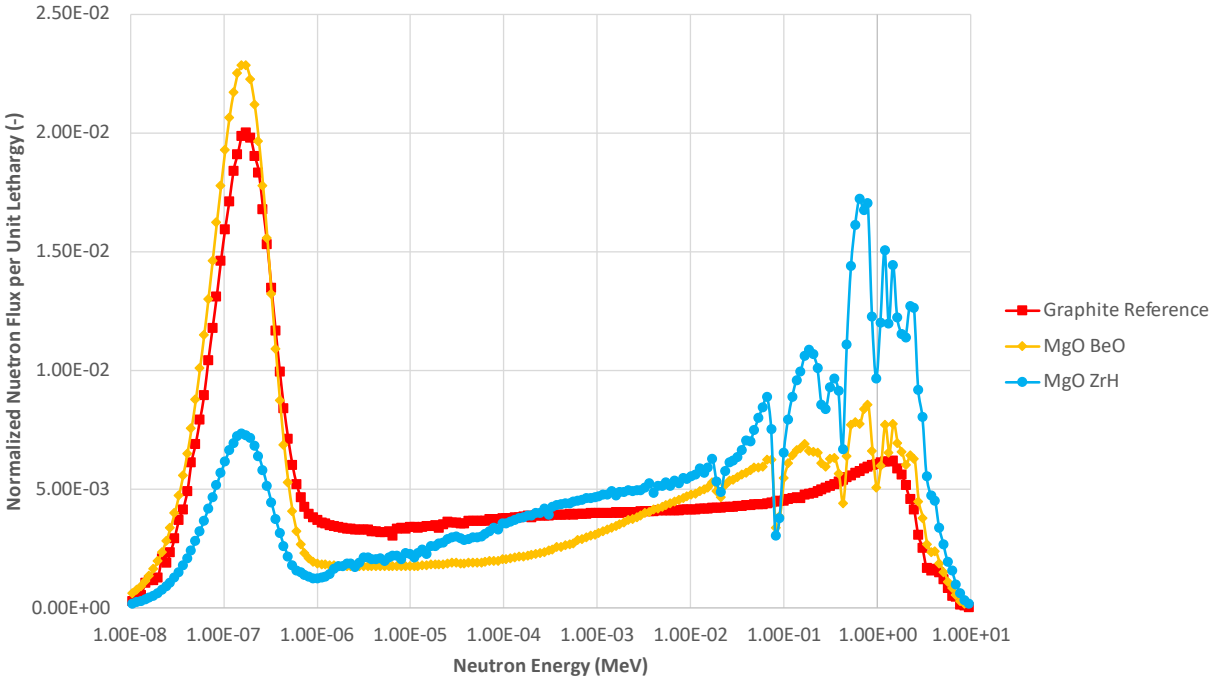

Figure 29. Normalized neutron flux per unit lethargy at BOC for graphite reference case, continuous recycle prismatic MgO $ZrH_{x=1.6}$ case, and continuous recycle pebble-bed MgO BeO case.

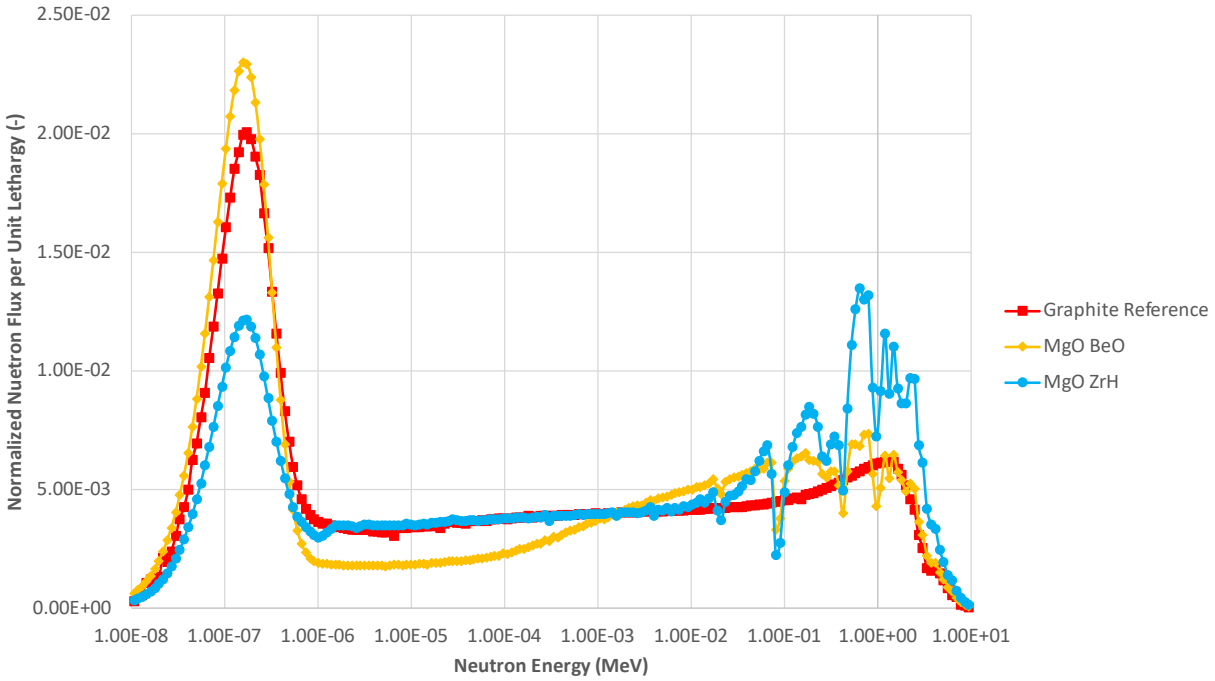

Figure 30. Normalized neutron flux per unit lethargy at EOC for graphite reference case, continuous recycle prismatic MgO ZrHx=1.6 case, and continuous recycle pebble-bed MgO BeO case.

When comparing the neutron flux in the continuous recycle pebble-bed cases to the graphite reference, the graphite reference has a larger thermal peak compared to the MgO $YH_{x=1.9}$ case only. The MgO Be, MgO BeO, and MgO $ZrH_{x=1.6}$ cases have larger thermal peaks compared to the graphite reference at BOC and EOC. Similar to the continuous recycle prismatic cases, valleys are seen at higher energies due to high-energy neutron interactions with the moderating material. Unlike the continuous recycle prismatic cases, the continuous recycle pebble-bed cases all have similar neutron flux distribution in an energy range between 1 eV to 10 keV. This similarity has to do with all four continuous recycle pebble-bed designs using the same optimized core configuration. When comparing the continuous recycle pebble-bed cases to each other, the Be-based moderator cases have larger thermal peaks and smaller fast peaks compared to the hydride-based moderator cases. The higher discharge burnup achieved in the Be-based moderator cases compared to the hydride-based moderator cases can be attributed to the relatively larger fraction of thermal neutrons. Although the MgO Be case has a larger thermal peak compared to the MgO BeO case, the MgO BeO case can achieve a slightly larger discharge burnup.

When comparing the prismatic MgO $ZrH_{x=1.6}$ case to the pebble-bed MgO BeO case, the pebble-bed MgO BeO case has a comparatively larger thermal peak. Despite the prismatic MgO $ZrH_{x=1.6}$ case having a smaller thermal peak compared to the graphite reference, it and the pebble-bed MgO BeO case achieve a higher discharge burnup than the graphite reference. When comparing the continuous recycle pebble-bed cases to the continuous recycle prismatic cases, the significant difference in discharge burnup achieved can be attributed to the difference in the fraction of thermal neutrons.

Looking at the terms in the six factor formula can also help shed light on the difference in burnups between designs. The six factor formula is used to determine the effective multiplication factor k_{eff}, which is a parameter representing the ratio of neutrons in one generation to neutrons in the previous generation. These six factors are the reproduction factor η, thermal utilization factor f, resonance escape probability p, fast fission factor ε, fast non-leakage probability P_{FNL}, and thermal non-leakage probability P_{TNL} [58]. **Figure 31** through **Figure 36** compare values for each of the six factors at the beginning of cycle (BOC) for the continuous recycle prismatic and pebble-bed designs to each other and the graphite reference. Shown in **Table 12** and **Table 13** are the values for the six factors for the continuous recycle prismatic and pebble-bed designs.

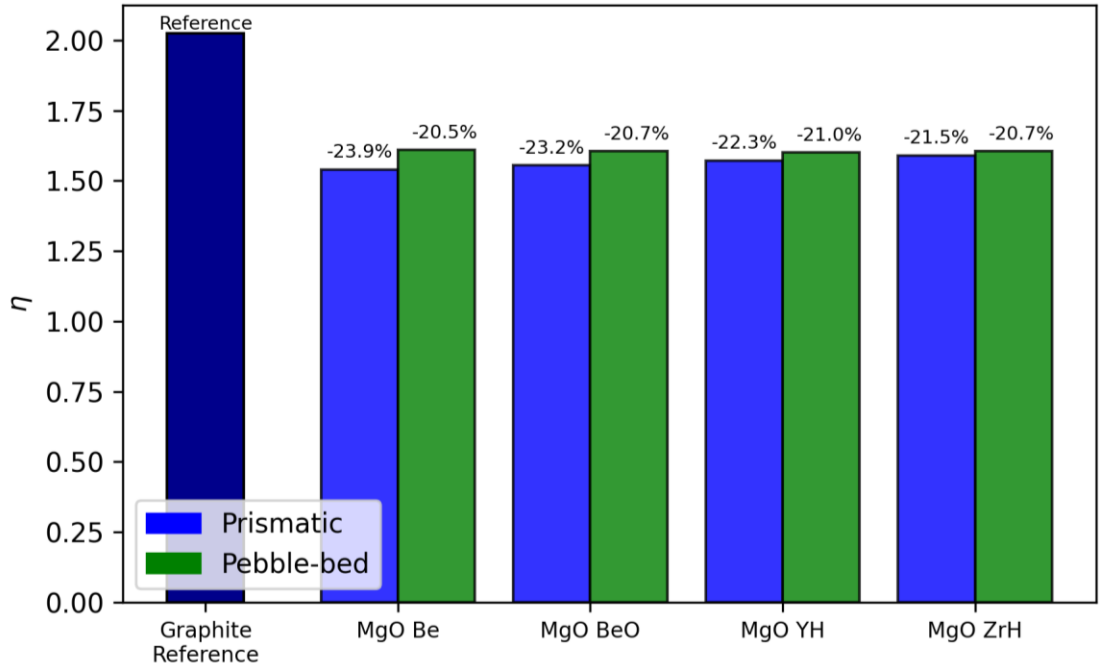

Figure 31. Reproduction factor for prismatic graphite reference and prismatic and pebble-bed concepts using TRU fuel in a continuous recycle fuel cycle.

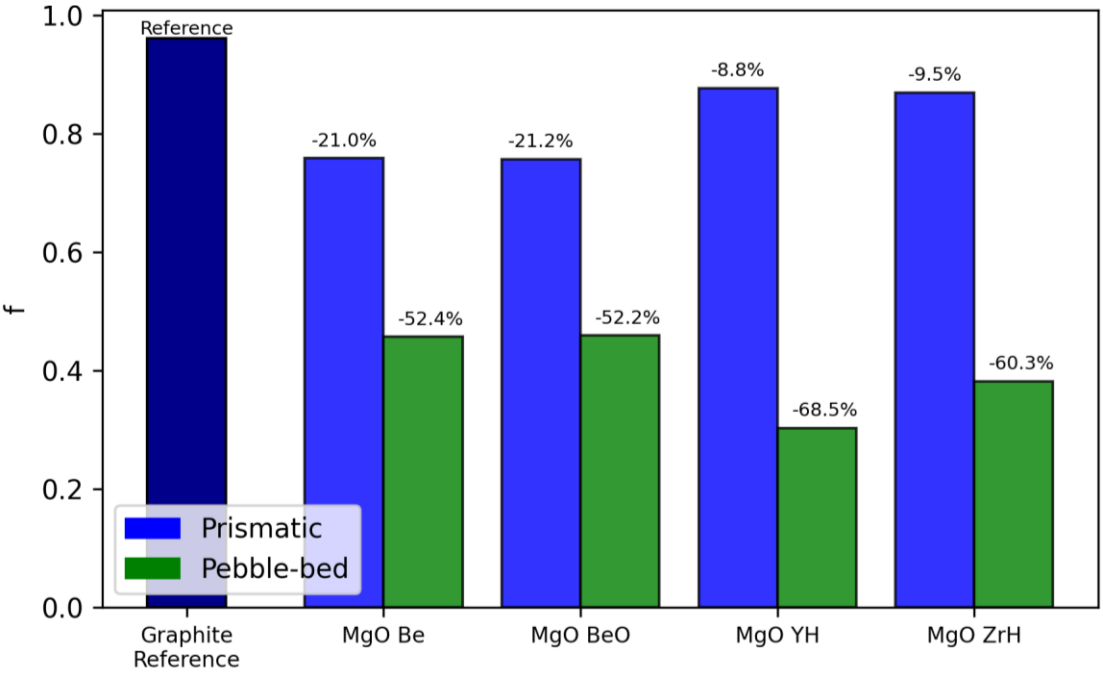

Figure 32. Thermal utilization factor for prismatic graphite reference and prismatic and pebble-bed concepts using TRU fuel in a continuous recycle fuel cycle.

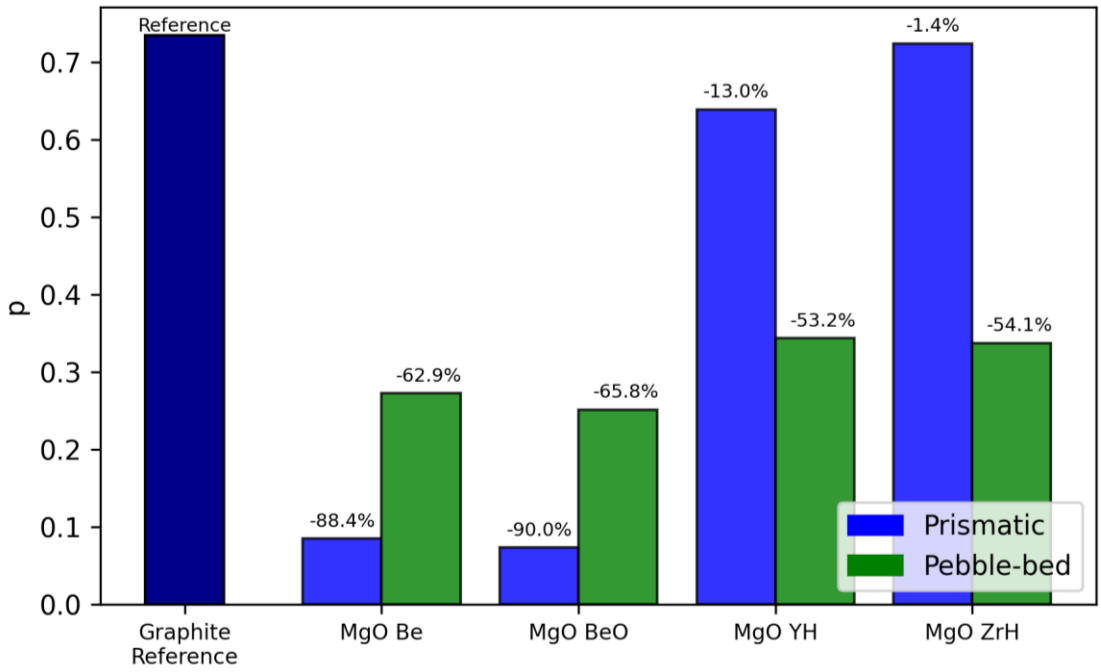

Figure 33. Resonance escape probability for prismatic graphite reference and prismatic and pebble-bed concepts using TRU fuel in a continuous recycle fuel cycle.

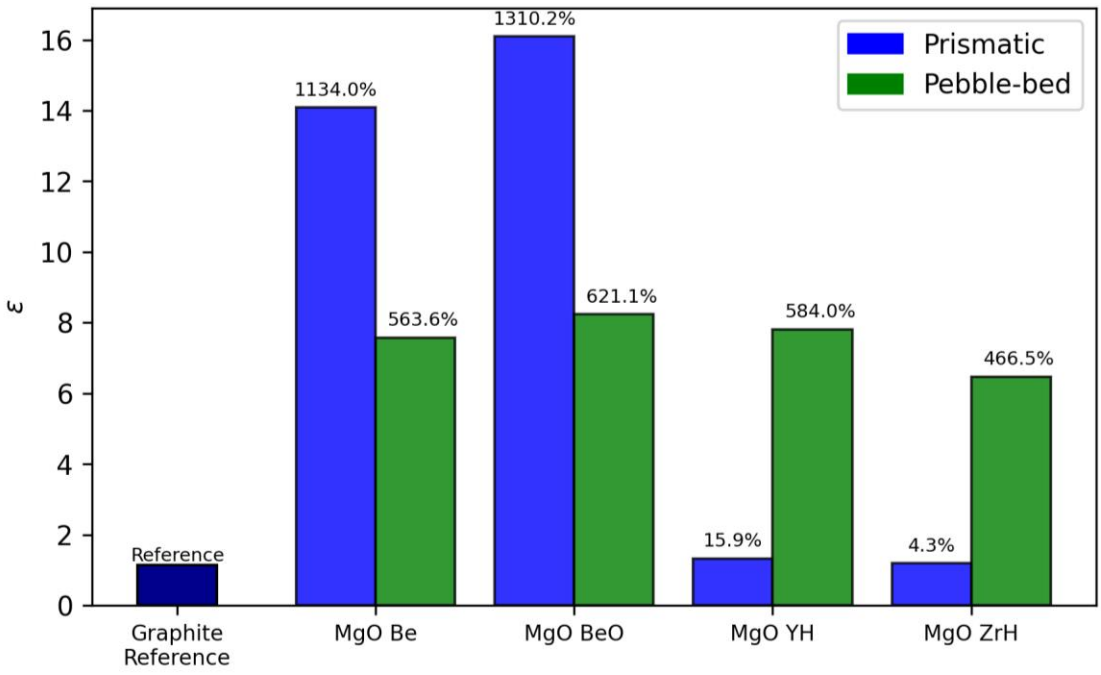

Figure 34. Fast fission factor for prismatic graphite reference and prismatic and pebble-bed concepts using TRU fuel in a continuous recycle fuel cycle.

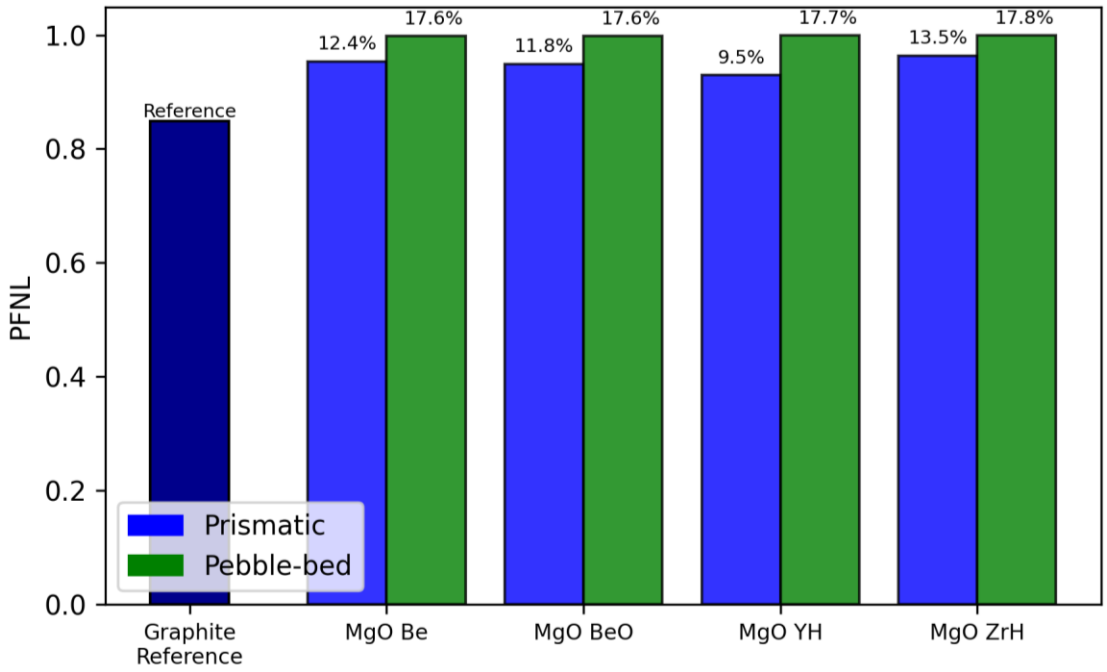

Figure 35. Fast non-leakage probability for prismatic graphite reference and prismatic and pebble-bed concepts using TRU fuel in a continuous recycle fuel cycle.

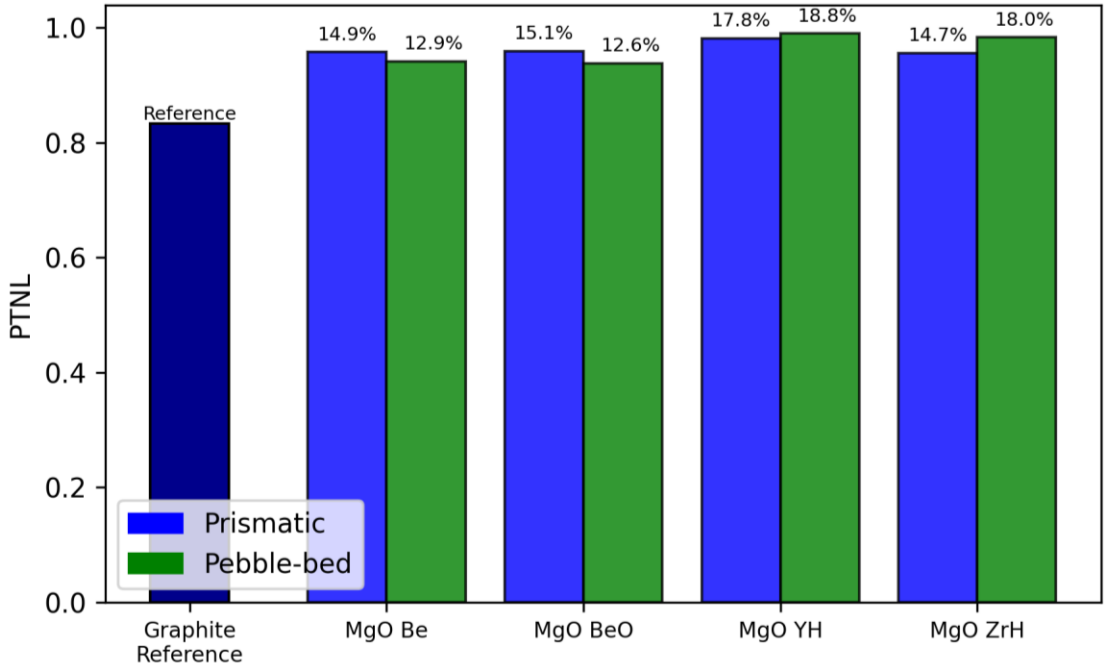

Figure 36. Thermal non-leakage probability for prismatic graphite reference and prismatic and pebble-bed concepts using TRU fuel in a continuous recycle fuel cycle.

Table 12. Six factor formula terms for continuous recycle prismatic designs.

Moderator	MgO Be	MgO BeO	MgO $YH_{x=1.9}$	MgO $ZrH_{x=1.6}$
Reproduction factor	1.539540	1.554340	1.572060	1.589850
Thermal utilization factor	0.758496	0.756641	0.876425	0.868888
Resonance escape probability	0.085052	0.073529	0.639150	0.724161
Fast fission factor	14.086100	16.098100	1.323530	1.190560
Fast non-leakage probability	0.953966	0.949117	0.929491	0.963674
Thermal non-leakage probability	0.957528	0.959718	0.981524	0.955963

Table 13. Six factor formula terms for continuous recycle pebble-bed designs.

Moderator	MgO Be	MgO BeO	MgO $YH_{x=1.9}$	MgO $ZrH_{x=1.6}$
Reproduction factor	1.609860	1.605280	1.599940	1.605120
Thermal utilization factor	0.456859	0.459133	0.302883	0.381726
Resonance escape probability	0.272673	0.251533	0.343661	0.337278
Fast fission factor	7.575240	8.232210	7.808170	6.467160
Fast non-leakage probability	0.998367	0.997898	0.999213	0.999417
Thermal non-leakage probability	0.941421	0.938275	0.990267	0.983243

The reproduction factor is the average number of fission neutrons produced per absorption of a thermal neutron in fuel [58]. This factor is not heavily impacted by the ratio of fuel to moderator and is much more dependent on what fuel is being used. The graphite reference has the highest value for the reproduction factor. This difference can be attributed to the use of UCO in the graphite reference and TRU oxide in the continuous recycle designs. The continuous recycle pebble-bed IMF concepts have slightly larger values for the reproduction factor compared to the continuous recycle prismatic IMF concepts. In the continuous recycle prismatic IMF concepts, the MgO $ZrH_{x=1.6}$ concept has the greatest reproduction factor value. In the continuous recycle pebble-bed IMF concepts, MgO Be has the greatest reproduction factor value.

The thermal utilization factor is the ratio of thermal neutron absorptions in fuel to total thermal neutron absorptions [58]. Unlike the reproduction factor, the thermal utilization factor can vary considerably depending on what the ratio of fuel to moderator is. The graphite reference has the highest value for the thermal utilization factor, similar to the reproduction factor. The continuous recycle prismatic IMF concepts have significantly larger values compared to the continuous recycle pebble-bed cases, indicating that a greater fraction of thermal neutrons is absorbed in fuel in the prismatic concepts than in the pebble-bed concepts. In the continuous recycle prismatic IMF concepts, the MgO $ZrH_{x=1.6}$ concept has the greatest thermal utilization factor value. In the continuous recycle pebble-bed IMF concepts, MgO BeO has the greatest thermal utilization factor value.

The resonance escape probability is the fraction of fission neutrons that slow down to thermal energy without being absorbed [58]. Similar to the thermal utilization factor, the resonance escape probability is also affected by the ratio of fuel to moderator. The graphite reference has the greatest value for the resonance escape probability, similar to both the reproduction and thermal utilization factors. In the continuous recycle prismatic IMF concepts, the MgO $ZrH_{x=1.6}$ concept has the highest resonance escape probability value. In the continuous recycle pebble-bed IMF concepts, the MgO $YH_{x=1.9}$ concept has the highest resonance escape probability value. When comparing thermal non-leakage probability values, the pebble-bed Be-based moderator concepts have larger resonance escape probabilities compared to their prismatic counterparts. The opposite is the case for the hydride-based moderator concepts, where the pebble-bed hydride-based moderator concepts have smaller resonance escape probabilities compared to their prismatic counterparts.

The fast fission factor is the ratio of fission neutrons produced by both fast and thermal fission to fission neutrons produced only by thermal fission [58]. Similar to the reproduction factor, the fast fission factor is also not heavily impacted by the ratio of fuel to moderator and is much more dependent on what fuel is being used. However, there is significant variance seen between the prismatic Be- based and hydride-based moderator cases, which could be attributed to a heterogenous reactor core being used and the ratio of fuel to moderator being much higher in the Be-based moderator cases than in the hydride-based moderator cases. The graphite reference has the smallest value for the fast fission factor. In the continuous recycle prismatic IMF concepts, the MgO BeO concept has the highest fission factor. In the continuous recycle pebble-bed IMF concepts, the MgO BeO concept has the highest fast fission factor. The larger fast fission factor values observed in the prismatic Be-based moderator concepts and the pebble-bed concepts can be attributed to the high fuel-to-moderator ratio used in their optimal configurations.

The fast non-leakage probability is the probability that a fast neutron will not leak from the core [58]. The thermal non-leakage probability is the probability that a thermal neutron will not leak from the core [58]. The graphite reference has the smallest value for both the fast non-leakage and thermal non-leakage probabilities. The continuous recycle pebble-bed IMF concepts have larger fast non-leakage probabilities compared to the continuous recycle prismatic IMF concepts. In the continuous recycle prismatic IMF concepts, the MgO $ZrH_{x=1.6}$ concept has the largest fast non-leakage probability. In the continuous recycle pebble-bed IMF concepts, the MgO $ZrH_{x=1.6}$ concept has the largest fast non-leakage probability but by a very small amount. When comparing thermal non-leakage probability values, the prismatic Be-based moderator concepts have larger thermal non-leakage probabilities compared to their pebble-bed counterparts. The opposite is the case for the hydride-based moderator concepts, where the prismatic hydride-based moderator concepts have smaller thermal non-leakage probabilities compared to their pebble-bed counterparts. In the continuous recycle prismatic IMF concepts, the MgO $YH_{x=1.9}$ concept has the largest thermal non-leakage probability. In the continuous recycle pebble-bed IMF concepts, the MgO $YH_{x=1.9}$ concept has the largest thermal non-leakage probability but by a very small amount. The differences in non-leakage probabilities between the continuous recycle prismatic and pebble-bed IMF concepts can be attributed to the use of cylindrical fueled compacts and fueled pebbles respectively.

The continuous recycle prismatic MgO $ZrH_{x=1.6}$ concept achieves the highest discharge burnup out of the four continuous recycle prismatic IMF concepts. In the continuous recycle prismatic MgO $ZrH_{x=1.6}$ concept, 96.36% of fast neutrons will not leak from the reactor core and 72.42% of those fast neutrons that do not leak will slow down to thermal energy without being absorbed. 95.60% of the now thermal neutrons will not leak from the reactor core. 86.89% of the thermal neutrons that do not leak will be absorbed in fuel and will each produce 1.59 fission neutrons on average. For every one fission neutron produced by thermal neutron absorption, 0.19 neutrons are produced on average by fast neutron absorption. The high non-leakage probabilities, resonance escape probability, and thermal utilization factor of the MgO $ZrH_{x=1.6}$ concept can explain the high discharge burnup it can achieve.

The continuous recycle pebble-bed MgO BeO concept achieves the highest discharge burnup out of the four continuous recycle prismatic IMF concepts. In the continuous recycle pebble-bed MgO BeO concept, 99.79% of fast neutrons will not leak from the reactor core and 25.15% of those fast neutrons that do not leak will slow down to thermal energy without being absorbed. 93.83% of the now thermal neutrons will not leak from the reactor core. 45.91% of the thermal neutrons that do not leak will be absorbed in fuel and will each produce 1.61 fission neutrons on average. For every one fission neutron produced by thermal neutron absorption, 7.23 neutrons are produced on average by fast neutron absorption. The high non-leakage probabilities, fast fission factor, and thermal utilization factor – out of the four continuous recycle pebble-bed concepts – of the MgO Be concept can explain the high discharge burnup it can achieve.

3.4 Pebble-bed Design Verification

A verification study was performed to verify the discharge burnup results found for the optimal pebble-bed designs using Serpent. This verification study involved running the optimized pebble-bed designs in OpenMC and comparing the burnup results found using OpenMC to those found using Serpent. See **Figure 37** through **Figure 44** for plots of the predicted discharge burnup using the linear and quadratic reactivity models. Compared to Serpent, larger time steps were used in OpenMC to speed up simulation time. The use of larger time steps affected the predicted discharge burnup, resulting in a slight discrepancy between Serpent and OpenMC discharge burnup results. Shown in **Table 14** is the predicted discharge burn-up using the quadratic reactivity model in Serpent and OpenMC. The percent differences in Serpent and OpenMC results are between 0.7 and 1.2%.

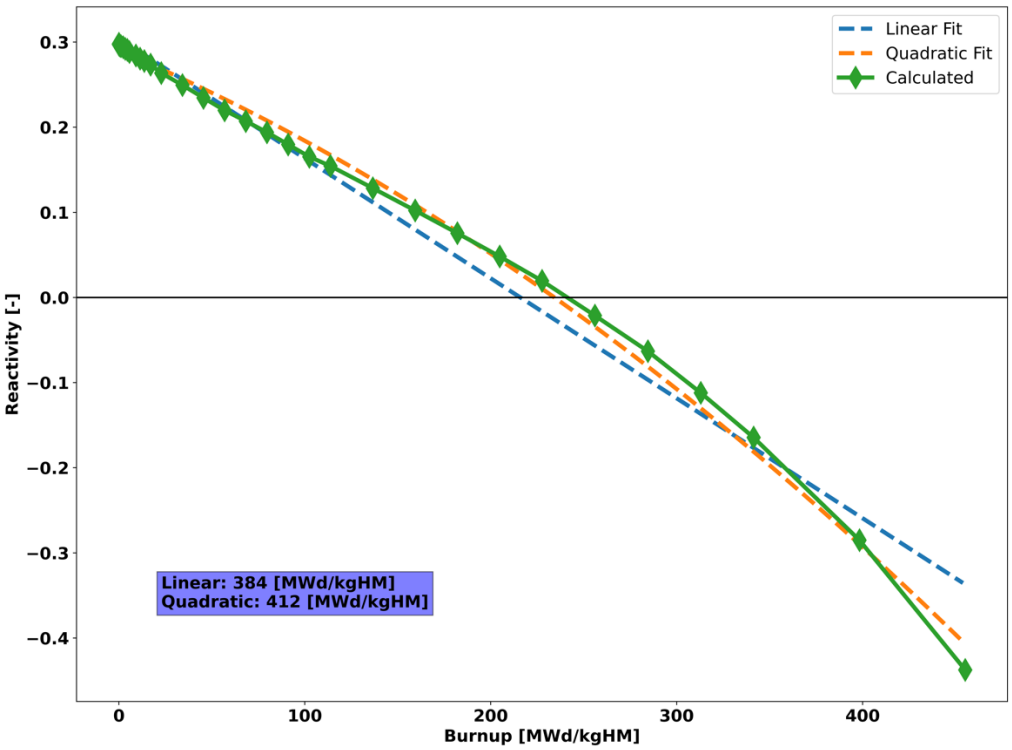

Figure 37. Linear and quadratic reactivity plot for pebble-bed MgO Be concept using Serpent.

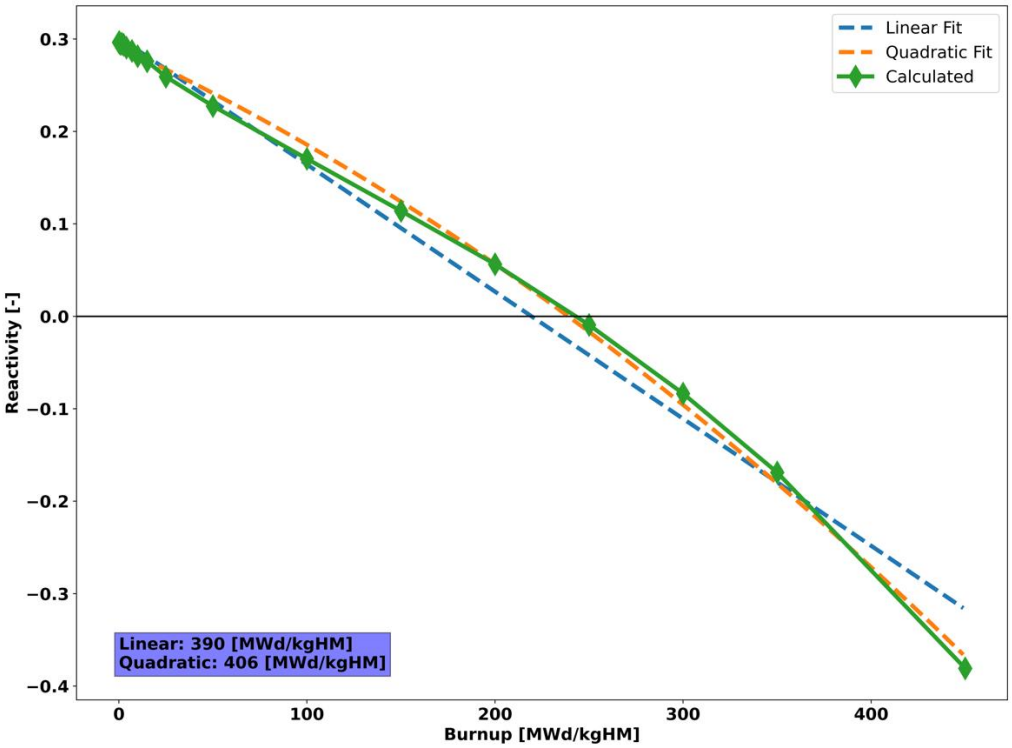

Figure 38. Linear and quadratic reactivity plot for pebble-bed MgO Be concept using OpenMC.

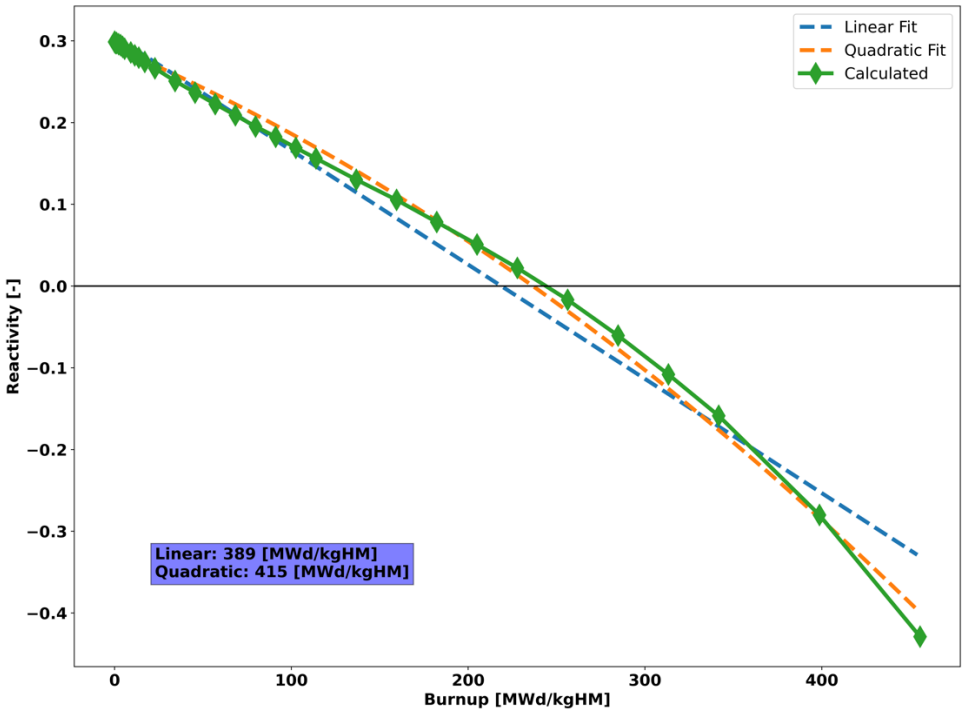

Figure 39. Linear and quadratic reactivity plot for pebble-bed MgO BeO concept using Serpent.

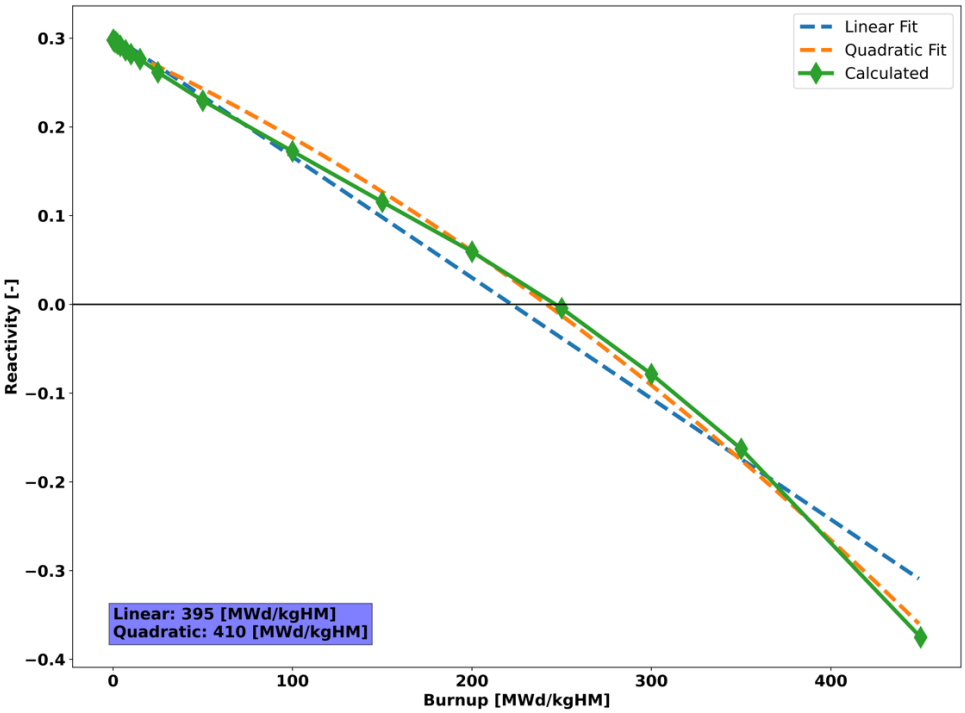

Figure 40. Linear and quadratic reactivity plot for pebble-bed MgO BeO concept using OpenMC.

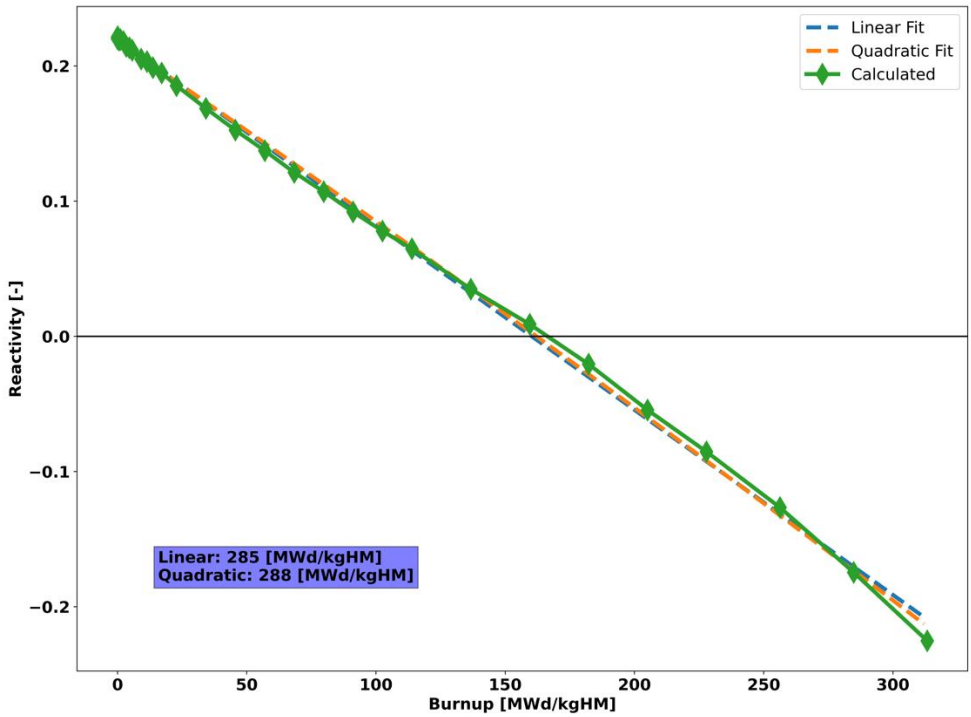

Figure 41. Linear and quadratic reactivity plot for pebble-bed MgO $YH_{x=1.9}$ concept using Serpent.

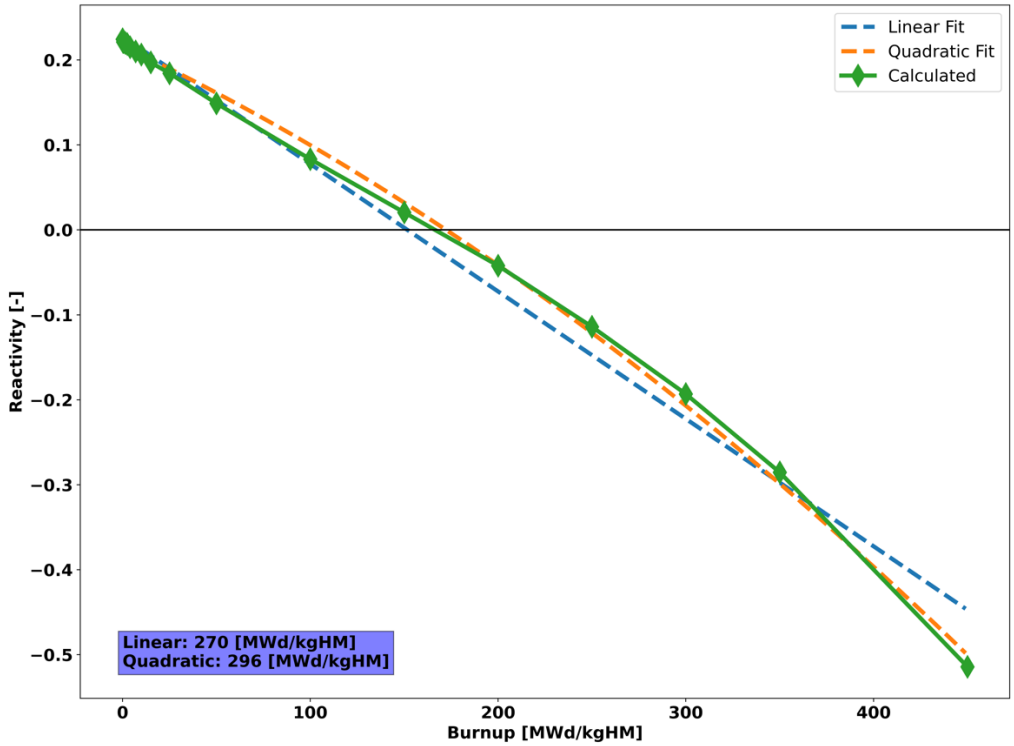

Figure 42. Linear and quadratic reactivity plot for pebble-bed MgO $YH_{x=1.9}$ concept using OpenMC.

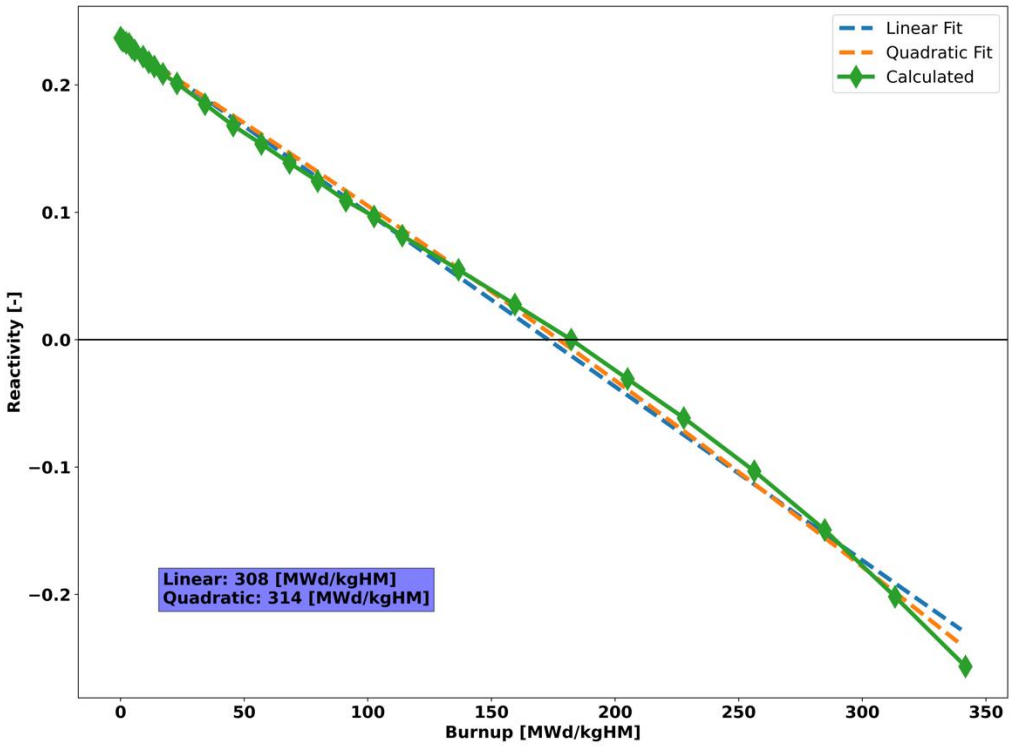

Figure 43. Linear and quadratic reactivity plot for pebble-bed MgO $ZrH_{x=1.6}$ concept using Serpent.

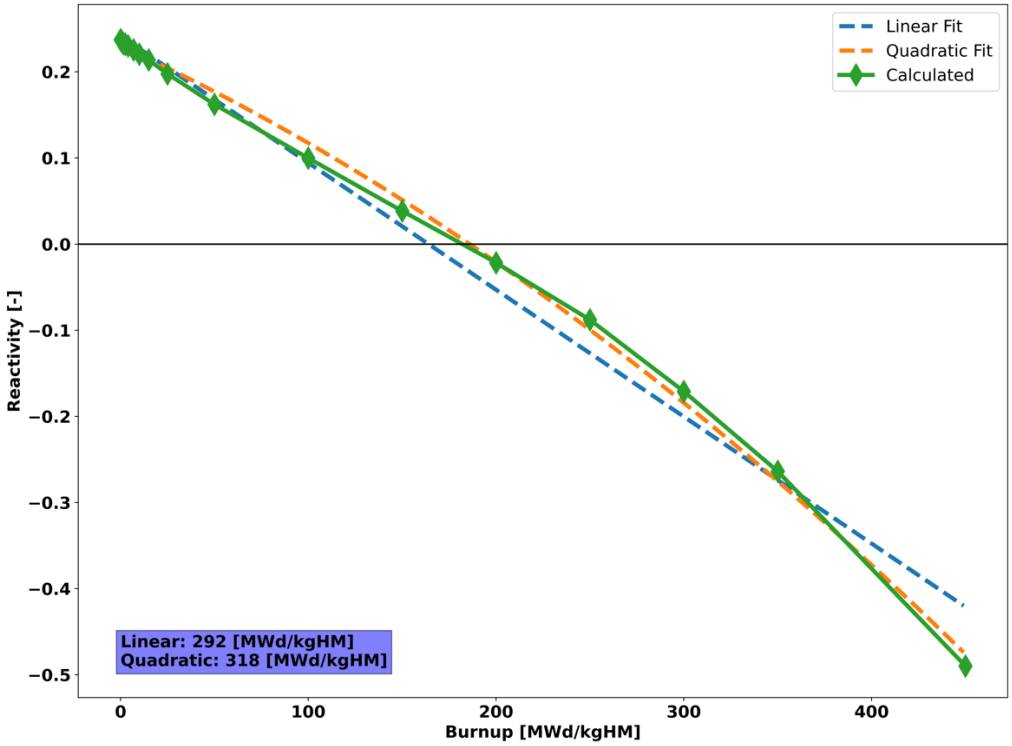

Figure 44. Linear and quadratic reactivity plot for pebble-bed MgO $ZrH_{x=1.6}$ concept using OpenMC.

Table 14. Predicted Discharge Burn-up using Quadratic Reactivity Model in Serpent and OpenMC.

Moderator	**Predicted Discharge Burn-up using Serpent (MWd/kgHM)**	**Predicted Discharge Burn-up using OpenMC (MWd/kgHM)**	**Percent Difference (%)**
MgO BeO	415	410	1.2
MgO Be	409	406	0.7
MgO $YH_{x=1.9}$	287	291	1.4
MgO $ZrH_{x=1.6}$	314	318	1.3

3.5 Prismatic Design Metric Results

Figure 45 shows the energy normalized mass of SNF&HLW for the continuous recycle prismatic IMF concepts using TRU fuel compared to a large-scale LWR, SMR, prismatic graphite reference, and once-through prismatic IMF concepts using LEU fuel. The results for the continuous recycle prismatic designs include the mass of SNF&HLW from the Stage 1 SFR and Stage 2 micro-HTGR. Compared to the graphite reference and the once-through prismatic IMF concepts, all four continuous recycle prismatic IMF concepts produce significantly less waste. Out of the four continuous recycle prismatic IMF concepts, the MgO $ZrH_{x=1.6}$ concept performs the best and reduces the mass of SNF&HLW by 92.7% compared to the graphite reference. This reduction in waste in the continuous recycle prismatic designs is largely due to recycling of all RU, Pu, and MA, meaning no SNF is sent to disposal. Only HLW and material losses are sent to disposal for the continuous recycle IMF concepts.

Figure 46 shows the energy normalized volume of LLW for the continuous recycle prismatic IMF concepts using TRU fuel compared to a large-scale LWR, SMR, prismatic graphite reference, and once-through prismatic IMF concepts using LEU fuel. The results for continuous recycle prismatic designs include the volume of LLW from the Stage 1 SFR and Stage 2 micro-HTGR. Compared to the graphite reference, all four continuous recycle prismatic IMF concepts produce less waste but do not perform better than the once-through prismatic IMF concepts. Out of the four continuous recycle prismatic IMF concepts, the MgO $ZrH_{x=1.6}$ concept performs the best and reduces the volume of LLW by 30.7% compared to the graphite reference.

Figure 47 shows the energy normalized mass of natural uranium required for the continuous recycle prismatic IMF concepts using TRU fuel compared to a large-scale LWR, SMR, prismatic graphite reference, and once-through IMF concepts using LEU fuel. The results for continuous recycle prismatic designs only include natural uranium used in the Stage 1 SFR as no natural uranium is used in the Stage 2 micro-HTGR. Compared to the graphite reference and the once-through prismatic IMF concepts, all four continuous recycle prismatic IMF concepts require significantly less natural uranium. The four continuous recycle prismatic designs perform just as well as each other, reducing MTNU by 99.8% compared to the graphite reference. This reduction in MTNU required in the continuous recycle prismatic designs is largely due to all RU in Stage 1 being recycled back into the Stage 1 SFR and the Stage 2 micro-HTGR not using any uranium.

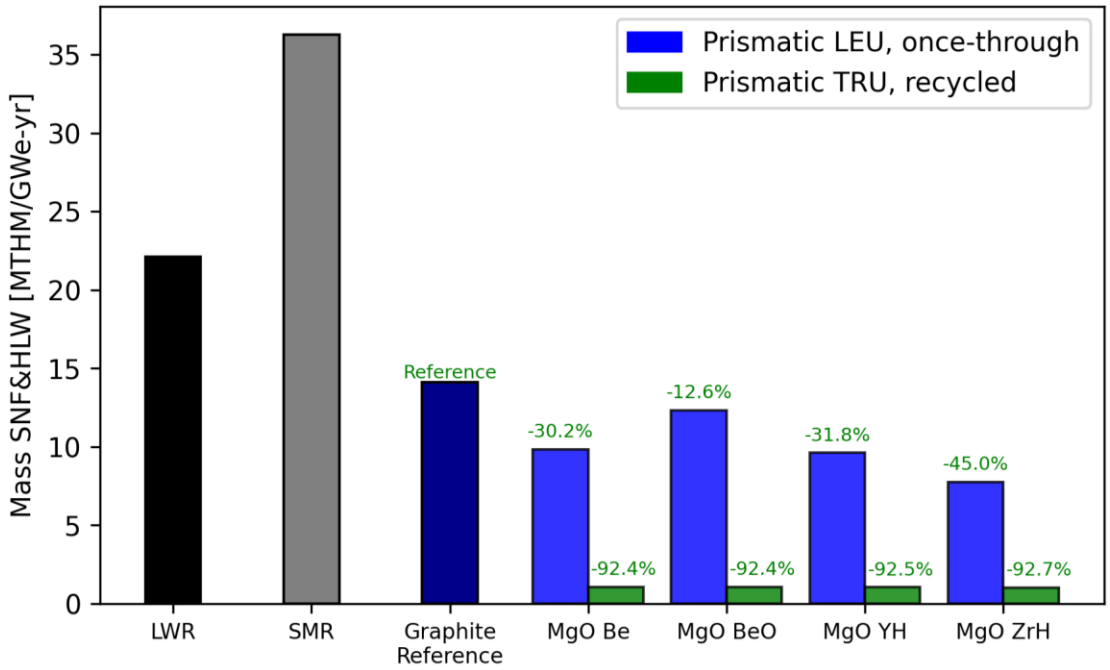

Figure 45. Energy normalized mass of SNF&HLW per unit energy generated for large-scale LWR, SMR, prismatic graphite reference, and prismatic IMF concepts using either LEU fuel in a once-through fuel cycle or TRU fuel in a continuous recycle fuel cycle.

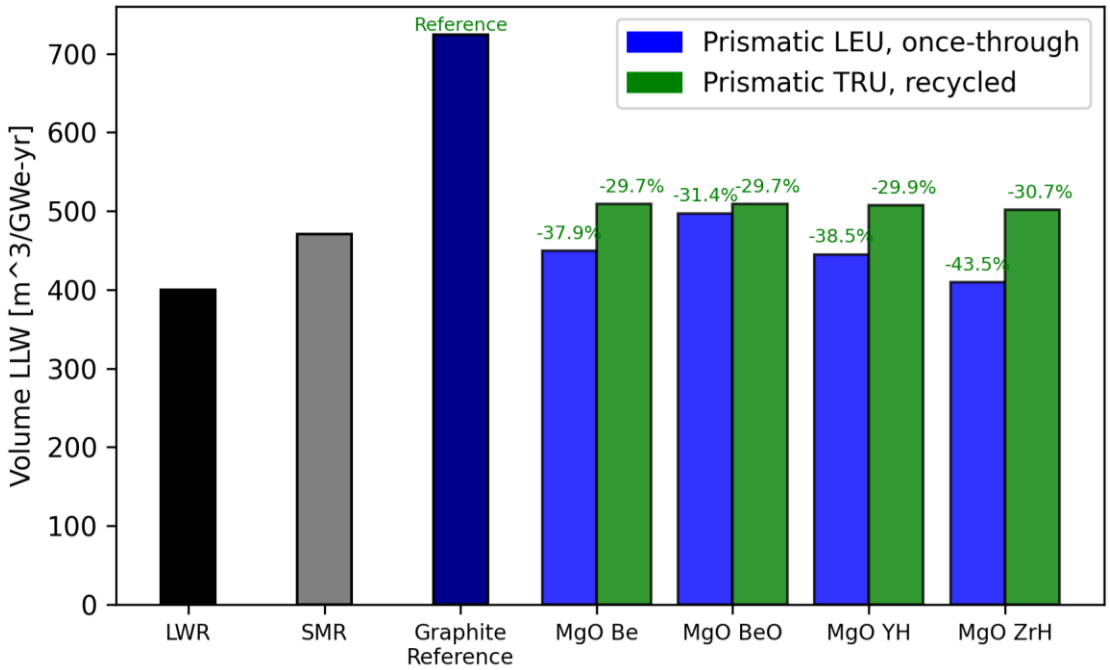

Figure 46. Energy normalized volume of LLW for large-scale LWR, SMR, prismatic graphite reference, and prismatic IMF concepts using either LEU fuel in a once-through fuel cycle or TRU fuel in a continuous recycle fuel cycle.

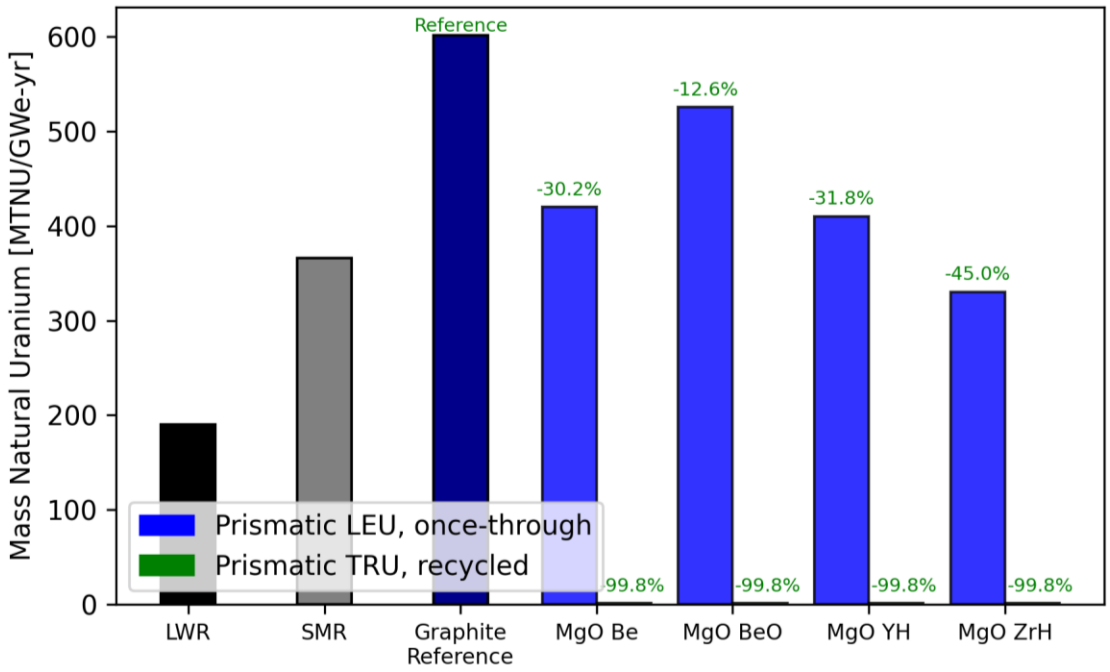

Figure 47. Energy normalized mass of natural uranium required for large-scale LWR, SMR, prismatic graphite reference, and prismatic IMF concepts using either LEU fuel in a once-through fuel cycle or TRU fuel in a continuous recycle fuel cycle.

Figure 48 shows the energy normalized area of land used for the continuous recycle prismatic IMF concepts using TRU fuel compared to a large-scale LWR, SMR, prismatic graphite reference, and once-through prismatic IMF concepts using LEU fuel. The results for continuous recycle IMF concepts include land used by processes for the Stage 1 SFR and Stage 2 micro-HTGR. Compared to the graphite reference and the once-through prismatic IMF concepts, all four continuous recycle prismatic IMF concepts require less land. The MgO $ZrH_{x=1.6}$ concept performs the best, reducing the area of land used by 76.9% compared to the graphite reference. The reduced area of land used in the continuous recycle prismatic IMF concepts is largely due to the significant reduction in MTNU required, which impacts how much land is needed for mining and milling of uranium. Additionally, the reduced mass of SNF&HLW disposed in the continuous recycle prismatic IMF concepts reduces how much land is needed for geological repository.

Figure 49 shows the energy normalized volume of water used for the continuous recycle prismatic IMF concepts using TRU fuel compared to a large-scale LWR, SMR, prismatic graphite reference, and once-through prismatic IMF concepts using LEU fuel. The results for continuous recycle IMF concepts include water used by processes for the Stage 1 SFR and Stage 2 micro-HTGR. Compared to the graphite reference and the once-through prismatic IMF concepts, all four continuous recycle IMF concepts require less water. The four continuous recycle prismatic designs perform just as well as each other, reducing the volume of water used by 2.3% compared to the graphite reference. This metric sees the least significant reduction for the continuous recycle IMF concepts due to the reactor operation multiplier constant being the most significant contributor to the metric by several orders of magnitude and all evaluated designs being normalized to be per unit energy generated.

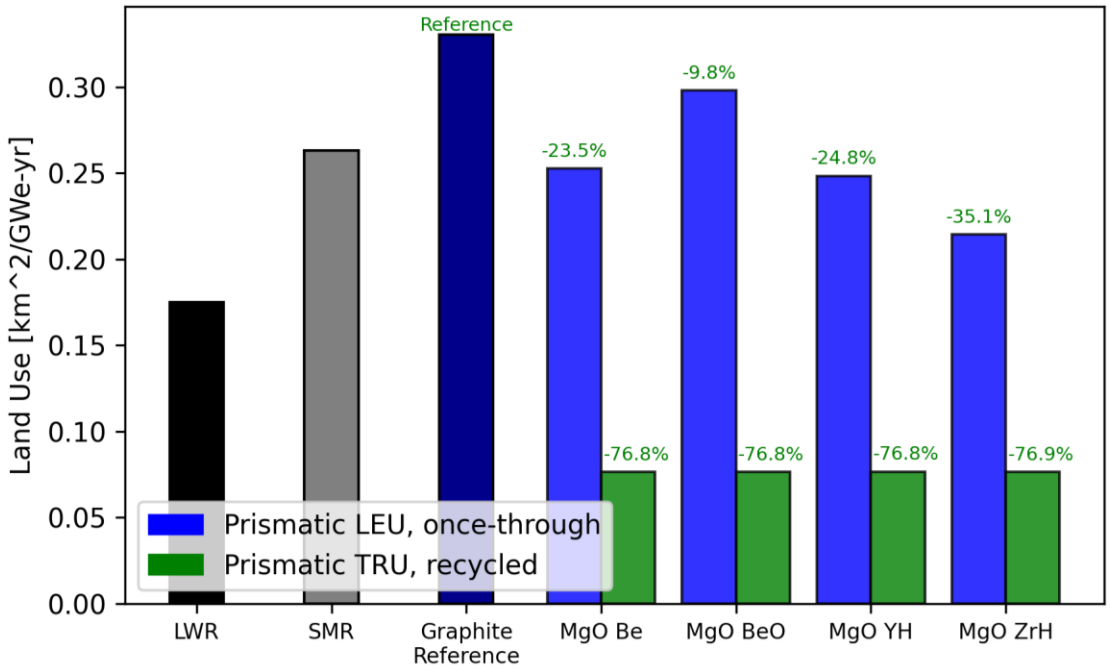

Figure 48. Energy normalized area of land used for large-scale LWR, SMR, prismatic graphite reference, and prismatic IMF concepts using either LEU fuel in a once-through fuel cycle or TRU fuel in a continuous recycle fuel cycle.

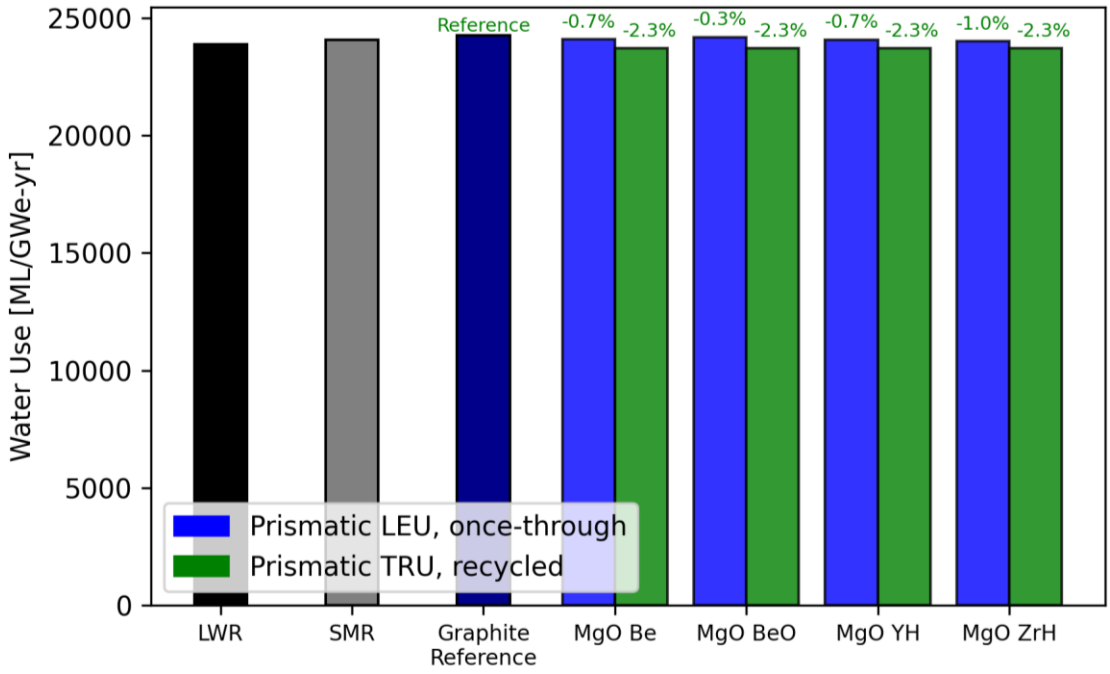

Figure 49. Energy normalized volume of water used for large-scale LWR, SMR, prismatic graphite reference, and prismatic IMF concepts using either LEU fuel in a once-through fuel cycle or TRU fuel in a continuous recycle fuel cycle.

Figure 50 shows the energy normalized mass of CO_2 produced for the continuous recycle prismatic IMF concepts using TRU fuel compared to a large-scale LWR, SMR, prismatic graphite reference, and once-through prismatic IMF concepts using LEU fuel. The results for continuous recycle prismatic IMF concepts include CO_2 produced by processes for the Stage 1 SFR and Stage 2 micro-HTGR. Compared to the graphite reference and the once-through prismatic IMF concepts, all four continuous recycle prismatic IMF concepts produce less CO_2. The MgO $ZrHx_{=1.6}$ concept performs the best, reducing mass of CO_2 produced by 72.3% compared to the graphite reference. This reduction in CO_2, similar to the reduction in the area of land used, is largely due to the reduced MTNU required in the continuous recycle prismatic designs. The reduced MTNU required reduces how much mining, milling, and enrichment of uranium is required, which reduces how much CO_2 is produced during these processes.

Figure 51 shows the activity of SNF&HLW at 100 years for the continuous recycle prismatic IMF concepts using TRU fuel compared to a large-scale LWR, SMR, prismatic graphite reference, and once-through prismatic IMF concepts using LEU fuel. The results for the continuous recycle IMF concepts only include the activity of SNF&HLW from the Stage 2 micro-HTGR. Compared to the graphite reference case and the once-through prismatic IMF concepts, all four continuous recycle IMF concepts have lower activity. The MgO Be concept performs the best, lowering activity by 58.6% compared to the graphite reference. The reduced activity of SNF&HLW at 100 years in the continuous recycle prismatic IMF concepts is due to the reduction in the mass of SNF&HLW from the recycling of RU, TRU, and MA in the Stage 1 SFR and Stage 2 micro-HTGR.

Figure 52 shows the activity of SNF&HLW at 100,000 years for the continuous recycle prismatic IMF concepts using TRU fuel compared to a large-scale LWR, SMR, prismatic graphite reference, and once-through prismatic IMF concepts using LEU fuel. The results for the continuous recycle IMF concepts only include the activity of SNF&HLW from the Stage 2 micro-HTGR. Compared to the graphite reference case and the once-through prismatic IMF concepts, all four continuous recycle IMF concepts have lower activity. The MgO ZrH concept performs the best, lowering activity by 77.3% compared to the graphite reference. The reduced activity of SNF&HLW at 100,000 in the continuous recycle IMF concepts is due to the recycling of Pu, TRU, and MA in the Stage 2 micro-HTGR, which is the same reason why activity of SNF&HLW at 100 years is reduced.

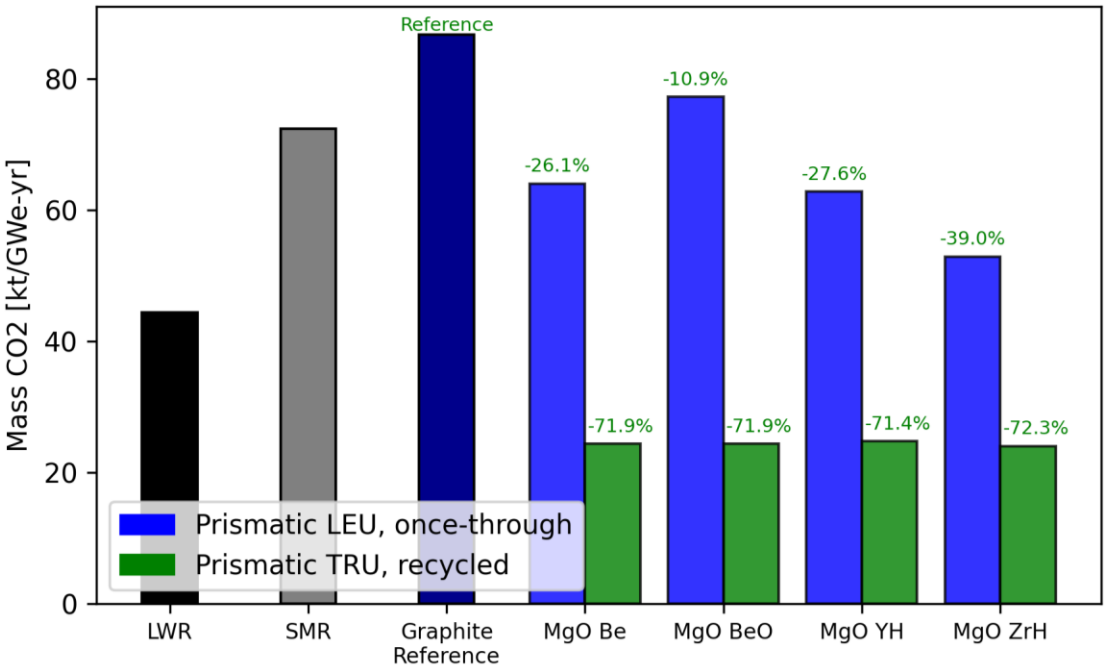

Figure 50. Energy normalized mass of CO_2 produced for large-scale LWR, SMR, prismatic graphite reference, and prismatic IMF concepts using either LEU fuel in a once-through fuel cycle or TRU fuel in a continuous recycle fuel cycle.

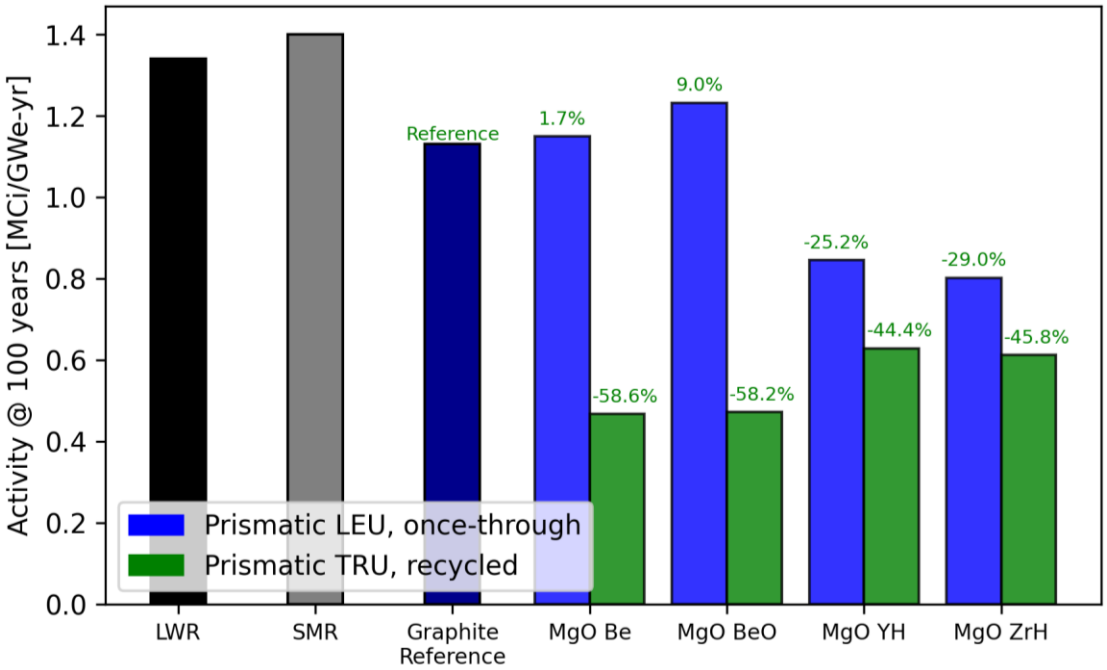

Figure 51. Activity of SNF&HLW at 100 years for large-scale LWR, SMR, prismatic graphite reference, and prismatic IMF concepts using either LEU fuel in a once-through fuel cycle or TRU fuel in a continuous recycle fuel cycle.

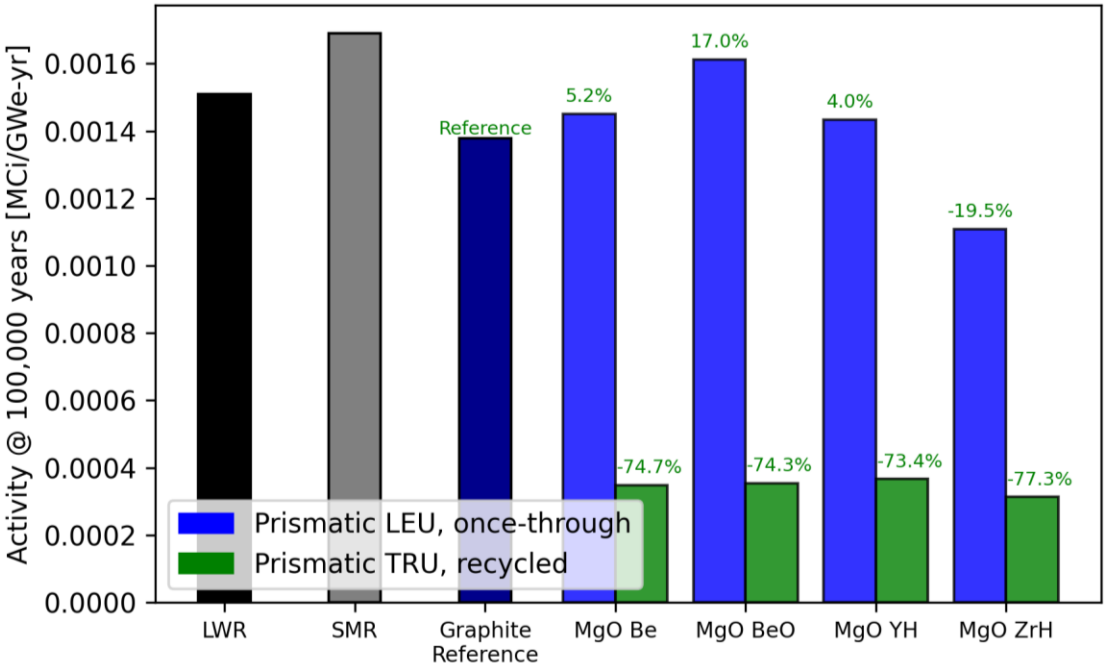

Figure 52. Activity of SNF&HLW at 100,000 years for large-scale LWR, SMR, prismatic graphite reference, and prismatic IMF concepts using either LEU fuel in a once-through fuel cycle or TRU fuel in a continuous recycle fuel cycle.

See **Table 15** for the reduction in each continuous recycle prismatic IMF concept compared to the graphite reference for each evaluated metric. For most of the evaluated metrics, the MgO $ZrH_{x=1.6}$ concept performs the best. The activity of SNF&HLW at 100 years is the only metric where the MgO $ZrH_{x=1.6}$ concept is outperformed by the MgO Be and MgO BeO concepts. This is due to the difference in fuel in-core residence time between the Be-based concepts and the hydride-based concepts. The in-core residence times of the MgO Be and MgO BeO concepts were 11629.51 and 11377.481 days respectively, compared to the in-core residence times of the MgO $YH_{x=1.9}$ and MgO $ZrH_{x=1.6}$ concepts being 1368.532 and 1462.43 days respectively. This significant difference in in-core residence times can be attributed to the optimal configurations for Be-based moderator concepts using significantly higher TRISO packing fractions than the hydride-based moderator concepts, therefore increasing the total fuel in the reactor core. The longer fuel in-core residence time for the Be-based concepts resulted in a lower activity of SNF&HLW at the time of discharge because highly radioactive fission products have comparatively more time to decay in the reactor core. Otherwise, all four continuous recycle prismatic IMF concepts showed substantial improvements compared to the graphite reference and also compared to the once-through prismatic IMF concepts, LWR, and SMR. The one metric where the continuous recycle prismatic designs are outperformed by the once-through prismatic designs is the volume of LLW disposed, which is largely due to the quantity of material being reprocessed in the SFR driver and blanket fuel.

3.6 Pebble-bed Design Metric Results

Figure 53 shows the energy normalized mass of SNF&HLW for the continuous recycle pebble-bed IMF concepts using TRU fuel compared to a large-scale LWR, SMR, prismatic graphite reference, and once-through pebble-bed IMF concepts using LEU fuel. The results for the continuous recycle pebble-bed designs include the mass of SNF&HLW from the Stage 1 SFR and Stage 2 micro-HTGR. Compared to the graphite reference and the once-through pebble-bed IMF concepts, all four continuous recycle pebble-bed IMF concepts produce significantly less waste. The four continuous recycle pebble-bed designs perform just as well as each other, reducing the mass of SNF&HLW by 92.7% compared to the graphite reference. Similar to what was observed in the continuous recycle prismatic IMF concepts, no SNF is sent to disposal and only HLW is sent to disposal for the continuous recycle pebble-bed IMF concepts which reduces the quantity of waste sent to disposal.

Table 15. Evaluated metric reduction percentages for the continuous recycle prismatic IMF concepts compared to the prismatic graphite reference.

IMF concept	MgO Be	MgO BeO	MgO $YH_{x=1.9}$	MgO $ZrH_{x=1.6}$
SNF&HLW	92.4 %	92.4 %	92.5 %	92.7 %
LLW	29.7 %	29.7 %	29.9 %	30.7 %
Natural Uranium	99.8 %	99.8 %	99.8 %	99.8 %
Land Use	76.8 %	76.8 %	76.8 %	76.9 %
Water Use	2.3 %	2.3 %	2.3 %	2.3 %
Mass CO_2	71.9 %	71.9 %	71.4 %	72.3 %
Activity at 100 years	58.6 %	58.2 %	28.7 %	45.8 %
Activity at 100,000 years	74.7 %	74.3 %	73.4 %	77.3 %

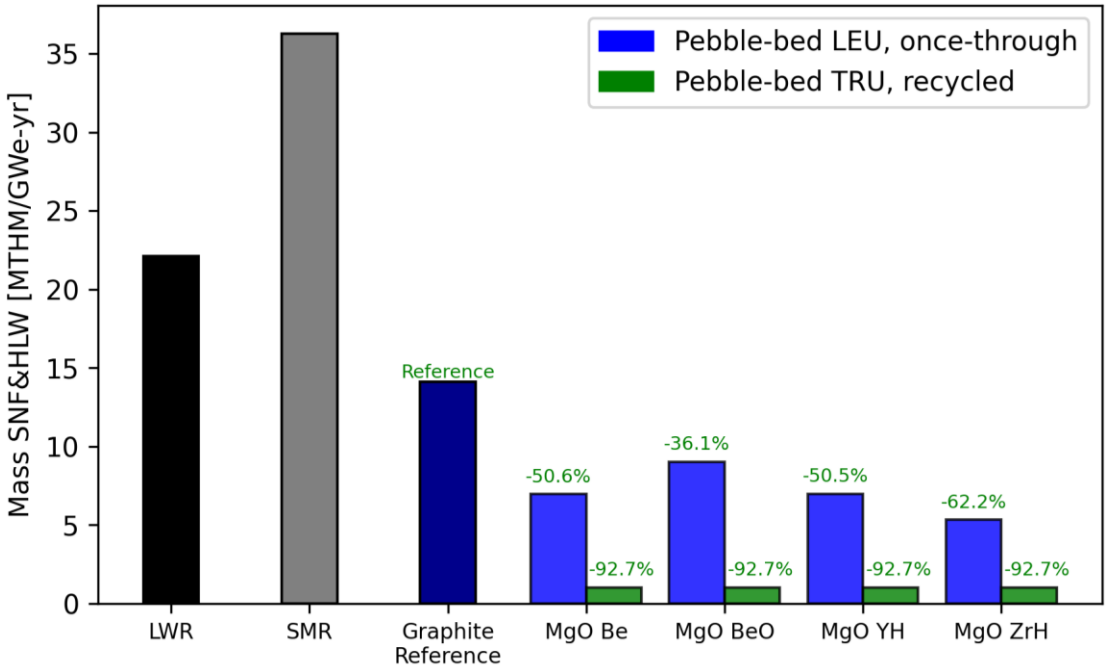

Figure 53. Energy normalized mass of SNF&HLW per unit energy generated for large-scale LWR, SMR, prismatic graphite reference, and pebble-bed IMF concepts using either LEU fuel in a once-through fuel cycle or TRU fuel in a continuous recycle fuel cycle.

Figure 54 shows the energy normalized volume of LLW for the continuous recycle pebble-bed IMF concepts using TRU fuel compared to a large-scale LWR, SMR, prismatic graphite reference, and once-through pebble-bed IMF concepts using LEU fuel. The results for continuous recycle pebble-bed designs include the volume of LLW from the Stage 1 SFR and Stage 2 micro-HTGR. Compared to the graphite reference, all four continuous recycle IMF concepts produce less waste but do not perform better than the once-through pebble-bed IMF concepts. This is also what was observed in the continuous recycle prismatic IMF concepts. Out of the four continuous recycle pebble-bed IMF concepts, the MgO BeO concept perform the best and reduces the volume of LLW by 31.1% compared to the graphite reference.

Figure 55 shows the energy normalized mass of natural uranium required for the continuous recycle pebble-bed IMF concepts using TRU fuel compared to a large-scale LWR, SMR, prismatic graphite reference, and once-through pebble-bed IMF concepts using LEU fuel. The results for continuous recycle pebble-bed designs only include natural uranium used in the Stage 1 SFR as no natural uranium is used in the Stage 2 micro-HTGR. Compared to the graphite reference and the once-through pebble-bed IMF concepts, all four continuous recycle IMF concepts require significantly less natural uranium and reduce MTNU required by 99.8% compared to the graphite reference. Similar to the continuous recycle prismatic IMF concepts, this reduction in MTNU required in the continuous recycle pebble-bed IMF concepts is largely due to all RU in Stage 1 being recycled back into the Stage 1 SFR and the Stage 2 micro-HTGR not using any uranium.

Figure 56 shows the energy normalized area of land used for the continuous recycle pebble-bed IMF concepts using TRU fuel compared to a large-scale LWR, SMR, prismatic graphite reference, and once-through pebble-bed IMF concepts using LEU fuel. The results for continuous recycle IMF concepts include the area of land used by processes for the Stage 1 SFR and Stage 2 micro-HTGR. Compared to the graphite reference and the once-through pebble-bed IMF concepts, all four continuous recycle pebble-bed IMF concepts require less land. Like the continuous recycle prismatic IMF concepts, the area of land used in the continuous recycle pebble-bed IMF concepts is reduced largely due to the significantly lower MTNU required which reduces how much land is needed for mining and milling of uranium. Additionally, only HLW is sent to disposal as all SNF is recycled which reduces how much land is needed for geological repository.

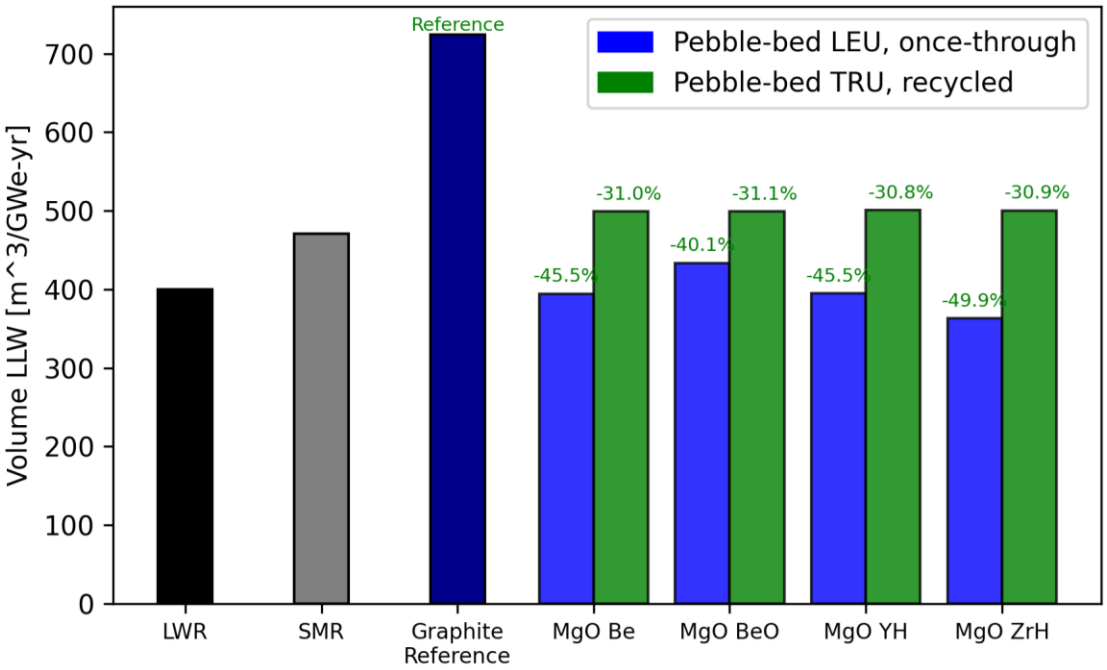

Figure 54. Energy normalized volume of LLW for large-scale LWR, SMR, prismatic graphite reference, and pebble-bed IMF concepts using either LEU fuel in a once-through fuel cycle or TRU fuel in a continuous recycle fuel cycle.

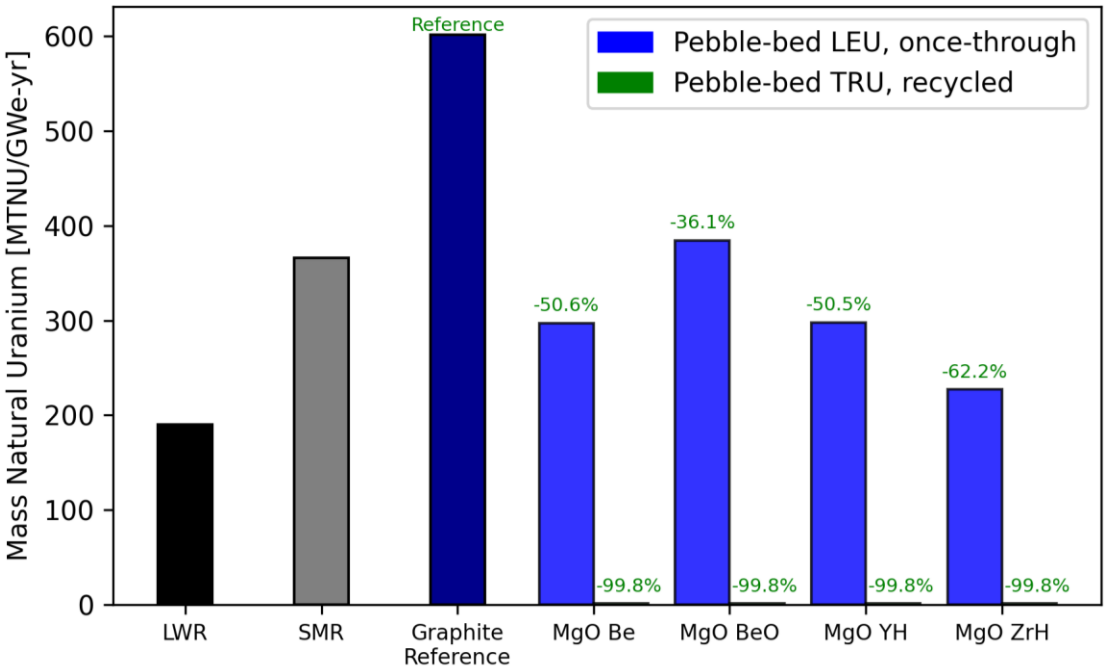

Figure 55. Energy normalized mass of natural uranium required for large-scale LWR, SMR, prismatic graphite reference, and pebble-bed IMF concepts using either LEU fuel in a once-through fuel cycle or TRU fuel in a continuous recycle fuel cycle.

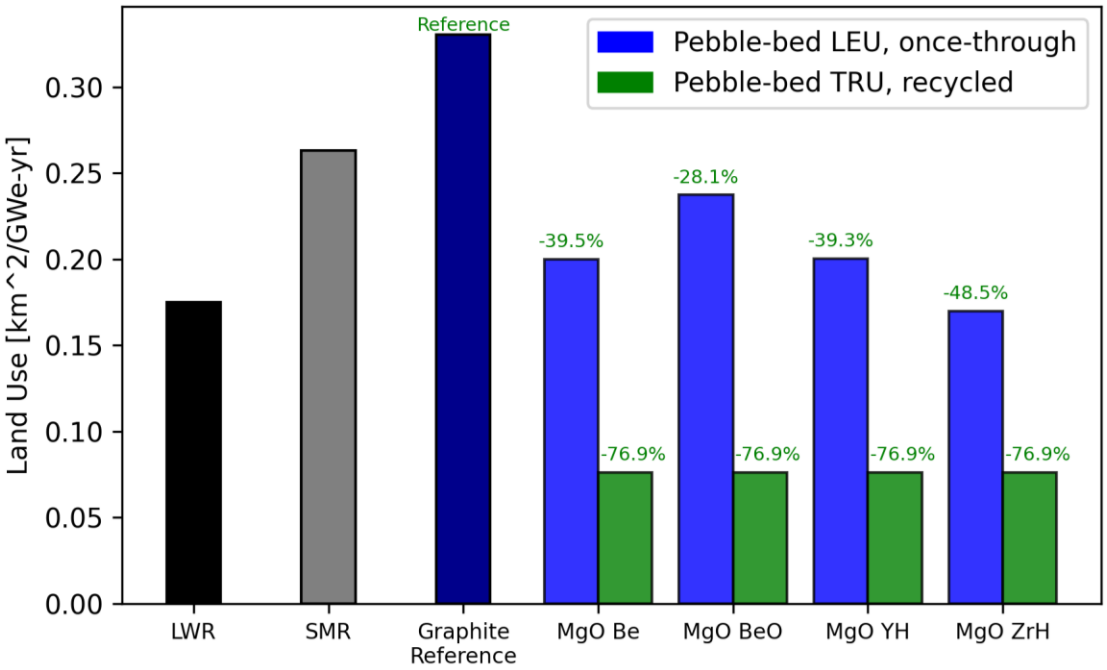

Figure 56. Energy normalized area of land used for large-scale LWR, SMR, prismatic graphite reference, and pebble-bed IMF concepts using either LEU fuel in a once-through fuel cycle or TRU fuel in a continuous recycle fuel cycle.

Figure 57 shows the energy normalized volume of water used for the continuous recycle pebble-bed IMF concepts using TRU fuel compared to a large-scale LWR, SMR, prismatic graphite reference, and once-through pebble-bed IMF concepts using LEU fuel. The results for continuous recycle IMF concepts include water used by processes for the Stage 1 SFR and Stage 2 micro-HTGR. Compared to the graphite reference and the once-through pebble-bed IMF concepts, all four continuous recycle pebble-bed IMF concepts require less water. This metric sees the least significant reduction for the continuous recycle pebble-bed IMF concepts for the same reasons as the continuous recycle prismatic IMF concepts. The reactor operation multiplier constant is the most significant contributor to the volume of water used by several orders of magnitude and all evaluated designs are normalized to be per unit energy generated.

Figure 58 shows the energy normalized mass of CO_2 produced for the continuous recycle pebble-bed IMF concepts using TRU fuel compared to a large-scale LWR, SMR, prismatic graphite reference, and once-through pebble-bed IMF concepts using LEU fuel. The results for continuous recycle IMF concepts include CO_2 produced by processes for the Stage 1 SFR and Stage 2 micro-HTGR. Compared to the graphite reference and the once-through pebble-bed IMF concepts, all four continuous recycle pebble-bed IMF concepts produce less CO_2. The MgO Be and MgO BeO concepts perform the best, producing 72.9% less CO_2 compared to the graphite reference. Like the continuous recycle prismatic designs, the mass of CO_2 produced is reduced largely due to the significantly lower MTNU required which affects how much CO_2 is produced during mining, milling, and enrichment of uranium.

Figure 59 shows the activity of SNF&HLW at 100 years for the continuous recycle pebble-bed IMF concepts using TRU fuel compared to a large-scale LWR, SMR, prismatic graphite reference, and once-through pebble-bed IMF concepts using LEU fuel. The results for the continuous recycle pebble-bed IMF concepts only include the activity of SNF&HLW from the Stage 2 micro-HTGR. Compared to the graphite reference case and the once-through pebble-bed IMF concepts, all four continuous recycle pebble-bed IMF concepts have lower activity. The MgO Be and MgO BeO concepts perform the best, lowering activity by 77.8% compared to the graphite reference. Similar to the continuous recycle prismatic designs, the reduced activity of SNF&HLW at 100 years in the continuous recycle pebble-bed concepts is due to the reduction in mass of SNF&HLW disposed from recycling SNF in the Stage 1 SFR and Stage 2 micro-HTGR as SNF is recycled and only HLW is sent to disposal.

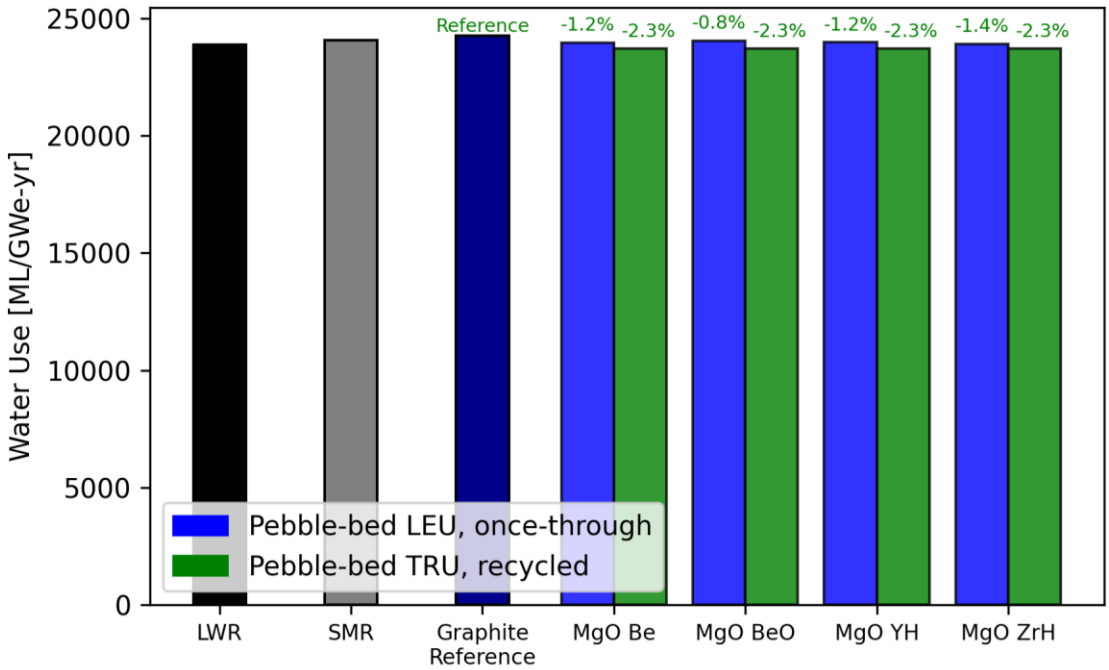

Figure 57. Energy normalized volume of water used for large-scale LWR, SMR, prismatic graphite reference, and pebble-bed IMF concepts using either LEU fuel in a once-through fuel cycle or TRU fuel in a continuous recycle fuel cycle.

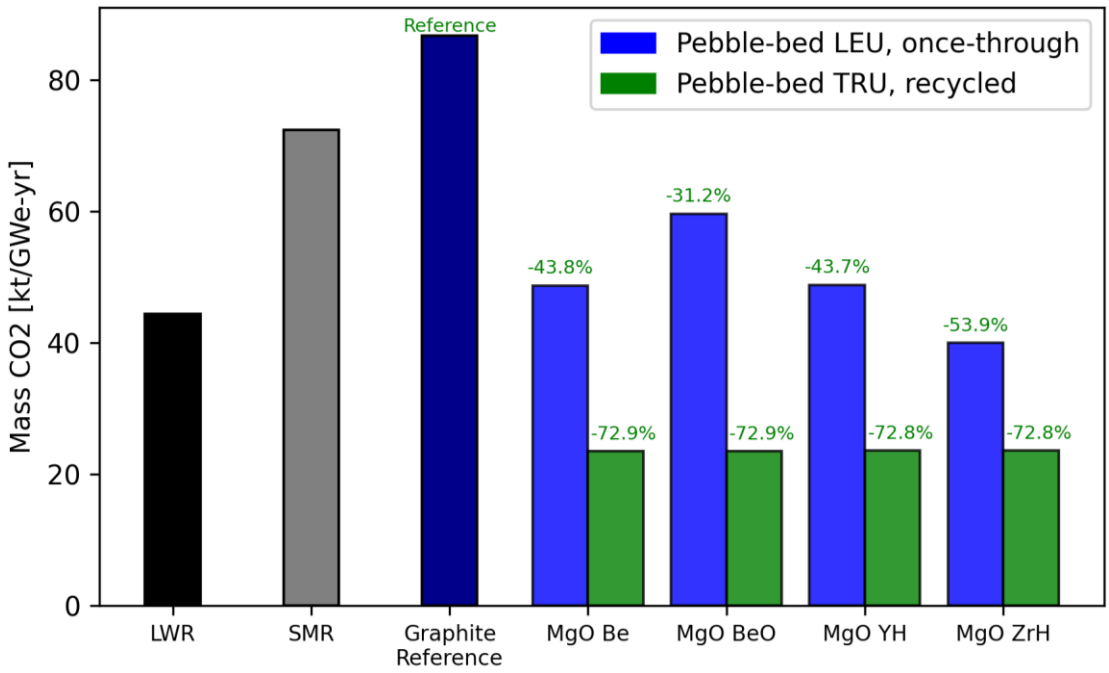

Figure 58. Energy normalized mass of CO_2 produced for large-scale LWR, SMR, prismatic graphite reference, and pebble-bed IMF concepts using either LEU fuel in a once-through fuel cycle or TRU fuel in a continuous recycle fuel cycle.

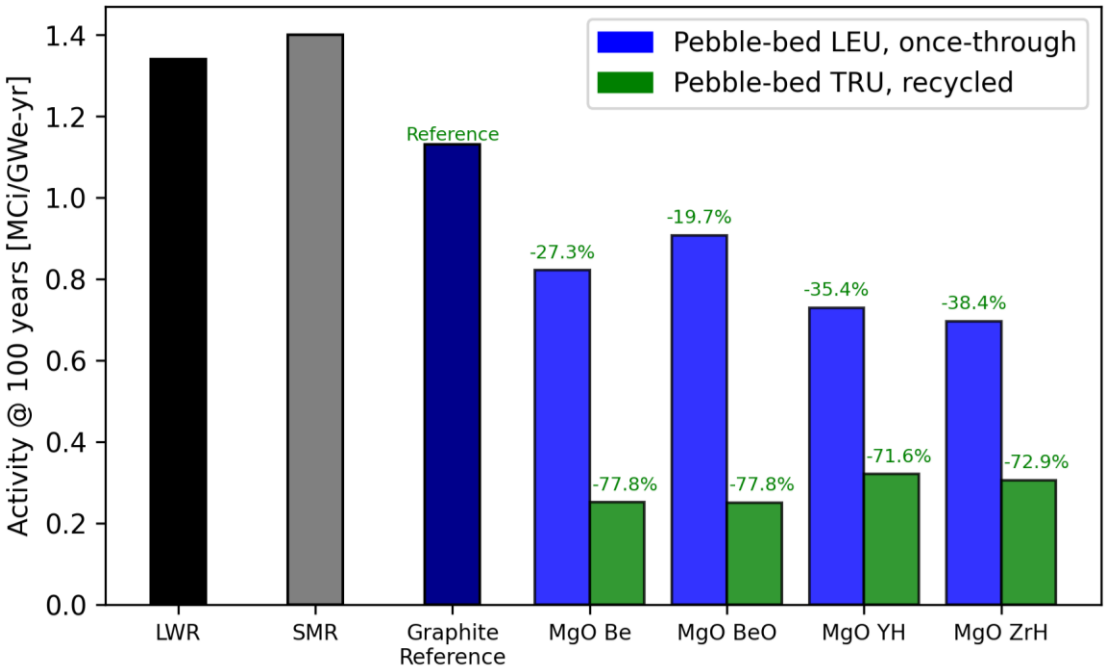

Figure 59. Activity of SNF&HLW at 100 years for large-scale LWR, SMR, prismatic graphite reference, and pebble-bed IMF concepts using either LEU fuel in a once-through fuel cycle or TRU fuel in a continuous recycle fuel cycle.

Figure 60 shows the activity of SNF&HLW at 100,000 years for the continuous recycle pebble-bed IMF concepts using TRU fuel compared to a large-scale LWR, SMR, prismatic graphite reference, and once-through pebble-bed IMF concepts using LEU fuel. The results for the continuous recycle pebble-bed IMF concepts only include the activity of SNF&HLW from the Stage 2 micro-HTGR. Compared to the graphite reference case and once-through pebble-bed IMF concepts, all four continuous recycle pebble-bed IMF concepts have lower activity. The MgO Be concept performs the best, lowering activity by 78.6% compared to the graphite reference. Similar to the continuous recycle prismatic designs and activity of SNF&HLW at 100 years, the activity of SNF&HLW at 100,000 years in the continuous recycle pebble-bed IMF concepts is reduced by recycling of SNF in Stages 1 and 2 which reduces the mass of SNF&HLW disposed.

See

Table *16* for the reduction in each continuous recycle pebble-bed IMF concept compared to the graphite reference for each evaluated metric. The Be-based concepts achieved the highest reductions in the evaluated metrics out of the four pebble-bed IMF concepts. The MgO Be concept reduced the activity of SNF&HLW by slightly more than the MgO BeO concept. All four pebble-bed IMF concepts showed substantial improvements compared to the graphite reference and also the once-through pebble-bed IMF concepts, LWR, and SMR. Like the continuous recycle prismatic designs, the reduction of LLW volume disposed in the continuous recycle pebble-bed designs is lower than it is in the once-through pebble-bed designs.

The mass of SNF&HLW disposed and volume of LLW disposed was also calculated for the continuous recycle pebble-bed MgO BeO concept where the active core radius is 60 cm instead of 30 cm, which is the core radius in the optimal core configuration that is used. This was done to see how much of an impact the larger discharge burnup achieved through a larger active reactor core would have on the evaluated metrics. Shown in **Figure 61** is the mass of SNF&HLW disposed for the large-scale LWR, the SMR, the graphite reference, the once-through pebble-bed MgO BeO design, the continuous recycle pebble-bed MgO BeO design where the active core radius is 30 cm, and the continuous recycle pebble-bed MgO BeO design where the active core radius is 60 cm. Shown in **Figure 62** is the volume of LLW disposed for the large-scale LWR, the SMR, the graphite reference, the once-through pebble-bed MgO BeO

design, the continuous recycle pebble-bed MgO BeO designs where the active core radius is 30 and 60 cm.

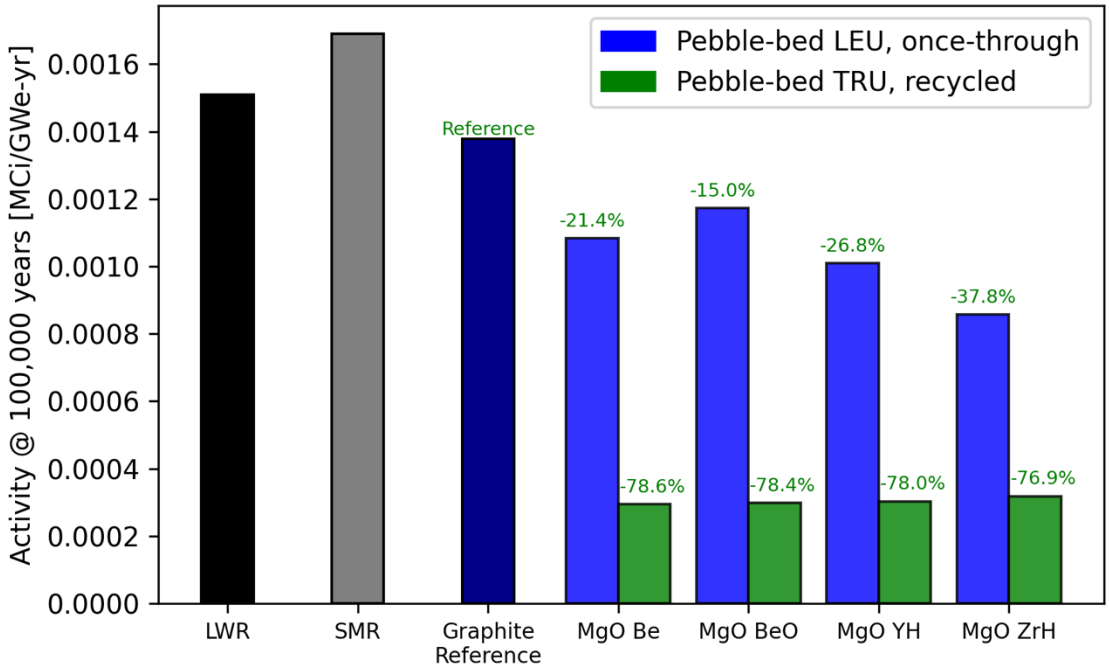

Figure 60. Activity of SNF&HLW at 100,000 years for large-scale LWR, SMR, prismatic graphite reference, and pebble-bed IMF concepts using either LEU fuel in a once-through fuel cycle or TRU fuel in a continuous recycle fuel cycle.

Table 16. Evaluated metric reduction percentages for the continuous recycle pebble-bed IMF concepts compared to the prismatic graphite reference.

IMF concept	MgO Be	MgO BeO	MgO $YH_{x=1.9}$	MgO $ZrH_{x=1.6}$
SNF&HLW	92.7 %	92.7 %	92.7 %	92.7 %
LLW	31.0 %	31.1 %	30.8 %	30.9 %
Natural Uranium	99.8 %	99.8 %	99.8 %	99.8 %
Land Use	76.9 %	76.9 %	76.9 %	76.9 %
Water Use	2.3 %	2.3 %	2.3 %	2.3 %
Mass CO_2	72.9 %	72.9 %	72.8 %	72.8 %
Activity at 100 years	77.8 %	77.8 %	71.6 %	72.9 %
Activity at 100,000 years	78.6 %	78.4 %	78.0 %	76.9 %

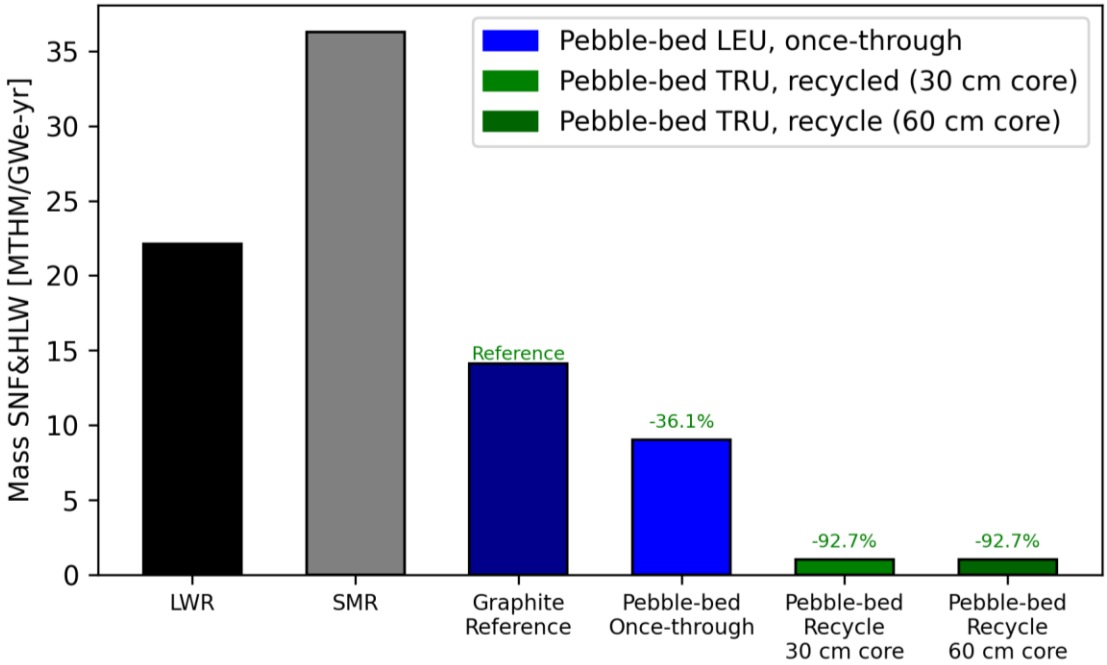

Figure 61. Energy normalized mass of SNF&HLW per unit energy generated for large-scale LWR, SMR, prismatic graphite reference, once-through pebble-bed MgO BeO design using LEU, and continuous recycle pebble-bed MgO BeO designs using TRU with an active core radius of 30 or 60 cm.

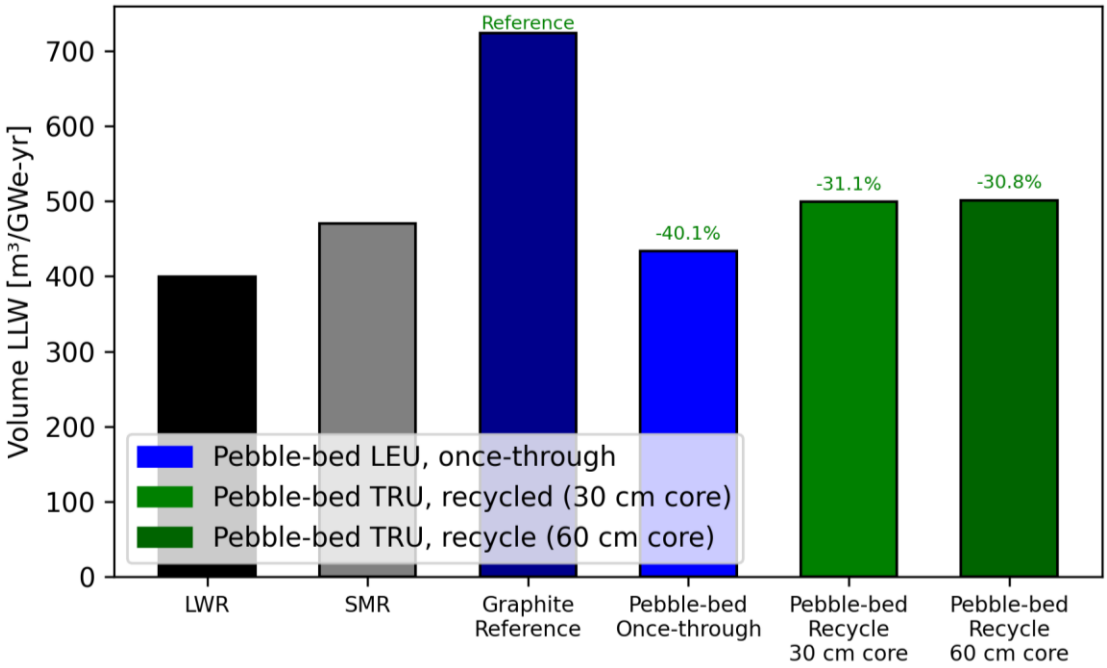

Figure 62. Energy normalized volume of LLW per unit energy generated for large-scale LWR, SMR, prismatic graphite reference, once-through pebble-bed MgO BeO design using LEU, and continuous recycle pebble-bed MgO BeO designs using TRU with an active core radius of 30 or 60 cm.

As seen in both figures for mass of SNF&HLW and volume of LLW, there is little to no difference between the reductions achieved by the continuous recycle pebble-bed MgO BeO designs using either a radius of 30 cm or 60 cm for the active core relative to the graphite reference. The mass of SNF&HLW disposed is reduced by 92.7% relative to the graphite reference in both continuous recycle pebble-bed MgO BeO designs using an active core radius of 30 cm or 60 cm. The volume of LLW disposed is reduced by slightly more in the continuous recycle pebble-bed MgO BeO design using an active core radius of 30 cm than the design using a core radius of 60 cm. In spite of the increased discharge burnup seen in the design using a 60 cm core radius, there is little to no difference in the shown metric results because of significant discrepancy between the electric power outputs of the Stage 1 SFR and Stage 2 micro-HTGR affecting power sharing fractions between stages and therefore affecting the results of mass flow balance. The design using a 30 cm core radius reduces volume of LLW slightly more than the design using a 60 cm core radius because it requires less Pu for recycled fuel, which shifts the power sharing fraction in favor of the micro-HTGR. This reduces the power sharing fraction of the Stage 1 SFR, which decreases the mass going into and out of the SFR, and that decreases LLW produced from reprocessing the SFR metal driver and blanket fuel. The optimal core configurations for the continuous recycle pebble-bed designs use the smaller core radius for this reason.

3.7 Comparison between Microreactor Designs

The pebble-bed and prismatic IMF concepts adapted to a continuous cycle using TRU fuel perform similarly when comparing the pebble-bed microreactor and the prismatic microreactor platforms for almost all levelized metrics. The pebble-bed reactor core has an additional degree of freedom in optimization as the ratio of fuel to moderating pebbles and reflector thickness were considered when optimizing the pebble-bed point design for waste performance. The prismatic microreactor could only modify the fuel-to-moderator ratio of the design by varying the TRISO packing fraction and the assembly lattice pitch. In contrast, the pebble-bed microreactor could modify the ratio by changing three parameters, including the TRISO packing fraction. See

for the levelized metrics in the best performing pebble-bed case and best performing prismatic case.

Table 17. Reduction percentages for the best performing pebble-bed and prismatic IMF concepts using TRU fuel compared to the prismatic graphite reference.

Reactor	**Pebble-bed**	**Prismatic**
SNF&HLW	92.7 %	92.7 %
LLW	31.1 %	30.7 %
Natural Uranium	99.8 %	99.8 %
Land Use	76.9 %	76.9 %
Water Use	2.3 %	2.3 %
Mass CO_2	72.9 %	72.3 %
Activity at 100 years	77.8 %	45.8 %
Activity at 100,000 years	78.4 %	77.3 %

The activity of SNF&HLW at 100 years sees the most significant difference between the pebble-bed and prismatic point designs. The pebble-bed designs have in-core residence times over 3 times larger than that of the prismatic designs. The longer in-core residence times in the pebble-bed designs allow for the decay of many shorter-lived fission products that dominate the radioactivity 100 years after reactor shutdown. To prove this point, the pebble-bed MgO Be micro-HTGR point design was modified to operate at 30 MWth instead of 10 MWth. This modification was done to see whether tripling the thermal power output of the reactor meant achieving close to the same discharge burn-up in roughly one-third of the in-core residence time in the 10 MWth pebble-bed MgO Be design. This trend was proven to be the case as the 30 MWth pebble-bed point design achieved a maximum discharge burn-up of 415.36 GWd/MTHM at 12,519 days compared to the 10 MWth pebble-bed point design, which achieved a maximum discharge burn-up of 411.55 GWd/MTHM at 36,165 days.

The activity of SNF&HLW at 100 years in the 30 MWth pebble-bed point design was compared to what was found in the 10 MWth pebble-bed and prismatic point designs. The in-core residence times are 36,165 days for the 10 MWth pebble-bed design and 11,629 days for the 10 MWth prismatic design. See **Figure 63** for a plot of the activity in the three cases. As seen in the plot, the SNF&HLW activity in the 30 MWth pebble-bed point design is very similar to that of the prismatic point design up to around 700 years. The 30 MWth pebble-bed point design has a higher activity than the 10 MWth design. These observations help explain the difference in SNF&HLW activity at 100 years between the optimized pebble-bed and prismatic point designs.

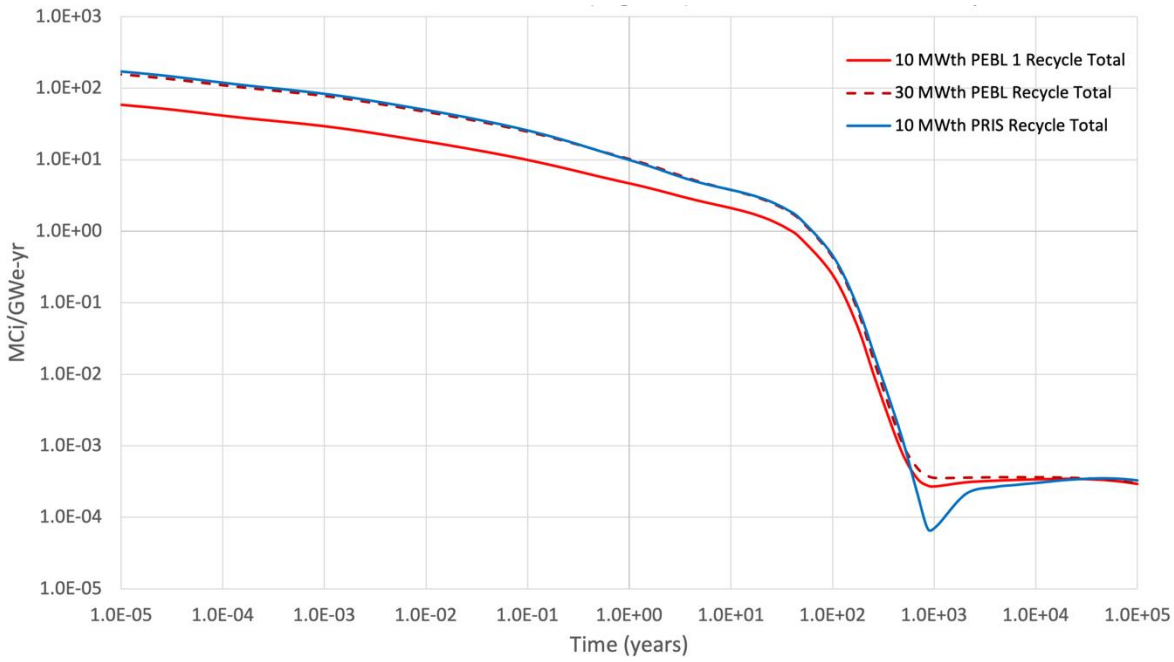

Figure 63. Activity per energy generated of SNF+HLW at 100 years in the 10 MWth pebble-bed, 30 MWth pebble-bed, and 10 MWth prismatic MgO Be micro-HTGR point designs.

Chapter 4 Conclusion

This work adapted once-through prismatic and pebble-bed IMF micro-HTGR concepts to a continuous recycle fuel cycle with the goal of reducing waste disposed, fuel cycle cost, and environmental impact. Optimization sweeps aiming to maximize discharge burnup were performed for prismatic and pebble-bed IMF concepts using the composite moderators MgO Be, MgO BeO, MgO $YH_{x=1.9}$, and MgO $ZrH_{x=1.6}$. For the prismatic concepts, TRISO packing fraction and lattice pitch were varied. For the pebble-bed concepts, TRISO packing fraction, fueled radius, ratio of fueled to unfueled pebbles, and reactor core radius were varied. Discharge burnup in the prismatic designs was found by identifying when reactivity reached zero whereas the linear and quadratic reactivity models were used to calculate it for the pebble-bed designs. After determining the optimal core configuration where discharge burnup was the highest for each IMF concept, mass flow balance was calculated between the Stage 1 SFR and Stage 2 micro-HTGR. Key metrics were calculated using values found in mass flow data tables and multiplier constants found in the E&S study. The metric results were compared between each continuous recycle design, the graphite reference, once-through designs, LWR, and SMR.

Metric results for the continuous recycle designs showed great improvement compared to not only the graphite reference but also the once-through designs in most metrics. For the prismatic microreactor continuous recycle point design, mass of SNF&HLW was reduced by up to 92.7%, volume of LLW was reduced by up to 30.7%, mass of natural uranium was reduced by up to 99.8%, area of land was reduced by up to 76.9%, volume of water was reduced by up to 2.3%, mass of CO_2 was reduced by up to 72.3%, activity of SNF&HLW at 100 years was reduced by up to 58.6%, and activity of SNF+HLW at 100,000 years was reduced by up to 77.3% compared to the state-of-the-art prismatic graphite once-through reference. For the pebble-bed microreactor continuous recycle point design, mass of SNF&HLW was reduced by up to 92.7%, volume of LLW was reduced by up to 31.1%, mass of natural uranium was reduced by up to 99.8%, area of land was reduced by up to 76.9%, volume of water was reduced by up to 2.3%, mass of CO_2 was reduced by up to 72.9%, activity of SNF+HLW at 100 years was reduced by up to 77.8%, and activity of SNF+HLW at 100,000 years was reduced by up to 78.6% compared to the state-of-the-art prismatic graphite once-through reference. Overall, adapting the once-through point designs to a continuous recycle fuel cycle shows excellent results.

List of References

[1] L. Wood LLNL, "Global warming and nuclear power," in *Report Number: UCRL-JC-131306; CONF-980751-*, Research Org.: Lawrence Livermore National Lab. (LLNL), Livermore, CA (United States), Jul. 1998. [Online]. Available: https://www.osti.gov/biblio/289886

[2] P. Lappi and J. Lintunen, "From cradle to grave? On optimal nuclear waste disposal," *Energy Econ.*, vol. 103, p. 105556, Nov. 2021, doi: 10.1016/j.eneco.2021.105556.

[3] A. Peakman, Z. Hodgson, B., and Merk, “Advanced micro-reactor concepts,” Prog. Nucl. Energy. Vol. 107, pp. 61-70, Aug. 2018. Doi: 1016/j.pnucene.2018.02.025.

[4] R. Testoni, A. Bersano, and S. Segantin, “Review of nuclear microreactors: Status, potentialities and challenges,” Prog. Nucl. Energy. vol. 138, p. 103822, Aug. 2021, doi:10.1016/j.pnucene.2021.103822.

[5] V. Kuznetsov, "Options for small and medium sized reactors (SMRs) to overcome loss of economies of scale and incorporate increased proliferation resistance and energy security," *Innov. Nucl. Energy Syst. Sustain. Dev. World Proc. Second COE-INES Int. Symp. INES-2 Novemb. 26-30 2006 Yokohama Jpn.*, vol. 50, no. 2, pp. 242–250, Mar. 2008, doi: 10.1016/j.pnucene.2007.11.006.

[6] D. E. Carlson and S. J. Ball, "Perspectives on understanding and verifying the safety terrain of modular high temperature gas-cooled reactors," *Nucl. Eng. Des.*, vol. 306, pp. 117–123, Sep. 2016, doi: 10.1016/j.nucengdes.2016.01.015.

[7] N. R. Brown and S. T. Revankar, "An endothermic chemical process facility coupled to a high temperature reactor. Part II: Transient simulation of accident scenarios within the chemical plant," *Nucl. Eng. Des.*, vol. 246, pp. 266–276, May 2012, doi: 10.1016/j.nucengdes.2011.12.026.

[8] N. R. Brown, V. Seker, S. T. Revankar, and T. J. Downar, "An endothermic chemical process facility coupled to a high temperature reactor. Part I: Proposed accident scenarios within the chemical plant," *Nucl. Eng. Des.*, vol. 246, pp. 256–265, May 2012, doi: 10.1016/j.nucengdes.2011.12.027.

[9] M. V. Ramana, “The checkered operational history of high-temperature gas-cooled reactors,” *Bull. At. Sci.*, vol. 72, no. 3, pp. 171-179, Apr. 2016, doi: 10.1080/0.00963402.2016.1170395.

[10] H. L. Brey, "Fort St. Vrain operations and future," *Energy*, vol. 16, no. 1, pp. 47–58, Jan. 1991, doi: 10.1016/0360-5442(91)90086-2.

[11] A. L. Habush and A. M. Harris, "330-MW(e) Fort St. Vrain high-temperature gas-cooled reactor," *Nucl. Eng. Des.*, vol. 7, no. 4, pp. 312–321, Apr. 1968, doi: 10.1016/0029-5493(68)90064-2.

[12] Z. Wu, D. Lin, and D. Zhong, "The design features of the HTR-10," *Nucl. Eng. Des.*, vol. 218, no. 1, pp. 25–32, Oct. 2002, doi: 10.1016/S0029-5493(02)00182-6.

[13] P. A. Demkowicz, B. Liu, J. D. Hunn, "Coated particle fuel: Historical perspectives and current progress," *J. Nucl. Mater.*, vol. 515, pp. 434-450, Mar. 2019, doi: 10.1016/j.jnucmat.2018.09.044

[14] H. R. Trellue, J. O'Brien, J. S. Carpenter, R. S. Reid, D. Guillen, and P. Sabharwall, "Microreactor Demonstration and Testing Progress in FY19," Los Alamos Nation Laboratory, Los Alamos, New Mexico, Tech. Rep. LA-UR-19-28768, Sep. 2019, doi: 10.2172/1566087

[15] N. R. Brown, "A review of in-pile fuel safety tests of TRISO fuel forms and future testing opportunities in non-HTGR applications," *J. Nucl. Mater.*, vol. 534, p. 152139, Jun. 2020, doi: 10.1016/j.jnucmat.2020.152139.

[16] J. McMurray, T. B. Lindemer, N. R. Brown, T. J. Reif, R. N. Morris, and J. D. Hunn, "Determining the minimum required uranium carbide content for HTGR UCO fuel kernels," *Ann. Nucl. Energy*, vol. 104, pp. 237-242, Jun. 2017, doi: 10.1016/j.anucene.2017.023.

[17] N. M. George, I. Maldonado, K. A. Terrani, A. Godfrey, J. Gehin, J. Powers, "Neutronics Studies of Uranium-Bearing Fully Ceramic Microencapsulated Fuel for Pressurized Water Reactors," *Nucl. Technol.*, vol. 188, no. 3, pp. 238-251, Mar. 2017, doi: 10.13182/NT14-3.

[18] K. A. Terrani, B. C. Jolly, J. M. Harp, "Uranium nitride-tristructural-isotropic fuel particle," *J. Nucl. Mater.*, vol. 531, p. 152034, Apr. 2020, doi: 10.1016/j.jnucmat.2020.152034.

[19] T. D. Burchell and L. L. Snead, "The effect of neutron irradiation damage on the properties of grade NBG-10 graphite," *J. Nucl. Mater.*, vol. 371, no. 1, pp. 18–27, Sep. 2007, doi: 10.1016/j.jnucmat.2007.05.021.

[20] L. L. Snead, T. D. Burchell, and Y. Katoh, "Swelling of nuclear graphite and high quality carbon fiber composite under very high irradiation temperature," *J. Nucl. Mater.*, vol. 381, no. 1, pp. 55–61, Oct. 2008, doi: 10.1016/j.jnucmat.2008.07.033.

[21] L. L. Snead and T. D. Burchell, "Thermal conductivity degradation of graphites due to nuetron irradiation at low temperature," *J. Nucl. Mater.*, vol. 224, no. 3, pp. 222–229, Sep. 1995, doi: 10.1016/0022-3115(95)00071-2.

[22] B. T. Kelly, *Physics of graphite*. United Kingdom: Applied Science, 1981.

[23] M. C. R. Heijna, S. de Groot, and J. A. Vreeling, "Comparison of irradiation behaviour of HTR graphite grades," *J. Nucl. Mater.*, vol. 492, pp. 148–156, Aug. 2017, doi: 10.1016/j.jnucmat.2017.05.012.

[24] E. M. Duchnowski, R. F. Kile, L. L. Snead, J. R. Trelewicz, and N. R. Brown, "Reactor performance and safety characteristics of two-phase composite moderator concepts for modular high temperature gas cooled reactors," *Nucl. Eng. Des.*, vol. 368, p. 110824, Nov. 2020, doi: 10.1016/j.nucengdes.2020.110824.

[25] B. Cheng, E. M. Duchnowski, D. J. Sprouster, L. L. Snead, N. R. Brown, and J. R. Trelewicz, "Ceramic composite moderators as replacements for graphite in high temperature microreactors," *J. Nucl. Mater.*, vol. 563, p. 153591, May 2022, doi: 10.1016/j.jnucmat.2022.153591.

[26] L. L. Snead, D. J. Sprouster, B. Cheng, N. R. Brown, C. Ang, E. M. Duchnowski, and J. R. Trelewicz, "Development and potential of composite moderators for elevated temperature nuclear applications," *J. Asian Ceram. Soc.* pp. 9-32, Oct. 2021, doi: 10.1080/21870764.2021.1993592.

[27] C. Lu, B. D. Hiscox, K. A. Terrani, and N. R. Brown, "Fully ceramic microencapsulated fuel in prismatic high temperature gas-cooled reactors: analysis of reactor performance and safety characteristics," *Ann. Nucl. Energy*, vol. 114, pp. 277–287, 2018.

[28] W. B. Cottrell, H. E. Hungerford, J. K. Leslie, and J. L. Meem, "OPERATION OF THE AIRCRAFT REACTOR EXPERIMENT," Oakridge National Laboratory, Oakridge, Tennessee. Tech. Rep. ORNL-1845(Del.), Sep. 1955, doi: 10.2172/4237975.

[29] F. C. Linn, *Heat Transfer Reactor Experiment No. 3: Comprehensive Technical Report*, Tech. Rep. US Atomic Energy Commission, Division of Technical Information, Jun. 1962.

[30] M. Ito and K. Morita, “The Solubility of MgO in Molten $MgCl_2$-$CaCl_2$ Salt,” *Mater. Trans.*, vol. 45, pp. 2712-2718, Jun. 2004, doi: 10.2320/matertrans.45.2712.

[31] M. F. Suárez and R. G. Compton, “Dissolution of Magnesium Oxide in Aqueous Acid: An Atomic Force Microscopy Study,” *J. Phys. Chem. B*, vol. 102, pp. 7156-7162, Sep. 1998, doi: 10.1021/jp982260x.

[32] E. M. Duchnowski, R. F. Kile, K. Bott, L. L. Snead, J. R. Trelewicz, and N. R. Brown, "Pre-conceptual high temperature gas-cooled microreactor design utilizing two-phase composite moderators. Part I: Microreactor design and reactor performance," *Prog. Nucl. Energy*, vol. 149, p. 104257, Jul. 2022, doi: 10.1016/j.pnucene.2022.104257.

[33] E. M. Duchnowski, V. Karriem, K. Skidmore, J. P. Gorton, L. L. Snead, J. R. Trelewicz, and N. R. Brown, “Pre-conceptual high temperature gas-cooled microreactor design utilizing two-phase composite moderators. Part II: Design space and safety characteristics,” *Prog. Nucl. Energy*, vol. 149, p. 104258, Jul. 2022, doi: 10.1016/j.pnucene.2022.104258.

[34] C. Rodriguez, A. Baxter, D. McEachern, M. Fikani, and F. Venneri, “Deep-Burn: making nuclear waste transmutation practical,” *Nucl. Eng. Des.*, vol. 222, pp. 299-317, Jun. 2003, doi: 10.1016/S0029-5493(03)00034-7

[35] L. Cecille, M. Casarci, and L. Pietrelli, *New Separation Chemistry Techniques for Radioactive Waste and Other Specific Applications*, pp. 21-29, 1991.

[36] S. Ansari, P. Pathak, P. Mohapatra, and V. Manchanda. “Aqueous Partitioning of Minor Actinides by Different Processes,” *Sep. Purif. Rev.*, vol. 40, pp. 43-76, Feb. 2011, doi: 10.1080/15422119.2010.545466.

[37] J. Mathur, M. Murali, and K. Nash, “ACTINIDE PARTITIONING-A REVIEW,” *Solvent Extr. Ion. Exc.* vol. 19, pp. 357-390, Feb. 2007, doi:10.1081/SEI-100103276.

[38] T. K. Kim, T. A. Taiwo, R. N. Hill, W. S Yang, and F. Venneri, “A feasibility study of reactor-based deep-burn concepts,” Argonne National Laboratory, Argonne, Illinois. Tech. Rep. ANL-AFCI-155, Aug. 2005, doi: 10.2172/861619.

[39] R. Wigeland, et al., "Nuclear Fuel Cycle Evaluation and Screening—Final Report," Tech. Rep. INL/EXT-14-31465, Idaho National Laboratory, Idaho Falls, Idaho, Oct. 2014.

[40] J. R. Burns, R. Hernandez, K. A. Terrani, A. T. Nelson, and N. R. Brown, “Reactor and fuel cycle performance of light water reactor fuel with 235U enrichments above 5%,” *Ann. Nucl. Energy*, vol. 132, Jul. 2020, doi: 10.1016/j.anucene.2020.107423.

[41] N. R. Brown, R. Hernandez, and A. T. Nelson, “High volume packing fraction TRISO-based fuel in light water reactors,” *Prog. Nucl. Energy*, vol. 146, p. 104151, Apr. 2022, doi: 10.1016/j.pnucene.2022.104151.

[42] R. Hernandez and N. R. Brown, “Potential fuel cycle performance of floating small modular light water reactors of Russian origin,” *Ann. Nucl. Energy*, vol. 144, p. 107555, Sep. 2020, doi: 10.1016/j.anucene.2020.107555.

[43] N. R. Brown, A. Worrall, and M. Todosow, “Impact of thermal spectrum small modular reactors on performance of once-through nuclear fuel cycles with low-enriched uranium,” *Ann. Nucl. Energy*, vol. 101, pp. 166-173, Mar. 2017, doi: 10.1016/j.anucene.2016.11.003.

[44] D. L. Doyle, E. M. Duchnowski, J. R. Trelewicz, N. R. Brown, “Ceramic Composite Inert Matrix Fuel Forms in High-Temperature Gas Cooled Micro-Reactors,” *Nucl. Sci. Eng.*, under review.

[45] P. Matveev, P. K. Mohapatra, S. N. Kalmykov, and V. Petrov, “Solvent extraction systems for mutual separation of Am(III) and Cm(III) from nitric acid solutions. A review of recent-state-of-the-art,” *Solvent Extr. Ion. Exc.*, vol. 39, pp. 679-713, Dec. 2020, doi:10.1080/07366299.2020.1856998.

[46] J. Leppänen, “Serpent-a continuous-energy Monte Carlo reactor physics burnup calculation code,” Research Center of Finland: VTT Technical, 2013.

[47] M. J. Driscoll, *The Linear Reactivity Model for Nuclear Fuel Management*, La Grange Park, Illinois: American Nuclear Society, 1990.

[48] K. Yonghee and F. Venneri, “Optimization of One-pass Transuranic Deep Burn in a Modular Helium Reactor,” *Nucl. Sci. Eng.*, vol. 160, pp. 59-74, Apr. 2017, doi: 10.13182/NSE160-59 .

[49] G. B. Bradshaw, N. I. Marsh, and C. F. Wallroth, “Safety analysis report for Fort. St. Vrain test elements FTE-1 through FTE-8. Proposed supplement to the Final Safety Analysis Report for Fort. St. Vrain Nuclear Generating Station,” General Atomic, San Diego, California, Tech. Rep. GA-A—13903, Aug. 1976.

[50] D. McEachern, “Deep-Burn Modular Helium Reactor Fuel Development Plan,”. Oak Ridge National Lab, Oak Ridge, Tennessee, Tech. Rep. ORNL/TM-2002/135; TRN: US0604097, Dec. 2002, doi: 10.2172/885771.

[51] W. V. Goeddel, E.O. Winkler, and C. S. Luby “HTGR FUEL IRRADIATION PERFORMANCE AND IMPLICATIONS ON FUEL DESIGN, ” General Atomic, San Diego, California, Tech. Rep. GA-10012, 1970.

[52] R. K. McGeary, “Mechanical Packing of Spherical Particles,” *J. Am. Ceram. Soc.*, vol. 44, pp. 513-522, Oct. 1961, doi: 10.1111/j.1151-2916.1961.tb13716.x.

[53] R. N Morris and P. J. Pappano, “Estimation of maximum coated particle fuel compact packing fraction,” *J. Nucl. Mat.*, vol. 361, pp. 18-29, Oct. 2006, doi: 10.1016/j.jnucmat.2006.10.017.

[54] K. A. Terrani et al., “Fabrication and characterization of fully ceramic microencapsulated fuels,” *J. Nucl. Mat.*, vol. 426, pp. 268-276, Jul. 2012, doi: 1016/j.jnucmat.2012.03.049.

[55] C. Ang, L. Snead, and Y. Kato, “A logical approach for zero-rupture Fully Ceramic Microencapsulated (FCM) fuels via pressure-assisted sintering route,” *J. Nucl. Mater.*, vol. 531, p. 151987, Apr. 2020, doi: 10.1016/j.jnucmat.2020.151987.

[56] C. Ang, G. Singh, L. Snead, and Y. Katoh, “Preliminary study of sintering zero-rupture Fully Ceramic Microencapsulated (FCM) fuel,” *Int. J. Appl. Ceram. Technol.*, vol. 16, pp. 1699-1707, May 2019, doi: 10.1111/ijac.13294.

[57] G. Kim and Y. Kim, “Processing of fully ceramic microencapsulated fuels with a small amount of additives by hot-pressing,” *J. Eur. Ceram. Soc.*, vol. 41, pp. 3980-3990, Jul. 2021, doi: 10.1016/j.jeurceramsoc.2021.02.020.

[58] J. J. Duderstadt and L. J. Hamilton, *Nuclear reactor analysis*, The University of Michigan, Ann Arbor, Michigan, pp. 74-86, 1976.

Vita

Venkata Vallabhaneni graduated from the University of Tennessee Knoxville with a Bachelor of Science in Nuclear Engineering in May of 2023. Venkata began graduate research at the University of Tennessee in June of 2023 to earn a Master of Science in Nuclear Engineering. His anticipated graduation date is May of 2025, after which Venkata plans on pursuing a Doctor of Philosophy in Nuclear Engineering at the University of Tennessee. Venkata will be presenting work at the American Nuclear Society Annual Conference in June of 2025.